POLITECNICO DI TORINO

MSc in Energy and Nuclear Engineering-
Innovation in Energy Production

Master Thesis

Modelling of Hydrogen production systems through Steam Methane Reforming and CO_2 capture for industrial applications

Supervisor
Prof. Pierluigi Leone

Co-supervisors
Prof. Andrea Lanzini
Prof. Stefano Campanari
Doc. Sonja Sechi

Candidate
Iacopo Ciuchi

Acknowledgements

Questo lavoro rappresenta per me, come per tutti gli studenti universitari, il punto di ancoraggio della "barca" accademica partita alla fine del XX secolo, quando mi divertivo a svolgere le prime operazioni o a contare i punti nelle prime partite a briscola. Mi sento dunque di ringraziare in primis i miei supervisors, che mi hanno permesso di gettare quest'ancora, con cui si è instaurato da subito un clima di serenità e disponibilità. Un grazie speciale a Pierluigi Leone, per essersi affezionato davvero come aveva promesso un anno e mezzo fa, portandomi avanti anche lungo tutto il progetto ASP. Ringrazio poi Andrea Lanzini e Sonja Sechi, per tutto il supporto tecnico e amministrativo datomi durante l'intero lavoro.

Lo scafo della barca, in ogni modo, non può che essere rappresentato dalla mia famiglia, base solida che mi ha accompagnato da sempre, sopportando le mie lamentele continue con una pazienza indescrivibile. Grazie Mamma, Papo, Lola e Pluto, per avermi saputo sempre prendere e concedere tutto l'affetto e il supporto di cui ho avuto bisogno: siete unici ed insostituibili.

Nella barca poi sono salite molte persone: alcune sono scese subito, altre dopo, altre invece sono rimaste. Focalizzerò la mia attenzione su di voi superstiti, che non vi siete allontanati subito all'apparenza di un carattere particolare e un po' arrogante, ma ne avete saputo cogliere tutti i lati positivi. Un grazie speciale alla mia nana del cuore, Alessandrina, per il premio di veterana assoluta in messaggi e chiamate di sfogo e supporto; ma mi sono legato al dito la pastiera mai pervenuta.

All'età di 19 anni sono poi sbarcato in quel di Pisa, dove tanta gente ha deciso di trascorrere tanti momenti piacevoli con me, sfruttando forse gli anni in cui siamo più carichi di energia. Grazie al gruppo di Lucca, per avermi accolto subito come uno di voi, facendomi sentire in una seconda casa anche quando ero relativamente lontano dalla prima. Doveroso poi il ricordo del mitico corso di ingegneria dell'energia. Grazie a Ame e Muarco, pikkoli elettriki sempre pronti a rispondere ai messaggi; a Clari, Ale e Nicco, per Meozzi, Casarosa e le dita tentacolose; a Pigna, per i discorsi sui massimi sistemi della meritocrazia pisana. Un ringraziamento speciale va però a Lisa e Michi, mie spalle sempre presenti, anche da Milano e dalla Danimarca: alla fine il gruppo tornerà ad essere usato per andare a correre, ne sono certo. Infine, non posso non ringraziare Vitino, che ha fatto l'errore di conoscermi e accettare la convivenza nel post triennale: grazie per aver attuato la modalità "sopportazione" anche quando un robot si sarebbe impiccato.

Il percorso si conclude qui al Poli, dove coi nuovi corsi la barca si comincia a ri-riempire. Grazie ad Andre, per tutti i progettini fatti insieme; a Marci, il mio alter ego polentone; a Edo e Vector, che mi hanno introdotto alla piemontesità con degli autoinviti ufficiali a cena; ai Reduci, che hanno contribuito a corroborare tale piemontesità. Un grazie doveroso a tutti gli amici veri che ho trovato in ASP; specialmente gli AfricASPers, per aver tollerato la mia ansia. Un grazie particolare poi agli spetteguless di Luca e Adriano, alla coinquilinanza 2.0 di Lukino, agli audio dal Giappone di Cri, alla Moscova di Piova, alla Milano di Franci.

Ovviamente, dovevo dedicare non solo un paragrafo, ma una pagina intera, a te, mia guida e mio Maestro, che mi guardi dalla poltrona più comoda di tutte (e non la tua col telo verde). Grazie per il parchetto, le partite a carte e la tua mentalità da Nonno-Sprint: le prossime parole sono quelle che sono sicuro ci dedicheremmo a vicenda, potessi ancora solo sgruntare un po' con te. Ti amo.

"La mia vita scorre mentre guardo te,
Quella voglia di riscatto so cos'è
E nessuno può comprenderti di più:
Nessun'altro prova ciò che provi tu."

Abstract

This work aims at providing a deeper insight into large scale hydrogen production facilities through Steam Methane Reforming and CO_2 capture, considered as a promising option for the decarbonization scenario that has to be reached by the end of 2050.

First of all, a technological overview was carried out in order to explore all the feasible options that are present in this moment at different scales, both in terms of size of the plants and development stage. Relevant parameters were extracted from literature, leading to the confidence that Chemical Looping Combustion (CLC) driven plants could become a worthy substitute of traditional Steam Methane Reforming ones.

Thus, both plant layouts were modelled in ASPEN PLUS, implementing operating parameters derived from literature or reasonable assumptions. A more detailed focus was carried on the fluid bed reactors of CLC plant, given the increased complexity of the model if proper block is chosen for its modelling.

The models then provided promising results, that were analyzed both at a component and system level. In particular, the attention was driven to the comparison between the total resources needed by both plants, at fixed hydrogen productivity, resulting in additional expenses for the CLC driven plant. Nevertheless, CLC has the advantage that all the CO_2 produced can be removed by simple condensation of the final exhaust, making it a competitive option from an environmental point of view.

Finally, a techno-economical analysis was performed in order to understand the feasibility of the investment in such plants. Results were comfortable, since they provided very high Net Present Values and low Payback Times, strengthening the idea that, with a proper infrastructure dedicated at its diffusion, hydrogen could play a dominant role for the energy panorama in the next future.

Contents

List of Figures

List of Tables

List of Acronyms

Acronym	Meaning
ACC	Annual Capital Cost
ASU	Air Separation Unit
BEC	Bare Erected Cost
BoP	Balance of Plant
CAPEX	CAPital EXpenditure
CCS	Carbon Capture and Storage
CEPCI	Chemical Engineering Plant Cost Index
CLC	Chemical Looping Combustion
CLR	Chemical Looping Reforming
CRF	Capital Recovery Factor
EEP	Energetically Enhanced Process
EPCC	Engineering, Procurement and Costruction Cost
GHG	Greenhouse Gases
IEER	Intesified Energetically Enhanced steam methane Reforming
IOU	Investor Owned Utility
IPCC	Intergovernmental Panel on Climate Change
IPP	Independent Power Producer
MEA	Mono-EthanolAmine
MMR	Mixed Membrane Reactor
MR	Membrane Reactor
NETL	National Energy Technology Laboratory
NIST	National Institute of Standards and Technologies
NPV	Net Present Value
NREL	National Renewable Energy Laboratory
OPEX	Operating Expense
PBIMR	Packed Bed Inert Membrane Reactor
PBT	PayBack Time
PSA	Pressure Swing Adsorption
PSD	Particle Size Distribution
SE-CL-SMR	Sorption Enhanced Chemical Looping Steam Methane Reforming
SE-SMR	Sorption Enhanced Steam Methane Reforming
SMR	Steam Methane Reforming
TPC	Total Plant Cost
VSA	Vacuum Swing Adsorption
WACC	Weighted Average Cost of Capital
WGS	Water Gas Shift

1 Introduction

"The pace of global warming is accelerating,
the scale of the impact is devastating.
The time for action is limited-
we are approaching a tipping point beyond which
the opportunity to reverse the damage of CO2 emissions will disappear."

Eliot Spitzer, 54th Governor of New York

It is with the approach followed by these words that Climate Change is entering our lives. A diffused sensibility about environmental aspects is spreading all over the world, employing public demonstrations where solutions to such an issue are proposed in terms of minor or major actions and operations.
Among the latter, it is clear that political arrangements are necessary to make the whole system work properly. The most important is represented by the Paris Agreement, whose main aim is setting strict limits to make EU decarbonization happen. Following this vision, the Intergovernmental Panel on Climate Change (IPCC) 2018 report states that global warming must not exceed 1.5 °C, with emissions that need to be reduced of 45% by 2030 from 2010 levels, reaching "net zero" by 2050 [1].
Consistently with this framework, new resources started to be inserred in the gas network to promote its reshaping towards a cleaner environment. **Renewable methane**, produced by power to gas systems or methanation of CO_2 present in biogas, will presumably dominate the EU transport and building heating sectors, while **hydrogen** is predicted to be the most used resource in industry and power ones. The Sankey below shows Navigant predictions about resources allocations in the "optimized gas" scenario, whose aim is to reach net-zero emissions by 2050, smartly combining the use of renewable electricity and low-carbon gases [2].

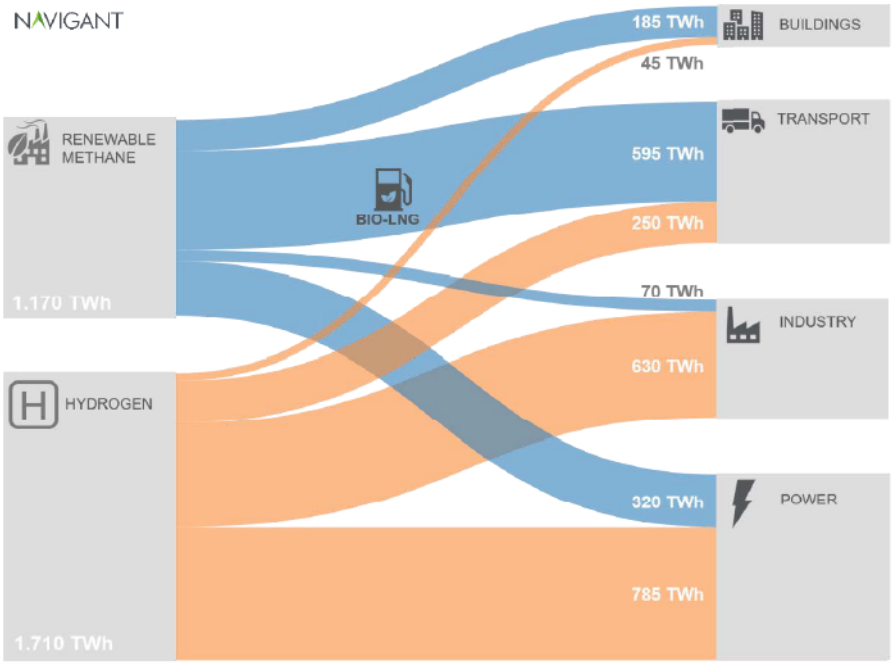

Figure 1: Resource allocation in the "Optimized Gas" Scenario [2]

Since hydrogen seems to be a fundamental resource for the decarbonization pathway, covering around 60% of the energy requirements of EU in the four sectors mentioned above [2], this work aims at investigating its large scale production systems in terms of efficiency and economic feasibility.
But why is hydrogen so important to make the low-carbon transition happen?
First of all, it has to be considered that electrification is not able to cover the whole energy supply by itself, since the actual gas grid is used to provide over 40% of EU **household heating** and around 15% of the **power generation** sector [3]. Moreover, part of the existing infrastructures is not electrificable: heat pumps can be used for space heating in new buildings, but they have a very high cost or can not be retrofitted in old ones, whose CO_2 emissions account for 90% of total buildings' ones [3].
Secondly, hydrogen is considered to be the best option for fuel cells in large vehicles (ships, trucks etc.), whose main disadvantages are the high costs and lower energy density of batteries that need to be installed if electrified. So, since **transport** sector accounts for around 33% of the CO_2 emissions in EU, actions are needed to make it become low-carbon as soon as possible [3].
Finally, since hydrogen is very useful in **industry** for high-temperature heat production or can be used as a reactant in several chemical processes, its importance is even more accentuated.
In spite of these major issues, another strength of hydrogen relies in its **flexibility**, that exhibits both in sectors and in time.
As far as **sectors** are concerned, it is clear that including renewables into the network is a need that has to be fulfilled, as well as the link between the different forms of energy needs a vector to be effectively implemented. Hydrogen can be the solution for both problems, as shown in figure 2 [4], thanks to the fact that electrolyzers can store directly renewable energy into it; moreover, H_2 can be used in different sectors as fuel for heat and power generation.

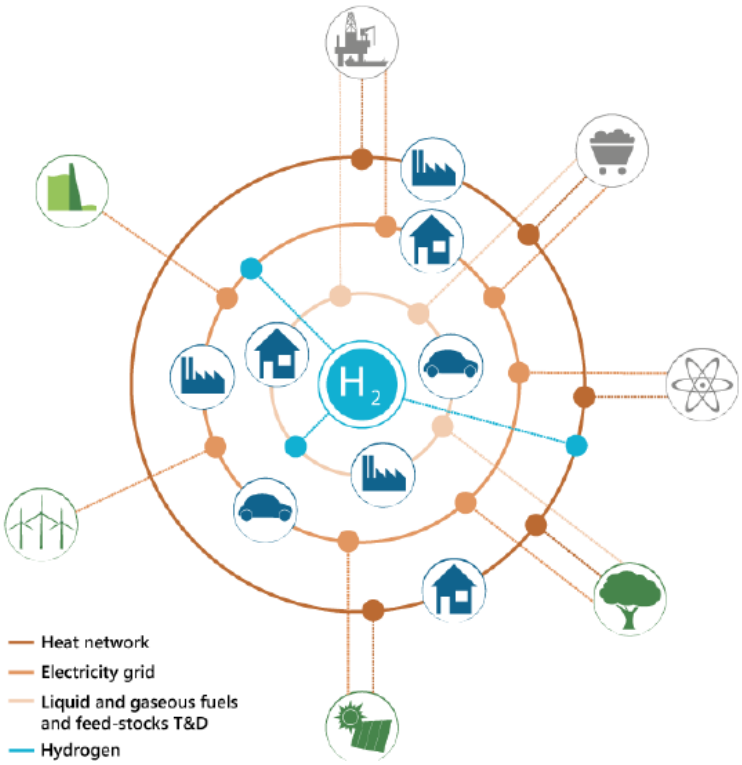

Figure 2: Hydrogen as connector of the different grids [4]

On the other hand, for the same capability of storing into it renewable energy through electrolysis, hydrogen can become the key point in **time** coupling, being able to overcome both seasonal and daily imbalances in generation and supply. Natural caverns, exhausted gas fields and the gas grid itself are the proper places to store low-cost energy in the form of hydrogen.
Concluding, in an ambitious scenario in 2050 great potentialities for hydrogen are foreseen. More in details, it is supposed to stand for around 2250 TWh of energy, accounting for 24% of EU's energy demand [3], with around 560 Mt of CO_2 in total and 0.5 Mt of NO_x abated per year, that stands, respectively, for 20% and 15% of the reductions that EU needs to carry out [3].
In addition, the EU hydrogen industry will create a business of around € 820 billion, with 5.4 million employers more created by its development [3].

Figure 3: Benefits of Hydrogen for the EU [3]

2 Technological Overview

At "State of the Art" level, hydrogen can be classified into two clusters, according to the way it is produced through:

- **Green Hydrogen**, that for its production exploits water electrolyzers, usually fed by renewable energy;
- **Blue Hydrogen**, whose generation pathway passes through thermochemical reactions between methane and steam, that have the disadvantage of producing CO_2 as by-product.

While the penetration of renewables in EU proceeds at a constant pace (9% share in 2005, 16,7% in 2015 and it is expected to grow up to 27% in 2030 [5]) and will become relevant only in several decades, the presence of a well-established gas infrastructure makes it possible to reach large scale productions of blue hydrogen in reasonably short timeframes. Nevertheless, hydrogen can be named as "Blue" only if its production plant is equipped with a Carbon Capture and Storage (CCS) system, that aims at limiting Greenhouse Gases (GHG) emissions in order to safeguard the environment; otherwise, hydrogen produced without CCS is called "Grey" [2].
This section wants to be an exploration of both existing and innovative ways of blue hydrogen production, as well as their CCS retrofitting if needed, highlighting their operation and potentialities.

2.1 H_2 production systems

A first analysis was carried out in order to investigate which is the state of the art of the technology and what are its future perspectives, both from modelling or experimental literature.
A series of parameters was identified in order to allow a comparison of the most relevant characteristics of each plant. More in details, the parameters chosen are:

- **Hydrogen Yield**, defined as [6]:

$$H_{2_{yield}}(\%) = \frac{nH_{2,out}}{nH_{2,stoic}} \cdot 100\% \tag{1}$$

  where $nH_{2,out}$ are the moles of H_2 effectively generated in the reactions and $nH_{2,stoic}$ are the moles of H_2 that would be produced if the reactions were stoichiometric. Thus, it indicates how far the real conditions are from stoichiometric ones.

- **Hydrogen Purity**, defined as [6]:

$$H_{2_{purity}}(\%) = \frac{nH_{2,out}}{nH_{2,out} + nCH_{4,out} + nCO_{,out} + nCO_{2,out}} \cdot 100\% \tag{2}$$

  where $nH_{2,out}$, $nCH_{4,out}$, $nCO_{,out}$, $nCO_{2,out}$ are, respectively, the moles of H_2, CH_4, CO and CO_2 that are present at the end of the reactions. It is fundamental for the correct working of the H_2 separation units.

- **Thermal Demand** [MJ_{th}/kmol], defined as the thermal energy that needs to be given in input to the plant to produce a unit kmol of H_2. It is an indicator of how energy-consuming the process is.

- **Methane Conversion**, defined as [6]:

$$CH_{4conversion}(\%) = \frac{(nCH_{4,in} - nCH_{4,out})}{nCH_{4,in}} \cdot 100\% \tag{3}$$

  where $nCH_{4,in}$ are the inlet moles of methane to the reactors and $nCH_{4,out}$ are the moles of methane that remain at the end of the reactions. It represents exactly the percentage of methane that reacts in the whole process.

- **Temperature** [°C] at which the isothermal reactor is maintained. It is interesting to be considered since it gives an idea of the temperature levels needed to sustain the reactions.

- **Pressure** [atm] of the inlet stream to the reactor. Also in this case, it gives an idea of the operating conditions needed to carry out the process.

- Type of **catalyst** used to foster the reactions. It is important to choose the proper catalyst in order to shift the reaction towards the products in the most effective way.

- **Complexity** of the system, evaluated on the basis of the equipment of the plants, as well as the number and quality of energy and material streams needed for the whole process.

- **Size** of the system, only subdivided into large scale production and laboratory tested ones. Since the aim of the work is to understand which plants can be inserted in the actual decarbonization scenario, it is important to deepen the knowledge on large scale systems that are currently used or that can be considered particularly promising in the next future.

- Type of **study**, that simply refers to whether the plant characteristics and results were investigated through a software modelling analysis or experimental tests.

Knowing that, a critical review of the various alternatives was undertaken, in order to better understand the technological details of each of them.

2.1.1 Steam Methane Reforming

The process that has been dominating the large-scale production of hydrogen for ages is Steam Methane Reforming (SMR). It is based on thermochemical conversion of CH_4 and H_2O into H_2 according to the following reaction:

$$CH_4 + H_2O \rightarrow 3H_2 + CO \qquad \Delta\bar{h} = 206\frac{kJ}{mol} \tag{4}$$

where $\Delta\bar{h}$ is the variation in specific reference enthalpy of reaction, calculated at T=298 K. As can be seen from the positive sign of this last value, the reaction is strongly endothermic and thus needs high temperatures (around 850 °C) and pressures (25 atm) to be completely substained [6]. Since H_2 generation needs to be maximized, a further step is added to convert the CO produced by the reforming reaction into H_2 and CO_2 according to the Water Gas Shift (WGS) reaction, as follows:

$$CO + H_2O \rightarrow H_2 + CO_2 \qquad \Delta\bar{h} = -41\frac{kJ}{mol} \tag{5}$$

where the negative sign of $\Delta\bar{h}$ and its absolute value suggest that the reaction is slightly exothermic.

So, combining (4) and (5), the overall reaction, called Total Reforming, results to be:

$$CH_4 + 2H_2O \rightarrow 4H_2 + CO_2 \qquad \Delta\bar{h} = 165\frac{kJ}{mol} \tag{6}$$

where 4 moles of H_2 per mole of CH_4 are produced stoichiometrically. So, $nH_{2,stoic}$ in (1) for hydrogen yield calculation is assumed to be 4 times the molar flow of inlet CH_4 to reformer.
A schematic of the plant can be represented as follows:

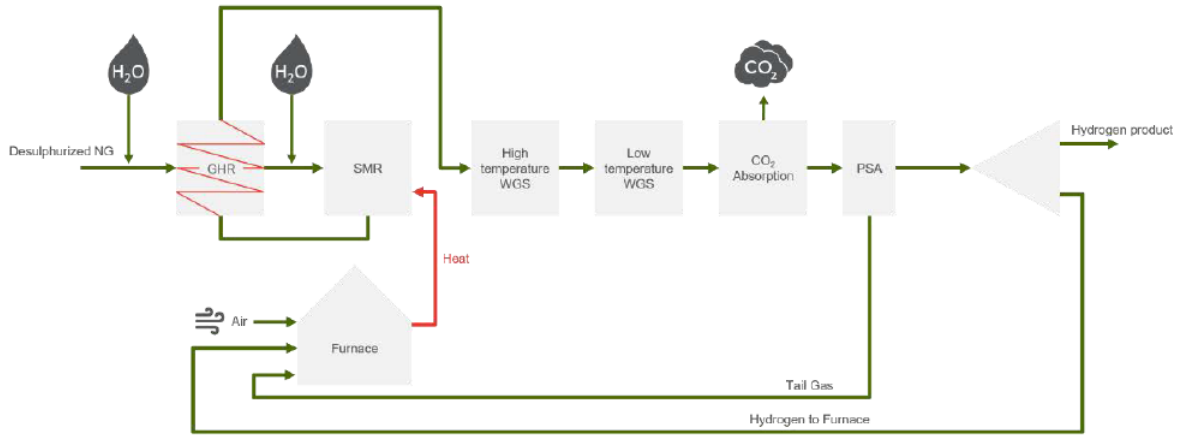

Figure 4: Steam Methane Reforming process [2]

After desulphurization, natural gas is mixed with steam and both enter the reformer, where under Nickel catalytic effect the SMR reaction occurs at high temperature. The reformer is basically a simple reactor that is surrounded by a furnace composed by multiple burners, spatially disposed in homogeneous way in order to guarantee isothermality. An example of reformer design is provided by figure 5:

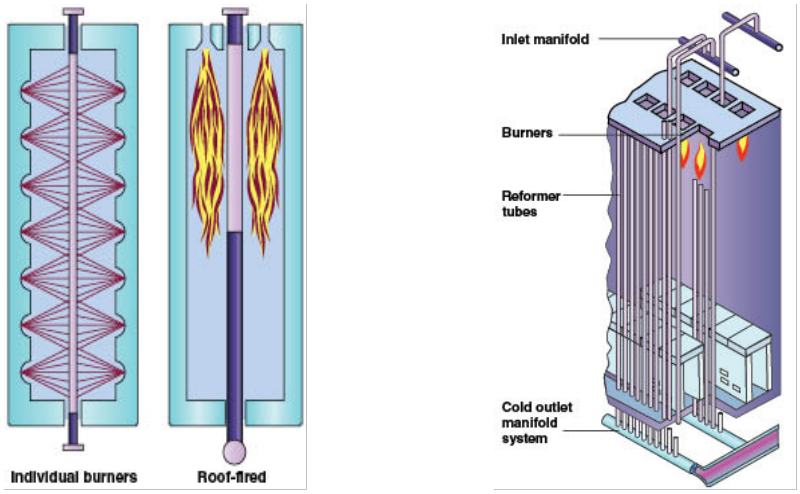

Figure 5: Reformer Design [7]

It is worth noting that burnerns can be both individual horizontal or vertical roof-fired ones, depending on the reactor design.
The hot fluegas exiting the reformer is sent to a heat exchanger to preheat the reacting

mixture itself, and then enters two WGS reactors that operate at different temperature levels (usually around 450 °C and 200 °C [6]), in order to maximize thermal recovery.
After that, a CO_2 capture system is usually present: it can be achieved through a chemical or physical washing technology, as well as through the use of pressure sensitive adsorbent mediums.
Hydrogen is then separated by the fluegas by means of a Pressure Swing Adsorption (PSA) process. In the traditional SMR process, H_2 purity after CO_2 separation reaches values of around 94% on dry basis [6]; nevertheless, common hydrogen applications, such as fuel cells, usually have very strict requirements on fuel purity (>99,995 %). In order to reach such values, PSA technology is used. In its simplest form, it basically consists in two colums filled with a selective solid adsorbent , that is able to bind to the desired gas at higher pressure and then release it when pressure decreases [8]. The reference cycle is the Skarstrom one [8], that can be represented in figure 6:

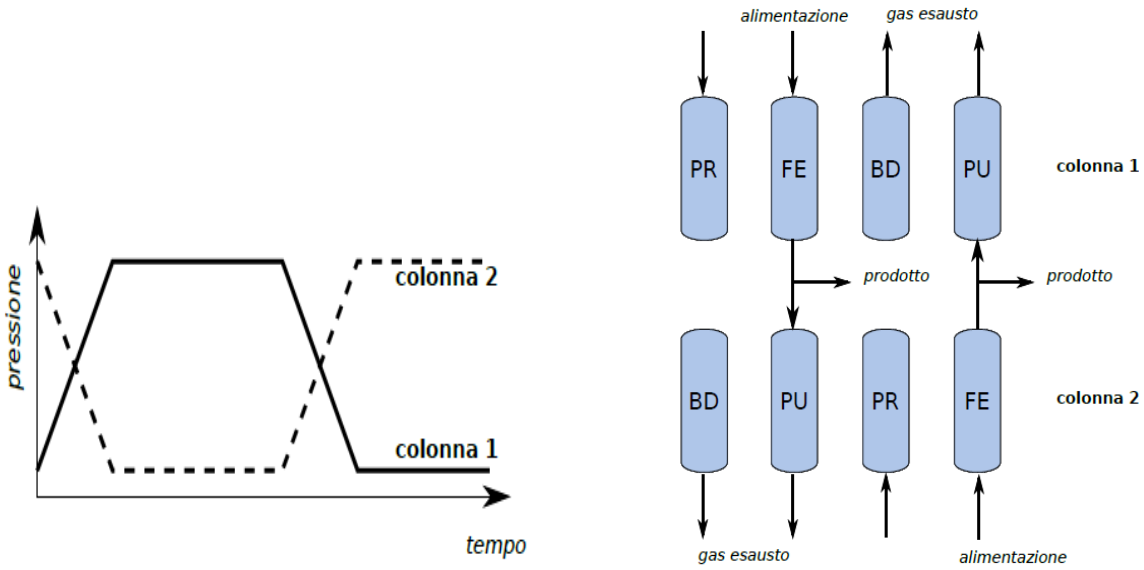

Figure 6: Skarstrom PSA cycle [8]

The cycle can be summed up into 4 phases:

1. **Pressurization (PR)**, where the column is pressurized;
2. **Adsorption (FE)**, where the gas to be treated enters the column and then the desired fluegas, enriched by the light component to be separated, exits the column;
3. **Blow-Down (BD)**, where the column is depressurized;
4. **Purge (PU)**, where the heavy component is separated and the adsorbption medium is regenerated.

The cycle is usually implemented with two different columns, that operate out of phase each other.
Finally, the tail gas obtained at the end of PSA is CH_4 rich, and thus it is sent, together with air and eventually part of the produced hydrogen, to the reformer furnace in order to generate the heat necesary to supply the SMR reaction.
Traditional SMR is able to reach high methane conversion and hydrogen yield, both of the order of 80 % [6]. Nevertheless, the main problems of traditional SMR remains its energy-intensity (around 100 $\frac{MJ_{th}}{kmol_{H2}}$) and CO_2 emissions [6]; this stokes the need for a new technology, able to overcome these issues.

2.1.2 Autothermal Reforming

An alternative to SMR is represented by Autothermal Reforming (ATR), where part of methane inserred into the reactor is combusted in order to thermally couple SMR with its heat supply process. A schematic of the process is shown in figure 7:

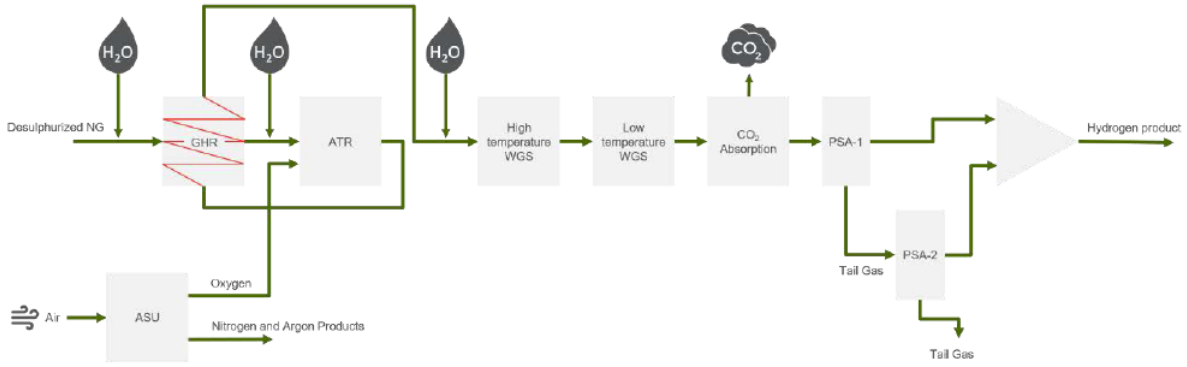

Figure 7: Autothermal Reforming process [2]

If the final part of the plant has the same structure as SMR (WGS, CCS system and PSA), the big difference relies on the type of reactor. As a matter of fact, oxygen is directly inserred into the reformer tubes, where lots of reaction, besides (4), (5) and (6) can happen [9]:

$$Methane\ \ Combustion: \qquad CH_4 + 2O_2 \rightarrow 2H_2O + CO_2 \qquad \Delta\bar{h} = -802\frac{kJ}{mol} \tag{7}$$

$$Partial\ \ Oxidation: \qquad CH_4 + \frac{1}{2}O_2 \rightarrow 2H_2 + CO \qquad \Delta\bar{h} = -36\frac{kJ}{mol} \tag{8}$$

$$Partial\ \ Combustion: \qquad CH_4 + O_2 \rightarrow 2H_2 + CO_2 \qquad \Delta\bar{h} = -71\frac{kJ}{mol} \tag{9}$$

$$Dry\ \ Reforming: \qquad CH_4 + CO_2 \rightarrow 2H_2 + 2CO \qquad \Delta\bar{h} = 247\frac{kJ}{mol} \tag{10}$$

$$Boudouard\ \ Reaction: \qquad 2CO \rightarrow C + CO_2 \qquad \Delta\bar{h} = -172\frac{kJ}{mol} \tag{11}$$

$$Methane\ \ Decomposition: \qquad CH_4 \rightarrow 2H_2 + C \qquad \Delta\bar{h} = 75\frac{kJ}{mol} \tag{12}$$

However, reactions (4), (5), (6) and (7) are known to be predominant in the process, that can be reduced to taking into account only those reactions [10]. The catalysts that can be used are mostly Ni-based one due to their lower cost, supported by $\gamma - Al_2O_3$ that gives higher mechanical stability [9], but in some applications also ZnO can become a valid alternative [11].
As far as reactor working, state of the art technologies are usually composed by a combustion chamber with a burner, and a catalytic section. But doing this way has a disadvantage related to the combustion reaction, that is so fast to be completed in a small portion of the reactor volume, releasing tempestively all the heat that may cause undesired temperature peaks [9]. The solution can be to separate the endothermic and exothermic processes in time, so that the reactor bed is heated by the combustion reaction and gradually releases heat for the SMR reaction that happens in a subsequent moment [9].
Another key aspect is oxygen distribution along the reactor. In order to supply the correct

quantity of heat to the SMR reaction, the use of a packed bed inert membrane reactor (PBIMR) can become the optimal solution [12]: the membrane selectivity can be chosen to provide only the right quantity of oxygen and prevent its accumulation, that can lead to hot spots formation and increase the safety of the process. Moreover, to maximize the performances of the system, a mixed membrane reactor (MMR) can be proposed, that enables high homogeneity of oxygen distribution by alternating permeable and impermeable layers in the tubes. Figure 8 shows the differences in the two configurations [12]:

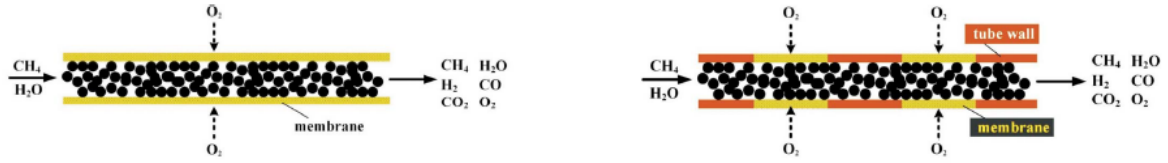

Figure 8: Membrane Reactor and Mixed Membrane Reactor [12]

In conclusion, several configurations can be adopted for ATR technology. Depending on which of them is chosen, operating parameters can be various: temperatures are maintained quite controlled and range from 570 to 650 °C, while reactors can be atmosferic or pressurized up to 28 bar [9] [11] [12]. Hydrogen yield is reported to be not so high (50-60 %), while methane conversion is very good, reaching also values near 100 % [9] [11] [12]. However, the system is not particularly complex in terms of equipment, and it can be scaled up to medium-high sizes.
The main disadvantage of ATR remains the necessity of an Air Separation Unit (ASU) for the production of the oxygen to be fed to the reactor. The ASU is a very energy-intensive component, and its electrical consumption may vanish the benefits obtained in terms of CO_2 emissions and heat to be supplied to the whole plant.

2.1.3 H_2 Membrane Reactor Reforming

Following the idea of oxygen semi-permeable membranes inside the reformer, another kind of reactor design is thought by using a different membrane which is H_2 permeable. By H_2 in-situ separation, with this kind of technology all the end-of-pipe hydrogen purification systems become useless and can be erased [13]. Moreover, since the concentration of products is reduced by the continuos removing of H_2, the reaction is more favoured because thermodynamic equilibrium is shifted towards the products, according to Le Chatelier's principle [14]. In other words, if an **affinity function y** is defined in such way:

$$y = -\sum_{i=1}^{N+M} \nu_i \mu_i(T, p_i) = \sum_{i=1}^{N} \nu_i \mu_i(T, p_i) - \sum_{i=N+1}^{N+M} \nu_i \mu_i(T, p_i) \tag{13}$$

where N and M are, respectively, the number of reactants and products present in the reaction, ν_i is the stioichiometric coefficient of the generic species i and $\mu_i(T, p_i)$ is the chemical potential of the generic species i (calculated at its temperature T and partial pressure p_i), the y function can be recognized to be equal to:

$$y = -\left(\frac{dG}{d\xi}\right)_{T,p} \tag{14}$$

where G is the Gibbs free energy of the reaction, that needs to me minimized to reach the equilibrium, ξ is the degree of advancement of the reaction, that increases if the reaction is moved towards the products and $_{T,p}$ subscript indicates that the exact differential is

calculated at constant temperature and pressure. At thermochemical equilibrium, y=0; if concentration of products is reduced through hydrogen separation, $\mu_{H_2}(T, p_{H_2})$ is reduced and consequently:

$$y = -\left(\frac{dG}{d\xi}\right)_{T,p} > 0 \implies \left(\frac{dG}{d\xi}\right)_{T,p} < 0 \tag{15}$$

Thus, to reach a lower value of G and reach a new equilibrium, ξ need to be increased, shifting the reaction towards the products.
Turning back to the technology, the reactor design can be outlined as in figure 9 [15].

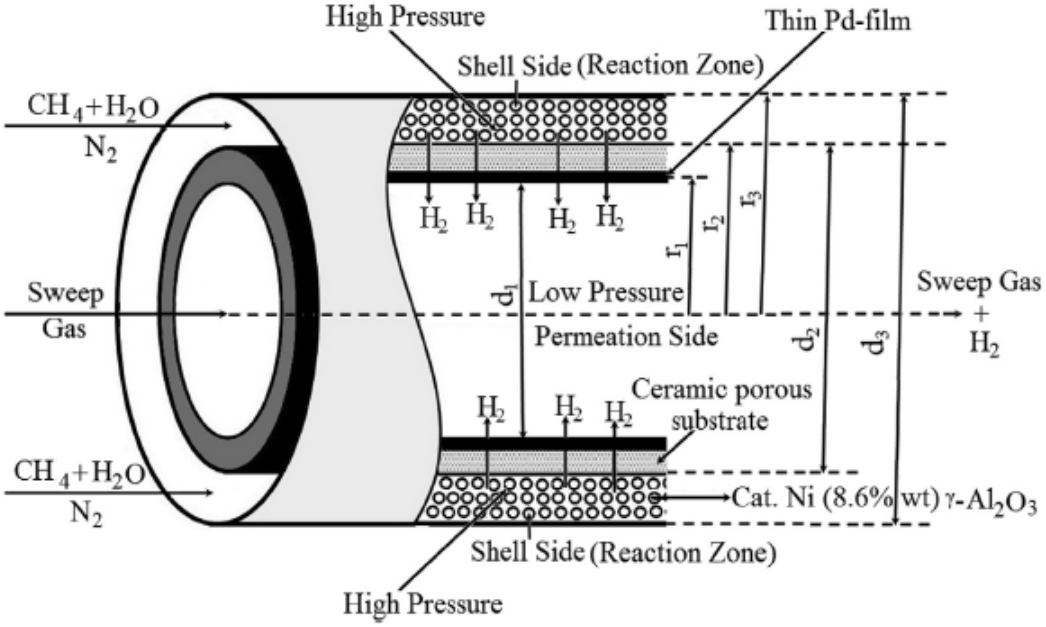

Figure 9: H_2 membrane reactor scheme [15]

As it can be seen, the component is formed by two concentric tubes. The external one is made of steel and is filled by a Ni-based catalyst and a continuous flowrate of reacting mixture (CH_4 and H_2O) passes through it; the internal one is instead represented by the membrane made of Palladium (Pd), through which the hydrogen generated by the SMR reaction permeates. Inside the internal tube, a slight pressure reduction is imposed in order to allow hydrogen to easily migrate from the outer layer, together with the use of a sweep inert gas that facilitates its removing [15].
In terms of operating parameters, this kind of reactor is usually pressurized (from 4.5 bar up to 20 bar) since hydrogen needs a driving force to permeate, and temperature is maintained quite low (550-600 °C) [13] [15] [16]. Good hydrogen yield (around 62,5%) and methane conversion (> 75%) can be achieved, and Ni-based catalysts can be substituted in some cases by Rubidium (Ru) ones [13] [15] [16]. Even if the complexity is not so high and both experimental and modelling studies were conducted to investigate the caractheristics of this technology, it was supposed not to be suitable for large scale applications at present. Some disadvantages of this kind of reactor rely on the attrition and catalyst entrainment that can be present due to the continuos and multidirectional flowrate of reactants and products, as well as the ingent heat fluxes and the erosion from the catalyst bed to be substained by the membrane; but the most important one is the fact that hydrogen is produced at lower pressure, and so it could need to be further compressed to be properly used for its various applications.

2.1.4 Chemical Looping Combustion coupled reactor Reforming

Among the novel technologies that can be proposed as alternatives to traditional SMR, chemical-looping based ones seem to be quite promising. In particular, an idea could be to keep the reformer reactor as it is but with heat supply given by a Chemical-Looping Combustion (CLC) system instead of a simple furnace. CLC allows the generation of ingent quantities of heat by trasnferring oxygen from air to the fuel through an oxygen carrier, that usually is a metal (Me) that can be easily found in its oxidized form (MeO). Conceptually, a CLC system is formed by two reactors, called **Fuel** and **Air** reactor, that respectively perform the reduction and oxidation of the oxygen carrier, generating heat. A scheme of the process is represented in figure 10 [17]:

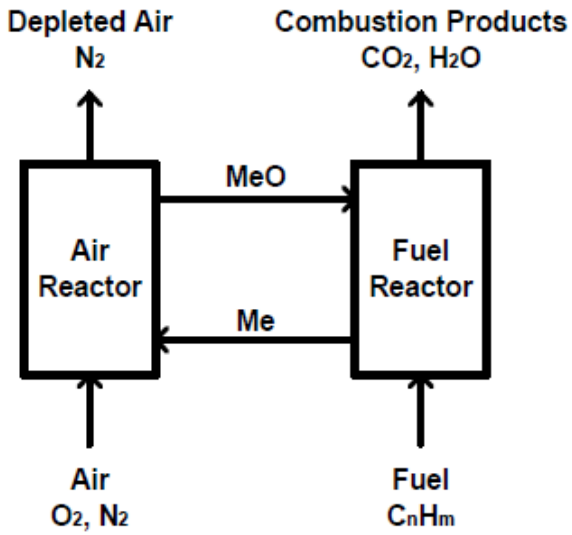

Figure 10: Chemical Looping Combustion system [17]

The generic reactions that occur during the process are the following:

$$Air \quad Reactor: \qquad O_2 + 2Me \rightarrow 2MeO \tag{16}$$

$$Fuel \quad Reactor: \qquad C_nH_m + (2n + \frac{1}{2}m)MeO \rightarrow nCO_2 + \frac{1}{2}mH_2O + (2n + \frac{1}{2}m)Me \tag{17}$$

Considering CH_4 as fuel and NiO as oxygen carrier, reactions (16) and (17) become:

$$Air \quad Reactor: \qquad O_2 + 2Ni \rightarrow 2NiO \qquad \Delta\bar{h} = -938,2\frac{kJ}{mol} \tag{18}$$

$$Fuel \quad Reactor: \qquad CH_4 + 4NiO \rightarrow CO_2 + 2H_2O + 4Ni \qquad \Delta\bar{h} = 136,5\frac{kJ}{mol} \tag{19}$$

It is worth noting that, summing (18) and (19), the enthalpy of reaction is equal to that of (7), highlighting that CLC process delivers exactly the same quantity of heat of a simple combustion.
Usually, the benefits related to the use of CLC technologies rely on the possibility of separating CO_2 from the offgas through a simple condenser, since it is not diluted with N_2 but only with H_2O steam. Moreover, since regeneration of the oxygen carrier occurs without a flame and at quite low temperatures, the formation of pollutants like NO_x is minimized [17].
A scheme of the plant is shown in figure 11 [17]:

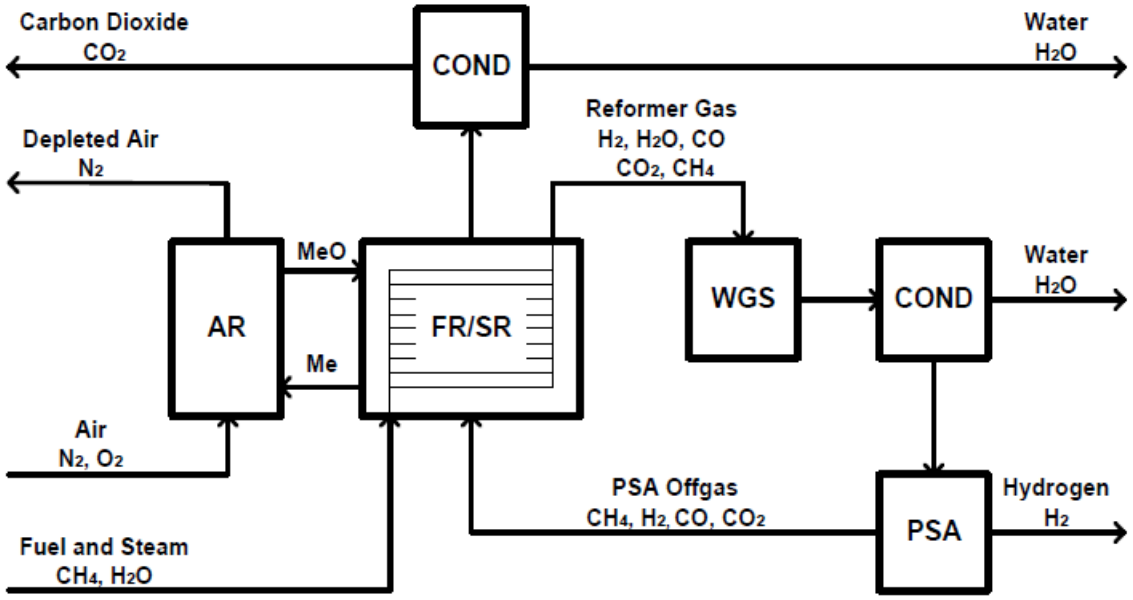

Figure 11: Chemical Looping Combustion SMR plant [17]

As can be easily seen, the process is very similar to traditional SMR; the only difference relies on the overall reactor design, that is composed by the two interconnected fluibed reactrs that deliver the necessary heat to the reforming one, that is composed by tubes as in the SMR plant. A focus on the reactor design can be observed in figure 12 [17].

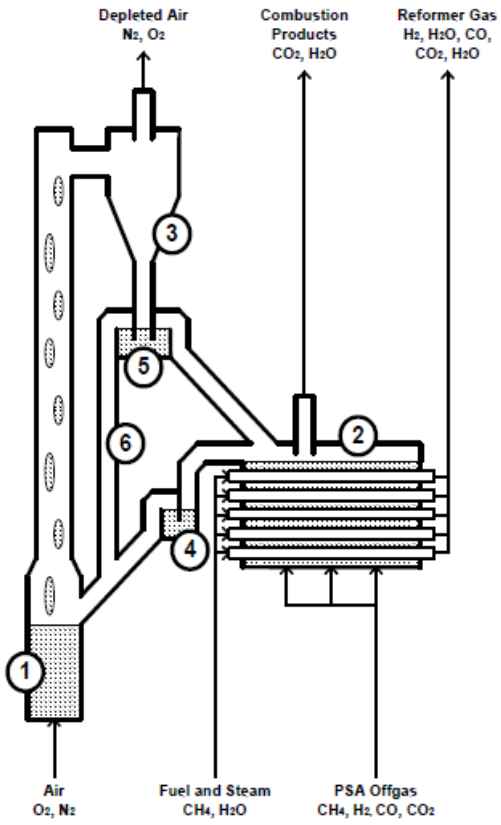

Figure 12: Chemical Looping Combustion coupled reactor [17]

The air reactor act as high-velocity fluidized one, that rises particles providing them

cinetic and thermal energy; those particles then enter the fuel reactor, that is a bubbling bed where lower velocities are reached and reformer tubes are placed, in order to receive the heat necessary for the SMR reaction.
From literature modelling data, this system is reported to have hydrogen yields of around 67%, with good methane conversion of over 76% [17]. The reformer reactor is pressurized (24,5 bar) and works at temperatures of around 800 °C, achieving a H_2 production of 1000 mol/s (242 MW of fuel) with a CH_4 input of around 300 MW [17]. Thus, the system size is medium, as well as the complexity of the system, that needs only additional studies in the chemical looping technology to become a completely proven one.

2.1.5 Chemical Looping Reforming

Another pathway of using Chemical Looping technology in this field is represented by Chemical Looping Reforming (CLR). It concerns the use of an oxygen carrier as oxidizing medium with the reacting mixture itself, not with an external fuel; in other words, the product of CLR is not heat to be supplied to SMR reaction, as it were for CLC, but is the H_2/CO mixture itself [18]. A schematic of the system is shown in figure 13 [19]:

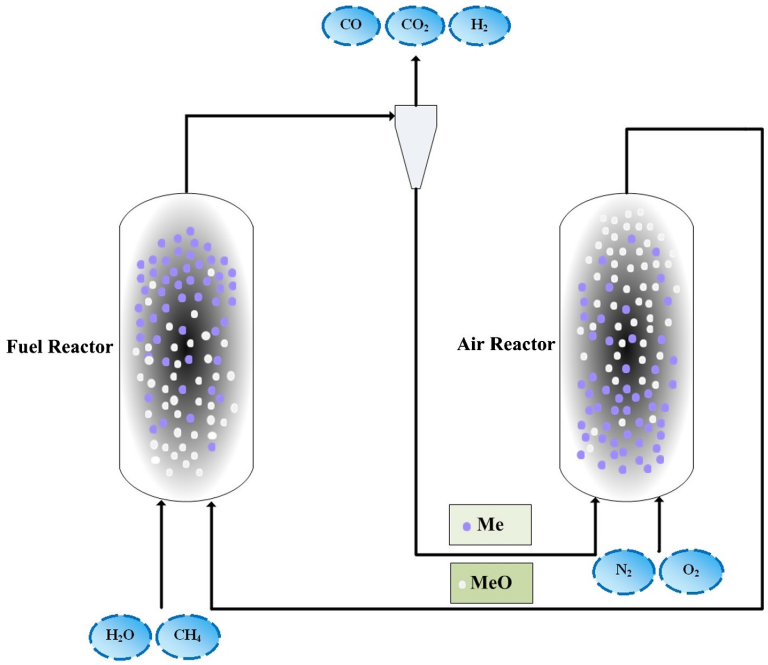

Figure 13: Chemical Looping Reforming scheme [19]

Oxidation and reduction of the oxygen carrier occur, respectively, in the air and fuel reactor according to the following reactions, if CH_4 is considered as fuel:

$$Air \quad Reactor: \qquad \frac{1}{2}O_2 + Me \rightarrow MeO \tag{20}$$

$$Fuel \quad Reactor: \qquad CH_4 + MeO \rightarrow CO + 2H_2 + Me \tag{21}$$

As can be easily seen, this kind of technology resembles ATR one, since H_2 production is obtained without providing heat from external sources. The main advantage of this system with respect to ATR one is that air can be used directly as oxidizing agent for the oxygen carrier, but N_2 is not present in the product gases since only the oxygen carrier is circulated from one reactor to another. In this way, no ASU and its ingent electrical feeding are necessary to make this system work, representing a great saving in terms of money and energy-input [19].

From experimental results, Ni-based oxigen-carriers appeared to be the right choice to carry on the reactions, since they show high catalytic properties and selectivity for H_2 generation [18]. CLR fuel reactors operate at around 700 °C and atmosferic pressure, reaching high H_2 purity, H_2 yield up to 85% and optimal methane conversion (99,7%) [19]. Finally, thanks to the benefits given by the low CO_2 emissions and costs associated to this technology, CLR is thought to be one of the potential alternative for large-scale H_2 production methods for the future.

2.1.6 Sorption Enhanced Steam Methane Reforming

It was seen that H_2 production usually requires three main steps to be accomplished: SMR reaction, WGS reaction and H_2 separation from the products. A fancy idea could be to try to restrict these processes in one single reactor, that can be achieved through the Sorption Enhanced Steam Methane Reforming (SE-SMR) technology. The process basically consists in the introduction of a selective CO_2 sorbent in the reformer, that can promote its remotion by fixation in another compound. Usually, the sorbent is constituted by CaO, that reacts with CO_2 according to the following carbonation reaction [20]:

$$CaO + CO_2 \rightarrow CaCO_3 \qquad \Delta\bar{h} = -178,8\frac{kJ}{mol} \tag{22}$$

where $\Delta\bar{h}$ is calculated at ambient temperature of 25 °C. Moreover, reaction (22) tends to decrease the moles of CO_2 present in the products, favouring the H_2 production from total reforming (6) according to Le Chatelier's principle [21].
A schematic of the system is shown in figure 14 [21]:

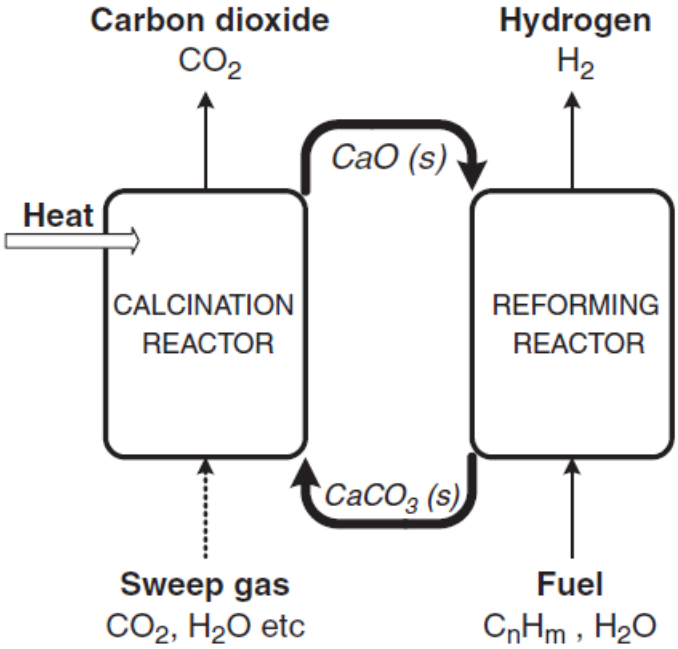

Figure 14: Sorption Enhanced Steam Methane Reforming scheme [21]

The plant design is very simple. Two reactor vessels are installed: one is used to perform the reforming reactions and the CO_2 fixation, whereas in the other calcination reaction (i.e. reverse carbonation reaction) takes place in order to regenerate the sorbent. Usually, a sweep gas is used in the calcination reactor in order to facilitate the removing of CO_2. The main disadvantage of this configuration is that calcination requires large amounts

of heat to be performed, that are obtained by CH_4 combustion, that produces CO_2 too [20]. Despite that, the overall process results to be less energy-intensive than traditional SMR $\left(62{,}1\ \frac{MJ_{th}}{kmol}\ \text{against}\ 100{,}7\ \frac{MJ_{th}}{kmol}\right)$, and allows to work at lower temperatures in the atmosferic reactor (around 650 °C), that in any case needs another calcination stage at 850 °C to properly work [6]. Very good hydrogen yield (90,9 %), H_2 purity (97-98 %) and methane conversion (92 %) can be achieved through this system, that despite great investigation and its possible application on large-scale has been remaining in state of research for ages [6] [20] [22].

2.1.7 Sorption Enhanced Chemical Looping Steam Methane Reforming

In a more complete vision, sorption enhanced and chemical looping technology can be combined to form a new innovative concept: Sorption Enhanced Chemical Looping Steam Methane Reforming (SE-CL-SMR). A schematic of the process is represented in figure 15 [21]:

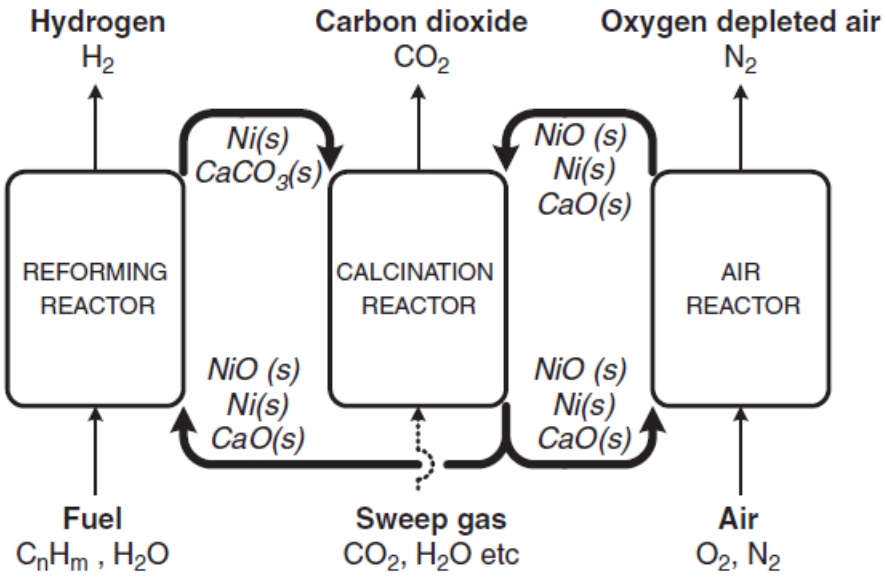

Figure 15: Sorption Enhanced Chemical Looping Steam Methane Reforming scheme [21]

The process is expected to be developed in three different reactors, namely:

1. **Reforming reactor**, where reactions between the oxygen carrier (in this case, NiO) and fuel-steam reacting mixtures are carried on. The reactions are, besides (19), the following:

$$CH_4 + NiO \rightarrow CO + 2H_2 + Ni \qquad \Delta\bar{h} = 203\frac{kJ}{mol} \tag{23}$$

$$CO + NiO \rightarrow CO_2 + Ni \qquad \Delta\bar{h} = -43\frac{kJ}{mol} \tag{24}$$

$$H_2 + NiO \rightarrow H_2O + Ni \qquad \Delta\bar{h} = -2\frac{kJ}{mol} \tag{25}$$

   The reactor operates at quite low temperature and in endothermicity, and contemporarely the carbonation reaction (22) occurs to fix the CO_2.

2. **Calcination reactor**, where calcination indeed is performed and released CO_2 is eliminated by means of a sweep gas. Operating temperature is intermediate, and the calcination reaction is endothermic too.

3. **Air reactor**, where the oxygen carrier is oxidized in presence of air by means of the following reactions, besides (18):

$$Ni + CO_2 \rightarrow NiO + CO \qquad \Delta\bar{h} = 43\frac{kJ}{mol} \tag{26}$$

$$Ni + H_2O \rightarrow NiO + H_2 \qquad \Delta\bar{h} = 48\frac{kJ}{mol} \tag{27}$$

   The overall reaction is exothermic and temperatures are quite high.

The idea is to make CO_2 adsorption happen in order to preserve the environment, but avoiding to provide heat from external source. If well designed, indeed, the oxidation reaction of Ni is able to provide all the heat necessary to regenerate the sorbent, that would lead to the creation of a self-sufficient system [21]. As a matter of fact, this plant would require the lower amount of thermal energy from outside $\left(45{,}8\ \frac{MJ_{th}}{kmol} \right)$ if compared to traditional SMR or SE-SMR, with reformer operating at atmospheric pressure and around 650 °C [6].
H_2 yield and purity are both satisfactory (83% and 94,7%), while methane conversion reach very good values around 97%, making this system to become a possible competitor for large-scale blue hydrogen production in the future [6] [20].

2.1.8 Intensified Energetically Enhanced Steam Methane Reforming

Actual research about design improvement of reforming system is focusing more and more on the reduction of energy input to the proper working of the plant. In this perspective, Intensified Energetically Enhanced Steam Methane Reforming (IEER) has been recently modelled and studied in University of California, in order to achieve spefific thermal demands of the order of $20\frac{MJ_{th}}{kmol}$ [23].
The idea is to go ahead an Energetically Enhanced Process (EEP), that by definition is "a process whose energy consumption at high temperature, in comparison to its traditional counterpart, is either reduced or eliminated, even if such reduction necessitates higher energy consumption at lower temperatures" [24], by introducing H_2 separation membranes in SMR and WGS reactors that can increase yields of reactions. In particular, EEP in reforming can be reached by CO recycling into the reformer, that makes WGS exothermic reaction happen more, decreasing the high temperature heat to be delivered.
The overall process is composed by a co-current membrane integrated WGS (WGS-MR), coupled with another countercurrent WGS-MR and a SMR-MR. The reactor, that operates at low temperatures (600 °C) but very high pressures (40 bar), would achieve not so high methane conversions (34,7 %) since the focus is to reduce thermal demand [23]. Nevertheless, this system is still at research level by modelling analysis, without actual implications in large-scale industry nor experimental testing.

2.1.9 Final Review

After analyzing all these technologies, main interest parameters are reported in table 1. It is worth noting that, in some cases, lack of literature data did not make possible to know some parameters, that would require precise modelling of each system to be estimated.

	T_{Ref} [°C]	P_{Ref} [atm]	CH_4 Conv. [%]	H_2 yi. [%]	H_2 pur. [%]	Th. Dem. $\left[\frac{MJ_{th}}{kmol}\right]$	Cat.	Compl.	Size	Study
SMR	850	25	80	79,4	93,8	100,7	Ni	Low	Large	Mod.
ATR	600-650	1-28	75-100	50-65	/	/	Ni or Zn	Low	Med.	Both
MR	550-600	4,5-20	75-82	62,5	97,7	/	Ni or Ru	Med.	Large	Both
CLC	800	24,5	76,5	67	82	/	Ni	Med.	Med.	Mod.
CLR	700	1	99,7	85	/	/	Ni	Med.	Med.	Sp.
SE-SMR	650	1	92	90,9	97-98	62,1	/	Med.	Large	Mod.
SE-CL-SMR	650	1	97	83	94,7	45,8	Ni	High	Large	Mod.
IEER	600	40	34,7	/	99,8	19,9	/	High	Small	Mod.

Table 1: Final Review, H_2 production methods parameters

2.2 CO_2 Capture

As extensively reminded during this work, CO_2 capture is an essential issue to be considered when designing an H_2 production plant. Since SMR facilities emit CO_2 in steady state conditions and well known technologies can be implemented for its capture and sequestration, they have received continuous attention in this field. Moreover, since usually flow streams are pressurized, CO_2 capture can be more cheap and efficient. Finally, being usually SMR plants near other industrial ones with a lot of waste heat, it can become attractive to re-use it inside the CCS process [25].
The technological overview, in this section, is related to two major aspects:

1. Type of **additional technology** requested, unless the plant design allows intrinsic CO_2 removal (as in case of CLC or SE-SMR, for example);
2. **Location** in the plant where this system is inserred.

As in the previous section, various parameters have been identified in order to make clearer comparisons.
As far as the technologies are concerned, the parameters are [25] [26] [30] [31]:

- CO_2 **capture efficiency** [%], defined as the ratio of the CO_2 captured over the CO_2 entering the system;
- CO_2 **purity** [%], defined as the ratio of the flowrate of CO_2 captured over the total flowrate of the stream where it is present;
- **Thermal energy** $\left[\frac{MJ_{th}}{kg_{CO_2}} \right]$ required for CCS process;
- **Electrical energy** $\left[\frac{MJ_{el}}{kg_{CO_2}} \right]$ required for CCS process;
- **Energy Penalty**, that can be expressed in various units of measure and represents the extra energy required to make CCS happen, with respect to the traditional process without CCS;
- Operative **costs** $\left[\frac{€}{ton_{CO_2}} \right]$ for CCS;
- **Complexity** of the system, evaluated on the basis of equipment and external resources needed.

On the other hand, the parameters individuated for better understand pros and cons of different locations are the following [32] [33]:

- CO_2 **mass ratio** [%], defined as the ratio of CO_2 present in the stream to be treated over the total CO_2 generated in the process;
- CO_2 **concentration** [%], defined as the molar fraction of CO_2 present in the stream to be treated;
- **Total pressure** [bar] of the stream to be treated;
- CO_2 **partial pressure** [bar] in the stream to be treated;
- N_{cc}, defined as product of CO_2 mass ratio, concentration and partial pressure in the stream to be treated;

- N_{cc} **after optimal** O_2 **enrichment**, that consists in the same parameter as before, calculated at the value of O_2 entering the furnace that represents the best compromise between the base case (21 % O_2 in the comburent mixture) and the ideal one (100 % O_2).
- Operative **costs** $\left[\frac{€}{ton_{CO_2}} \right]$ for CCS.

In this work, only two main kinds of technologies are analzyed, even if in literature other examples can be found. The possible locations, instead, are only three and each one is considered in the analysis.

2.2.1 Gas absorption through MEA

The traditional way of capturing a gas for its sequestration is to fix it into a chemical or phisical solvent, and then release it by means of temperature or pressure changes. Chemical solvents have better absorption properties when working at low partial pressures of the gas that needs to be absorbed; for this reason, absorption through organic chemical solvents as Mono-EthanolAmine (MEA), whose chemical formula is $NH_2CH_2CH_2OH$ (C_2H_7NO). MEA are a good choice for their ability to react with CO_2 at low pressure and concentration, but also for their commercial readiness on the market [34].
The basic scheme of an absorption process is shown in figure 16 [35]:

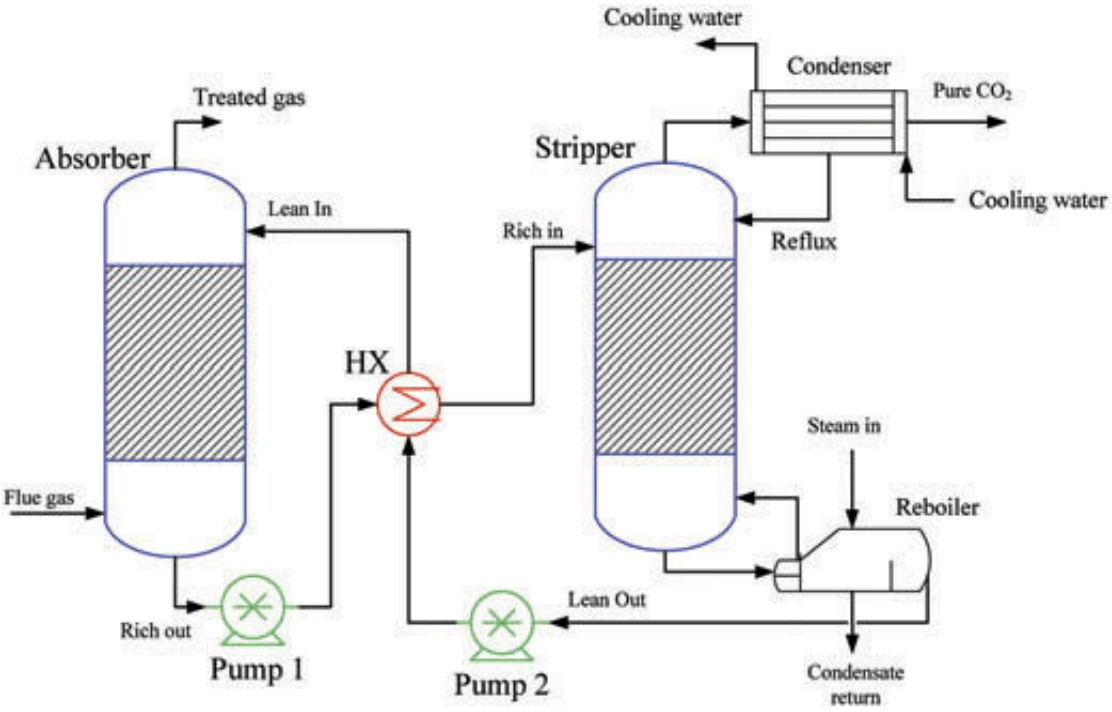

Figure 16: MEA absorption scheme [35]

The system basically consists in an **absorber**, that is a column where the flue gas is put in contact with the lean solvent, and a **stripper**, another column where the solvent is regenerated by heat supply and CO_2 is separated by it [26]. Auxiliaries that complete the Balance of Plant (BOP) are, respectively:

- A **heat exchanger** (HX) that is used to re-use the low-temperature heat of the lean regenerated solvent to heat up the rich one exiting the absorber;

- Two **pumps** that are used to give small pressure increases to win pressure drops and make the system work at proper operating conditions;
- A **reboiler** at the bottom of the stripper that, by the use of hot steam or fuel for combustion, provides the heat necessary to regenerate the lean solvent starting from CO_2 rich one;
- A **condenser** at the top of the stripper that, by the use of cooling water from outside, is able to separate part of the H_2O vapour present in the flue gas exiting the stripper, recirculating it into the stripper.

As far as pressure is concerned, experimental studies found out that 2 bar seems to be a reasonable value [27]. As a matter of fact, if increasing pressure of the rich solvent decreases both electrical energy in input for CO_2 compression after its caputre (since compressing a liquid is much less energy-intesive with respect to a gas) and reboiler duty for CO_2 stripping, on the other hand it implies an increase lean regenerated solvent temperature, that may lead to its degradation [27]. Here is reported the trend of reboiler duty and solvent temperature as pressure varies [28] :

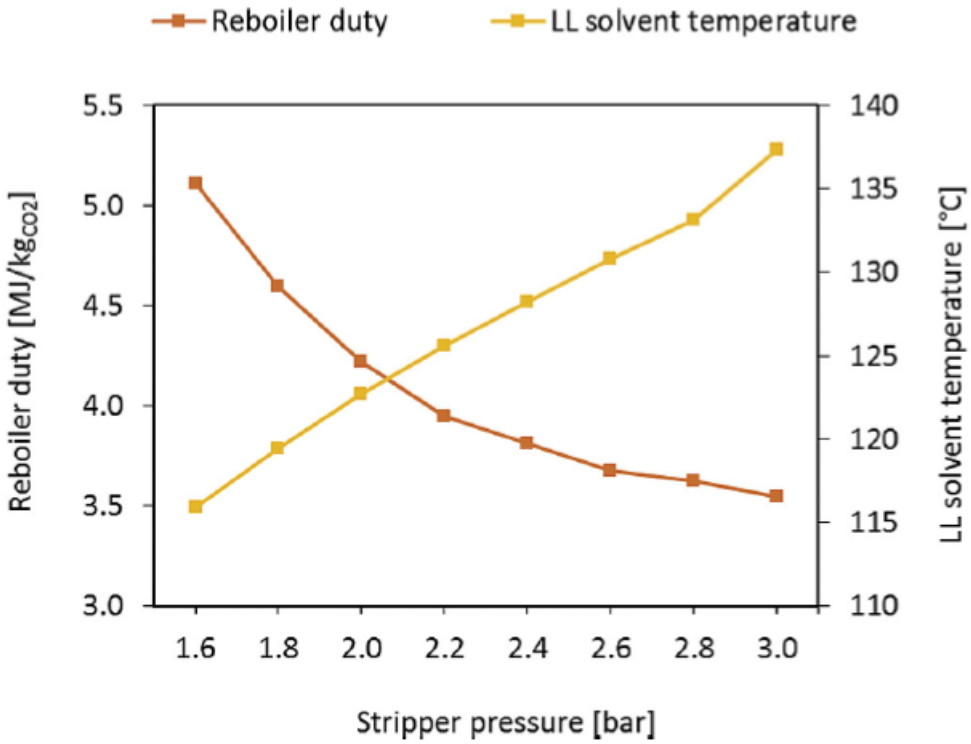

Figure 17: Influence of Stripper pressure [28]

This system, that is usually set just before PSA, allows to reach high CO_2 purity and very high capture efficiencies (about 95 %) [25]. Moreover, thermal requirements are on the order of 3,2-5,5 $\frac{MJ_{th}}{kg_{CO_2}}$, while electric input power that is used mainly for CO_2 compression are estimated to be around 0,4 $\frac{MJ_{el}}{kg_{CO_2}}$ [25] [26]. Nevertheless, costs for this additional technologies are not-neglibigle and accounts for about 35 $\frac{€}{ton_{CO_2}}$, while energy penalty results to be of the order of 100 $\frac{MJ}{MJ_{H_2}}$ [25].

2.2.2 Vacuum Swing Adsorption

The other pathway that can lead to CCS is to play with selective solvents that can release the compound they adsorb by pressure changes, and not temperature ones as in the case of MEA-based systems. An option is represented by Vacuum Swing Adsorption (VSA), that basically consists in the same multi-column system of PSA, with the difference that in this case pressure is reduced starting from atmospheric one, and not increased.
This technology has been implemented for the firs times in the Port Arthur refinery, where H_2 was intensively produced by means of SMR, aiming at the achievement of high CO_2 purity and low energy input standards [29].
The basic design of the process is represented in figure 18 [29]:

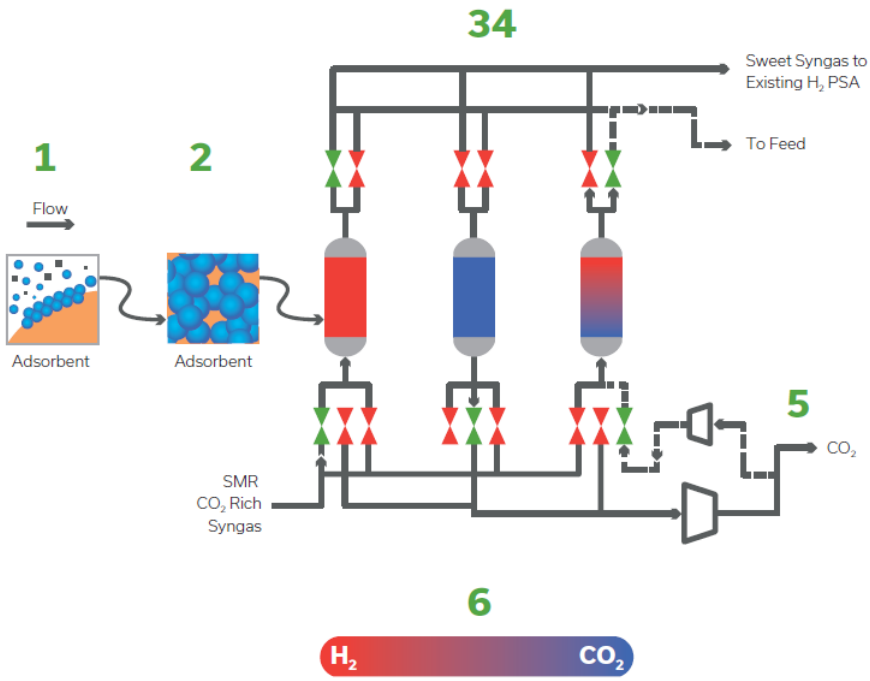

Figure 18: VSA process scheme [29]

The working principle is the same of PSA: it exploits different pressure levels to make adsorption and desorption of CO_2 happen. In particular, different steps can regognized as follows [29]:

- **1-2**: selective pressurized CO_2 adsorbents are inserred into VSA vessels, occupying great areas;
- **3**: the flue gas at around 25-27 bar is sent into one vessel for CO_2 adsorption, with other parallel vessels at various pressure levels for solvent regeneration;
- **4**: the H_2 rich offgas is sent to PSA for separation, reaching H_2 purities of over 99,99 %;
- **5**: the vessel then undergoes different pressure reduction steps in order to desorb the CO_2, that is finally evacuated by means of an under-atmospheric separation step;
- **6**: offgas recirculation from one vessel to another at higher pressure can be done in order to improve CO_2 removal efficiency.

With this system, very high CO_2 purity and capture efficiency can be achieved (both around 93-94 %), but it requires from 0,52 to 0,87 $\frac{MJ_{el}}{kg_{CO_2}}$ to work, resulting in an energy penalty of 12-20 % of the total energy required by the H_2 production process [30] [31]. General CO_2 abatement costs for this technology range from 18 to 32 $\frac{€}{ton_{CO_2}}$ [31].
The performance indicators of this technology, compared with MEA's, can be found in Appendix B.

2.2.3 CCS Locations

In all those processes that are not able to intrinsically remove CO_2, three different points of the plant are identified as possible locations for installing CCS systems, as shown in figure 19 [33].

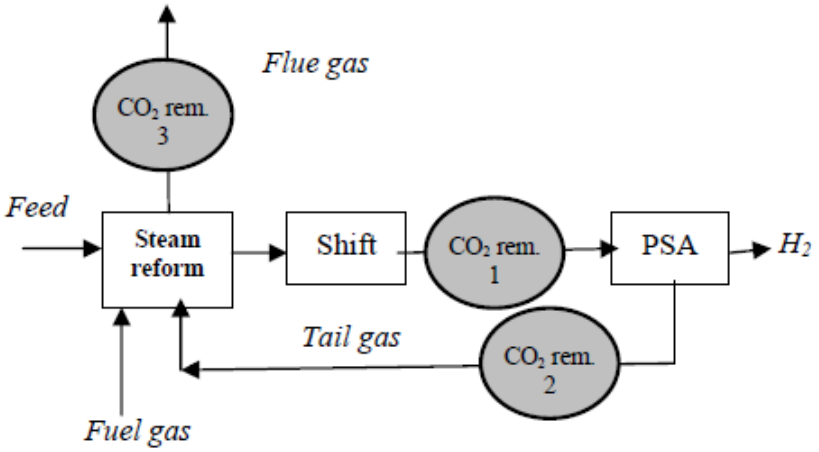

Figure 19: 3 locations for CCS [33]

As can be easily seen, the 3 locations potentially identified are:

1. **Pre-PSA** shifted syngas;
2. **Post-PSA** tail gas;
3. **End-of-Pipe** after reformer furnace flue gas.

Each location has different characteristics in terms of pressure and CO_2 concentration. In particular, pressure is atmospheric at location 2 and 3, while it is about 15-20 bar at location 1; on the other and, only location 2 is characterized by high CO_2 concentrations (about 50%), due to the fact that H_2 has just been removed, while other locations have lower CO_2 concentrations (around 18%) [32]. The major advantage of putting the CO_2 removal equipment at the very end of the process is that the totality of the CO_2 produced during SMR is present there, while locations 1 and 2 have a significant part missing (up to 27% of the total), that is the one associated to the fuel combustion in the reformer furnace [32]. All the parameters of interests are resumed in Appendix C [32] [33].
In order to take into account contemporarily the effect of CO_2 partial pressure, concentration and mass ratio, a suitable index, called CO_2 capture number (N_{cc}), has been defined as follows [32]:

$$N_{cc} = I_{pressure} \cdot I_{concentration} \cdot I_{mass} \tag{28}$$

where $I_{pressure}$ is the CO_2 partial pressure (in bar), $I_{concentration}$ is the CO_2 concentration in the stream and finally I_{mass} is the CO_2 mass ratio over the total produced. Calculated values of N_{cc} for the 3 locations are reported in Appendix C [32], showing that location 1 seems to be the best option to host such an abatement system: this because higher partial pressure is a very strong plus to have, since CO_2 needs to be compressed again for storage purposes, resulting in lower energy consumptions. On the other hand, location 3 seems to be quite inefficient, due to its low CO_2 concentration and pressure. Location 3 could become of relevant importance only when the decarbonization scenario will be significantly developed: as a matter of fact, an increase in compression energy, if provided by renewables, would not lead to additional CO_2 emissions by fuel combustion to produce that power. In this phase, trying to capture almost all the CO_2 produced by the SMR process could become interesting from an environmental point of view, towards the achievement of "net-zero" emissions.
Moreover, oxygen enrichment in reformer furnace is an issue to be carefully considered. Finding the best O_2 enrichment has two major benefits [32]:

- Parassitic N_2 concentration in the offgas is reduced, increasing the quantity of heat that can be exploited by the SMR process;
- Flame temperature and gas emissivities in the furnace are increased, resulting in overall better heat transfer conditions during SMR.

This clearly leads to better conversion rates and, consequently, fewer CH_4 input and CO_2 emissions at fixed H_2 production. The optimal O_2 enrichment has been evaluated and studied in literature [32], providing the variation in N_{cc} that is reported in Appendix C. Finally, abatement costs $\left[\frac{€}{ton_{CO_2}} \right]$ have been reported, showing that location 1 remains the 1st preference also from economic point of view: as a matter of fact, estimated costs for location 1 range from 31 to 36 $\frac{€}{ton_{CO_2}}$, while in location 3 for example they are between 43 and 52 $\frac{€}{ton_{CO_2}}$ [33].

	CO_2 capt. eff. [%]	CO_2 pur. [%]	Th. En. $\left[\frac{MJ_{th}}{kg_{CO_2}}\right]$	El. En $\left[\frac{MJ_{el}}{kg_{CO_2}}\right]$	En. Penalty	Op. Costs $\left[\frac{€}{ton_{CO_2}}\right]$	Compl.
MEA	95	High	3,2-5,5	0,4	101 $\frac{MJ}{GJ_{H_2}}$	35	Low
VSA	93,66	94,3	/	0,52-0,87	12-20% of power	18-32	Med.

Table 2: Final Review, CCS technologies parameters

	CO_2 mass ratio [%]	CO_2 conc. [%]	Tot. Pres. [bar]	CO_2 Par. Pres. [bar]	N_{cc}	N_{cc} O_2 enr.	Op. Costs $\left[\frac{€}{ton_{CO_2}}\right]$
Loc. 1	73	17,90	16,06	3,04	0,40	0,42	31-36
Loc. 2	73	51,49	1,03	0,53	0,20	0,21	/
Loc. 3	100	17,81	1,03	0,18	0,03	0,10	43-52

Table 3: Final Review, CCS locations parameters

2.3 Choice of modelled technologies

It is clear that SMR is the most used process to produce Hydrogen in the industrial panorama nowadays. This is a mature and well-known technology whose parameters have been investigated and optimized by lots of researches. But, after the clear picture about technological review provided by the previous sections, it is worth noting that a certain room for improvement is present for novel large-scale technologies. The upgradings mostly imply the redesign of the reactor in a synergic view, where more than one single effect is achieved in the component [36].
In particular, **Chemical Looping** technologies appear to be suitable for this implementation, provided that the oxygen carrier is selected in a wise way for which trasport capacity, reactivity and chemical stability are maximed as well as carbon deposition is minimized [18], so that it can be used for large-scale applications. The most performative oxygen carriers were recognized to be Ni-based ones [18], since it is also a very effective catalyst of the reforming reaction.
The most promising way to implement chemical looping seems to be **CLC**, where the oxygen carrier does not get in contact with the reactants but its oxidation provides only the necessary heat for reforming.
This technology has been modelled for medium-scale H2 production (1000 mol/s, corresponding to 242 MW of H_2 produced) [17], due to the substantial proof given from the last three decades studies that it will be reliable in industrial applications. Lots of demo CLC plant concepts have been analyzed, passing from a 10 to 1000 MWth CLC-based boilers [37]: studies expect a fully commercial development of 10 MWth ones from 2020 on. As stated in the previous sections, the main advantages of this technology are that the offgas is not mixed with N_2 and thermal NO_x are not produced since the flame is not present and temperatures are lower. Moreover, exergy efficiency will increase from 65.2 % of conventional SMR to 71,% of CLC-SMR [37]. By doing this way, only a condenser is needed to separate CO_2, making the process easier and cost-effective, even with the addition of another reactor in terms of capital costs. Levelized Cost Of Hydrogen for the two technologies is indeed estimated to be almost equal (around 3.28 $\frac{€}{kg}$ for conventional SMR and 3.24 $\frac{€}{kg}$ for CLC-SMR [37]), fact that shows CLC's opportunities of implementation also in economic terms.
In conclusion, since a comparison with SMR facilities could be relevant both in terms of operation and economic viability of the projects, in this work it was chosen to model both a traditional SMR plant with CCS and a CLC one, trying to highlight potentialitis and limits of each one.

3 Description of the models

After choosing the two kinds of technologies to be analyzed, a steady-state model for each of them was elaborated with the help of ASPEN plus software. Models of similar plants with the same software can be extensively found in literature [6] [38] [39] [40] [44]. A first description of the processes was presented, followed by a more detailed investigation on each single component in terms of inputs and constraints required.

3.1 Traditional SMR plant with MEA-based CCS

The first plant that was modelled resembles the traditional and well-established way of blue H_2 production through SMR, retrofitted with a MEA-based system for CCS. A schematic of the plant is shown in figure 20.
The plant layout can be subdivided in 3 parts, on the basis of their function.
In the H_2 **production** part, pure methane is compressed and mixed with steam obtained by pressurization and vaporization of water in ambient conditions. Steam is assumed, for simplicity, to be produced in a water boiler, fed by methane too. The reacting mixture is then preheated in a heat exchanger before entering the reformer, by means of the hot products of the SMR reaction themselves. In the reformer, great part of the entering CH_4 and H_2O react to form H_2 and CO at high temperature (800-850 °C), that are sent to preheat the reacting mixture. As described in the previous section, two WGS reactors at different temperature levels are installed in order to maximize heat recovery inside the plant. The same structure (preheater + reactor) is maintained in the two WGS stages, that operate at different temperature levels in order to increase the efficiency of the conversion and maximize heat recovery by providing it at different temperatures levels. At the end of the reactors, almost all CO is converted into a consistent quantity of CO_2, that needs to be properly managed and sequestrated. First of all, water present at the end of the reactions is eliminated through condensation, so that the H_2 and CO_2 rich stream is ready to be properly treated.
The second section is the CO_2 **capture** one, that basically consists in an absorber-stripper configuration. The H_2O free and pressurized offgas is sent to the bottom of the absorber, while a MEA-rich water solution is inserred from the top. When the streams get in contact, CO_2 is absorbed by being fixed in MEA liquid compounds, leaving the absorber from its bottom stage. Since MEA solution is sent at atmospheric pressure, the liquid CO_2 rich solution needs to be pressurized before entering the stripper; but thanks to the effect of pressurized gas, outlet temperauture results to be quite high, eliminating the need for a preheater. Once inside the stripper, in the bottom stage a reboiler fed by waste heat at quite low temperature performs the regeneration of the solvent solution, that is recirculated in the absorber after being cooled down. On the other hand, a H_2O and CO_2 mixture gets out from the top of the stripper: part of the H_2O is already removed by the condenser put at the first stage of the stripper, while the remaining one is eliminated in an external condenser. A high-purity CO_2 stream is then ready to leave the plant for its compression and storage, while removed water is recirculated to the beginning of the plant. Coming back to the absorber, the CO_2 poor stream is then sent to the PSA for H_2 separation, even if, in a global view, this last component has been aggregated to the H_2 separation part since thanks to it very pure H_2 can be obtained.
Finally, a **heat production** part for SMR reaction is present. It is composed by a condenser, where H_2O accumulated in the absorber is condensed and removed, and the furnace of the reformer, where tail gas, additional methane and air are inserred. in the end, an exhaust mainly composed of CO_2, H_2O and N_2 leaves the plant.

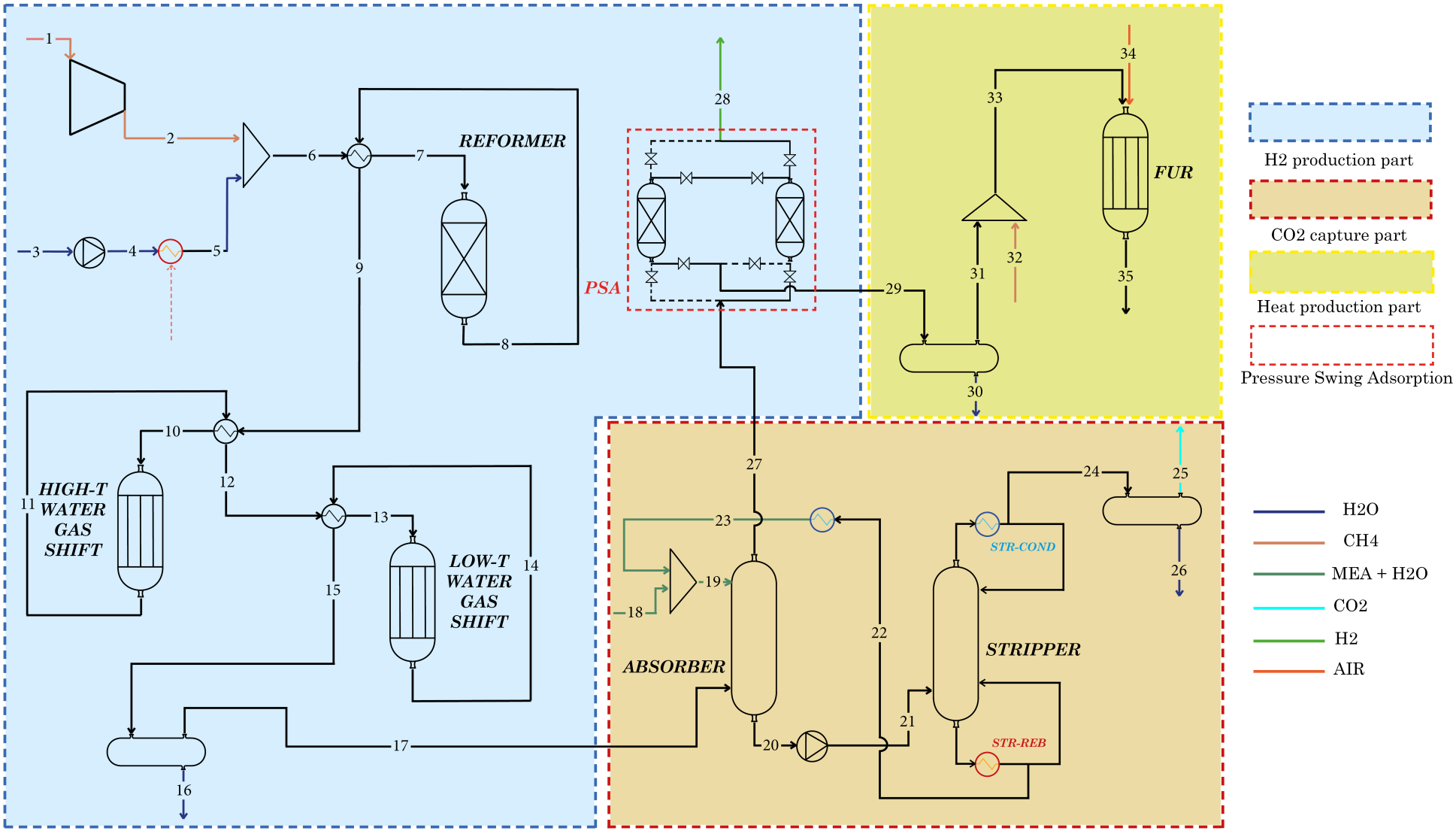

Figure 20: Traditional SMR with MEA-based CCS system plant

3.1.1 H_2 Production section

The first part that is analyzed more in depth is the H_2 production one, whose most relevant components are the reactors where SMR and WGS occur. The scheme, with details of components and streams, is shown in figure 21 .

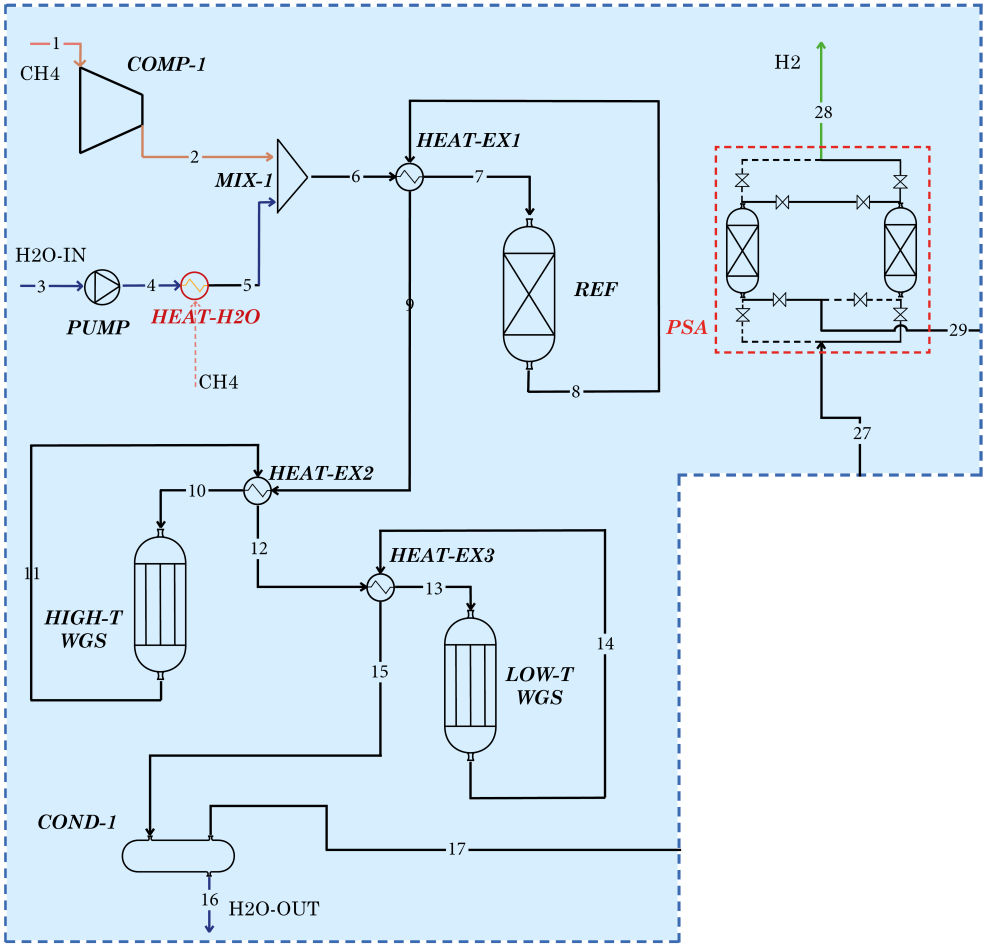

Figure 21: H_2 production section, Traditional plant

The external **inputs** are represented by pure CH_4 and H_2O at ambient conditions (T=25 °C and p=1 bar): their starting molar flow values are not so interesting, since they would be overwritten by other requirements.
As far as **components** are concerned, they can be summed up as follows:

- A compressor (**COMP-1**) that is used to pressurize methane up to 25 bar [6], with an isotropical efficiency of 0,85 [41], defined as follows [42]:

$$\eta_{ic} = \frac{W_{id}}{W_{re}} \tag{29}$$

  where W_{id} is the ideal work required to compress the gas, if the compression were isentropic, and W_{re} is the real work required by the process. It is an indicator of how much entropy is generated while pressurizing.

- A pump (**PUMP**), that is necessary to pressurize liquid water too, since liquid compression is much less energy consuming than vapor one. Water is thus pumped at 25 bar [6], with an isotropical efficiency of 0,85 too [41].

- A water boiler (**HEAT-H2O**), modelled as a heater with no pressure drops and an outlet temperature of 468 °C. This temperature is quite high because no thermal integration has been forseen for this part of the plant, and so a higher value can be achieved. The boiler is assumed to be fed by pure methane, so another input needs to be calculated starting from the combustion duty in order to take into account each external resource to the plant.

- A mixer (**MIX-1**) with no pressure drops and liquid-vapour valid phases, used to model the blending of steam inside the methane.

- A preheater (**HEAT-EX1**) used to increase the temperature of the reacting mixture by exploiting heat of the hot products. It is modelled as a countercurrent HeatX, with hot stream outlet temperature of 700 °C.

- A reformer (**REF**) that is the key point of the entire plant. Modelled as an equilibrium reactor that perform only both SMR (5) and WGS (6) reactions, the product gases are calculated starting from those reaction in order to reach the equilibrium. The choice of the block used relies in the reason that, being the reactions strongly catalyzed by Nichel, the others that could happen are negligible. The reactor is assumed to operate isothermally at T=800 °C [43], with an assumption of pressure drops equal to 1 bar.

- A high temperature recovery heat exchanger (**HEAT-EX2**), aimed at maximizing thermal integration inside the plant. As the preheater, it is modelled as a countercurrent HeatX, with hot stream outlet temperature of 450 °C.

- A high temperature WGS reactor (**HIGH-T WGS**) that performs WGS (6) at a consistent temperature level in order to improve CO conversion. It is modelled as an equilibrium reactor too, performing only WGS (6) at T=350 °C [41] with an assumption of pressure drops equal to 1 bar.

- A low temperature recovery heat exchanger (**HEAT-EX3**), that has the same scope of the previous one. Also in this case, the heat exchanger is modelled as a countercurrent HeatX, with hot stream outlet temperature of 350 °C.

- A low temperature WGS reactor (**LOW-T WGS**), whose aim and modelization are the same of the previous one, except for the lower temperature of 200 °C [41] at which it operates isothermally.

- A condenser (**COND-1**) that operates in pressure and removes unreacted water present in the product gas, in order to increase partial pressure of CO_2 for its removal. It is modelled as a Flash-2 separator, operating at T=35 °C and same pressure of the stream exiting LOW-T WGS (22 bar in this case).

- The Pressure Swing Adsorption (**PSA**), that belongs to this section but treats the flue gas exiting the CCS part. Since from literature it is well known that this component can achieve a very high H_2 purity (over 99.995 % [30]), modelization was done with a very simple separator, where composition of the outlet H_2 stream was imposed (99,995 % H_2, rest equally divived between other compounds).

In order to have a more compact vision of the assumptions, they were summed up in table 4 .

Block Name	Block Type	Assumptions/Specifications
COMP-1	Compr	Discharge pressure 25 bar, isentropic efficiency 0,85
PUMP	Pump	Discharge pressure 25 bar, efficiency 0,85
HEAT-H2O	Heater	Flash type: pressure. Pressure drop: 0 bar. Outlet temperature=468 °C
MIX-1	Mixer	Pressure drops=0 bar. Valid phases: Vapor-liquid
HEAT-EX1	HeatX	Hot stream outlet temperature: 700 °C. Countercorrent
REF	REquil	1 bar pressure drop; Temperature 800 °C; specified SMR and WGS reactions
HEAT-EX2	HeatX	Hot stream outlet temperature: 450 °C. Countercorrent
HIGH-T WGS	REquil	Temperature 350 °C, pressure drop 1 bar, specified WGS reaction
HEAT-EX3	HeatX	Hot stream outlet temperature: 350 °C. Countercorrent
LOW-T WGS	REquil	Temperature 200 °C, pressure drop 1 bar, specified WGS reaction
COND-1	Flash-2	Valid Phases: Liquid-Vapor. Temperature 35 °C, Pressure 22 bar
PSA	Sep2	Outlet Stream H_2: Split fractions defined (0,99995 H_2, rest others)

Table 4: Assumptions for H_2 production part, traditional plant

3.1.2 CO_2 Capture Section

After H_2O condensation, the pressurized and H_2 rich offgas is ready for CO_2 removal in the CCS part of the plant, whose detailed scheme is shown in figure 22.

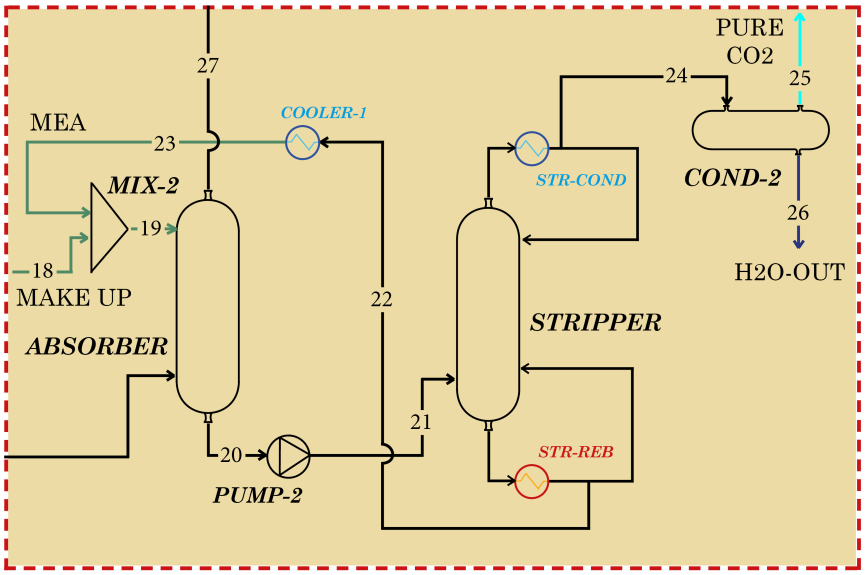

Figure 22: CO_2 Capture section, Traditional plant

The inputs of the system are represented by the water-MEA solution (molar fraction 0,8 H_2O, 0,19 MEA and 0,01 CO_2, to consider eventual CO_2 still dissolved in the solution), that enters the top of the absorber at T=40 °C and p=1 bar, and the make-up streams to compensate lacks of MEA and water in the flue gases exiting the section. The water-MEA solution entering the absorber is an input to be given to ASPEN since modelization was carried out in open loop, allowing faster convergence: the make-up streams are thus calculated in order to preserve mass balance, considering the outlet water-MEA stream completely equal to the inlet one.
The components used in this part are the following:

- An absorber (**ABSORBER**), that was modelled as a 20 stage column without condenser nor reboiler. The input specifications were decided to be of rate mode, as described by Ferrara et al. [44], that in this case result in providing only the valid phases (both vapor and liquid), and the flows direction (imposed as counter-current, since the gas to be treated is supposed to enter the bottom stage of the absorber). In any case, this rate-based approach is a very complete and rigorous one, taking into account each aspect regarding heat transfer, mass transfer, kinetics and hydrodinamics of the system by adopting a stage-discretized two films theory [45]. In any case, the reactions between MEA, H_2O and CO_2 need to be specified in the "Reactions" section of the worksheet, in order to allow the absorber model to properly run. In general, ammine react with H_2O and CO_2 according to the following overall reaction [44]:

$$C_2H_4OHNH_2 + CO_2 + H_2O \longleftrightarrow C_2H_4OHNH_3^+ + HCO_3^- \tag{30}$$

  However, the global reaction can be seen as the result of simulatenous ones, that occur or through equilibrium calculation or with imposed kinetics due to the operative conditions of the system. The ones that reach the equilibrium can be summed up as follows [44]:

$$2H_2O \longleftrightarrow H_3O^+ + OH^- \tag{31}$$

$$2H_2O + CO_2 \longleftrightarrow H_3O^+ + HCO_3^- \tag{32}$$

$$H_2O + HCO_3^- \longleftrightarrow CO_3^{--} + H_3O^+ \tag{33}$$

$$MEA + H_3O^+ \longleftrightarrow MEAH^+ + H_2O \tag{34}$$

$$MEA + HCO_3^- \longleftrightarrow MEACOO^- + H_2O \tag{35}$$

  The equilibrium constants for these reactions have been computed from the reference state Gibbs free energy of the components.
  On the other hand, the reactions that involve kinetic definition are the following:

$$MEA + CO_2 + H_2O \rightarrow MEACOO^- + H_3O^+ \tag{36}$$

$$MEACOO^- + H_3O^+ \rightarrow MEA + CO_2 + H_2O \tag{37}$$

$$CO_2 + OH^- \rightarrow HCO_3^- \tag{38}$$

$$HCO_3^- \rightarrow CO_2 + OH^- \tag{39}$$

  Built-in Power Law expressions were used for kinetic factor k_j definition, whose form follows the Arrhenius one:

$$k_j = A_j exp\left(-\frac{E_{aj}}{RT_j}\right) \tag{40}$$

where A_j is a pre-exponential factor expressed in $\frac{m^3}{kmols}$, E_{aj} is the activation energy expressed in $\frac{J}{kmol}$, R is the universal gas constant, whose value is around 8,314 $\frac{J}{kmolK}$ and T_j is the temperature, in K, at which reaction j occurs.
A_j and E_{aj} used for each reaction are reported in table 5 [46].

Reaction n	$A_j \left[\frac{m^3}{kmols} \right]$	$E_{aj} \left[\frac{J}{kmol} \right]$
36	$9{,}77 \cdot 10^{10}$	$4{,}12643 \cdot 10^{7}$
37	$3{,}23 \cdot 10^{19}$	$6{,}55444 \cdot 10^{7}$
38	$4{,}32 \cdot 10^{13}$	$5{,}54709 \cdot 10^{7}$
39	$2{,}38 \cdot 10^{17}$	$1{,}23305 \cdot 10^{8}$

Table 5: Kinetic parameters for k_j evaluation

Pressure in the absorber was set constant at 21 bar, with an assumption of 2 bar of pressure drops for the gaseous phase. Moreover, this component requires also some geometrical dimensions in input, to be given in the "Packing rating" section; basing the hypothesis on Ferrara et al. [44], a Mellapack Sulzer Standard, dimensions 250Y, with section diameter of 3 meters and section packed height of 4 meters, was chosen. Values of section diameters and section packed height were chosen proportionally to the ones given by Ferrara et al. [44], considering the ratio between the gas flowrates that passes through the absorber, if residence time of the reactants is maintained constant.

- A first valve (**VALVE1**) not represented in the scheme, but used only to model the fact that liquid solution enters and exit the absorber at a pressure different from the one specified in the block, making it necessary to implement another "dummy" component. The only valid phase accepted is liquid one, while outlet pressure was imposed to the value of 1 bar.

- A second "dummy" valve (**VALVE2**) not represented in the scheme, but used to model the additional pressure drops that outlet product gases has to encounter to preserve the assumption of 2 bar pressure drops. In this case, valid phases are both liquid and vapour, while pressure drops were set to 1 bar, indeed.

- A pump (**PUMP-2**), that is used to pressurize the liquid CO_2 rich solution up to 2,1 bar, that has been identified as the best tradeoff pressure for stripper working [28]. As far as efficiency is concerned, it was assumed to be equal to the one of PUMP-1 (0,85).

- A stripper (**STRIPPER**), where regeneration of the solvent occurs and a CO_2 and H_2O rich stream leaves from. Like the absorber, it has been modelled as a 20 stage column, where rate-based reactions take place at a pressure of 1.6 bar set in the first stage. Valid phases are both liquid and vapour, and gases and condensed liquid react in countercurrent. Dimensions were set at 16 meters of section diameter, as

well as 13,5 meters of section packed height, for the same reason of proportionality; type of column was set as Mellapack Sulzer Standard, dimensions 250Y [44].
But in this case, a kettle reboiler and a partial-vapour condenser are present, needing additional specification to run properly. The first one is distillate to feed ratio, defined as the ratio, in molar basis, of the CO_2 and H_2O rich gas that exits the stripper over the feed stream, set at 0.12 [44]; the second one is reboiler duty, set as first attempt at 56 MW, but then modified from further specifications on MEA regeneration.

- A cooler (**COOLER-1**), used to cool down the liquid regenerated water-MEA solution exiting the bottom stage of the stripper up to the absorber inlet temperature. Thus, outlet temperature has been set equal to 40 °C, with no pressure drops.
- A mixer (**MIX-2**) that is used to model the mixing between the regenerated water-MEA solution and the make up one. Valid phases are both vapour and liquid, with no pressure drops.
- A condenser (**COND-2**), used to separate gaseous H_2O from the outlet stream from the top of the absorber, in order to have a high-purity CO_2 stream ready to be compressed and stored. It has been modelled as a flash separator, like the one in the previous section, at a pressure of 1,6 bar and a temperature of 30 °C [44].

Also in this case, all the assumptions and specifications for each block are summarized in table 6.

Block Name	Block Type	Assumptions/Specifications
ABSORBER	RadFrac	Rate based approach, 20 stages. No reboiler or condenser. Vapor-liquid valid phases, countercurrent. Pressure=21 bar (2 bar total pressure drops). Packing Rating: Mellapack Sulzer Standard, 3 meters section diameter, dimensions 250Y, 4 meters section packed height.
VALVE1	Valve	Valid phases: liquid only; outlet pressure=1 bar
VALVE2	Valve	Valid phases: liquid only; pressure drops=1 bar
PUMP-2	Pump	Discharge pressure: 2,1 bar, efficiency 0,85
STRIPPER	RadFrac	Rate based approach, 20 stages. Partial Vapor condenser, Kettle reboiler. Vapor-liquid valid phases, countercurrent. Distillate to feed ratio (molar base)=0,12. Reboiler duty= 56 MW. Stage 1 pressure= 1,6 bar. Packing Rating: Mellapack Sulzer Standard, 16 meters section diameter, dimensions 250Y, 13.5 meters section packed height.
COOLER-1	Heater	Pressure drop: 0 bar. Outlet temperature= 40 °C.
MIX-2	Mixer	Pressure drop: 0 bar. Valid phases: Vapor-liquid
COND-2	Flash2	Valid Phases: Liquid-Vapor. Temperature 30 °C , Pressure 1,6 bar

Table 6: Assumptions for CCS part

3.1.3 Heat supply section

Since SMR is a highly endothermic, tail gas and additional methane need to be burned to provide heat to the reformer. A clearer picture of the system is shown in figure 23.

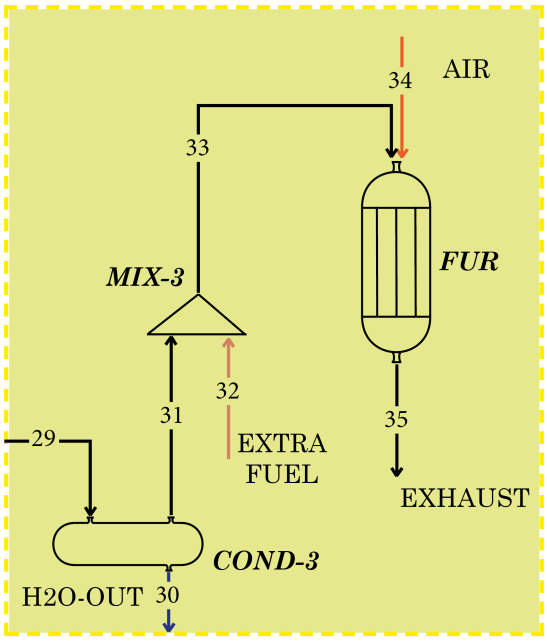

Figure 23: Heat supply section, Traditional plant

The external inputs of the system are the extra fuel needed to substain the reaction and comburent air that gets into the furnace. Both enter the plant at ambient conditions (25 °C and 1 bar), and the value of their molar flow is then changed to satisfy further specifications of the plant.
Only 3 components were necessary to model this part, namely:

- A condenser (**COND-3**), whose aim is to remove the vapour phase water present in the mixture leaving PSA after H_2 separation, in order to save additional fuel requested. This stream cointains water since part of the liquid solvent solution vaporizes by receiving heat from exothermic adsorption reactions. As in the previous cases, the condenser is modelled as a flash separator, at T=35 °C and p=1 bar.

- A mixer (**MIX-3**) used to simulate the blending of the additional fuel in the offgas. Valid phases are both liquid and vapour, with no pressure drops.

- The reformer furnace (**FUR**), modelled as a simple reactor where only combustion occurs. Obviously, the temperature is set equal to the one of the reformer (800 °C [43]), while pressure is atmospheric. Reactions that are allowed in this block are methane combustion (7) and CO one, whose stoichiometry is:

$$CO + \frac{1}{2}O_2 \rightarrow CO_2 \tag{41}$$

  CO combustion is considered too since small parts of it are present in the offgas, and due to its high exothermicity it would surely be a favoured reaction. As assumption on fractional conversion of CH_4 and CO, a value of 0.97 was chosen.

Characteristics of each block are summed up in table 7.

Block Name	Block Type	Assumptions/Specifications
COND-3	Flash2	Valid Phases: Liquid-Vapor. Temperature 35 °C , Pressure 1 bar.
MIX-3	Mixer	Pressure drop: 0 bar. Valid phases: Vapor-liquid.
FURNACE	Rstoic	Temperature: 800 °C. Pressure=1 bar. Reactions: CH_4 and CO combustion, 0,97 fractional conversion of both.

Table 7: Assumptions for heat supply part

3.1.4 Calculator Blocks and Design Specifications

In order to proper manage the inputs given to the plant and to some model blocks, a set of constraints need to be implemented. In ASPEN, there are mainly two methods to impose some conditions to the plant, overwriting the initial trial values:

- Calculator Blocks, that are strict equality conditions that can modify a parameter according to external imposed realationships;
- Design Specifications, that basically consist in setting a target value for specific variables or their combinations, that is reached by manupulating the value of another variable within an imposed range.

In this model, both methods were extensively used in order to guarantee optimal performances from the plant.
Starting from **Calculator Blocks**, only 2 of them were implemented:

- **SCRATIO**, where a first steam to carbon ratio equal to 2,5 was imposed by changing the initial value of the entering H_2O molar flow, making it equal to 2,5 times the CH_4 to the reformer.
- **AIRIN**, that calculates the inlet molar flow of air according to stoichiometry of the CH_4 and CO combustion reactions, without air excess. The amount of air needed to perform the calculation is given by the following relationship:

$$Air_{IN} = CH_{4reac} \cdot \frac{2}{0,21} + CO_{reac} \cdot \frac{0,5}{0,21} \tag{42}$$

  where CH_{4reac} and CH_{4reac} are, respectively, the molar flow of CH_4 and CO that burn in the combustion reaction. The multipliers come from stoichiometry of the reactions.

Passing to **Design Specifications**, more constraints needed to be satisfied. In particular, following the model proposed by Ferrara et al [44], they can be explained as follows:

- **CH4IN**, used to calculate the CH_4 needed to be given to the reformer in order to have, at the end of Low-T WGS reactor, an hydrogen productivity of 1000,05 mol/s, as proposed by Lyngfelt et al. [17].
- **FINALCH4**, used to calculate the molar flow of additonal fuel necessary to provide the right amount of heat to be given to the reformer.

- **CAPRATE**, used to calculate the MEA-water inlet solution molar flow by imposing a certain amount of CO_2 captured over the total entering the absorber (in this case, 90% has been chosen [44]).
- **H2OMAKEU**, used to calculate the molar flow of the make-up water for CCS section. At this point, it was useful to define some properties of the MEA, H_2O and CO_2 components that do not take into account their electrolites and ions that can be dissolved in the solutions, but consider a single neutral component, called *apparent*, for each of them. Thus, make-up water was calculated by imposing that the molar fractions of apparent H_2O in the inlet and outlet stream of the closed loop were the same.
- **MEAMAKEU**, used to calculate the molar flow of the make-up MEA for CCS section. As in the previous specification, make-up MEA was calculated by imposing that the molar fractions of apparent MEA in the inlet and outlet stream of the closed loop were the same.
- **REB**, used to calculate the right amount of duty to be given to the reboiler in order to completely regenerate the solvent. The reboiler duty is varied until the ratios between apparent molar fractions of CO_2 and MEA, respectively in the inlet and outlet streams of the closed loop, were the same.

In order to make each assumption clearer, table 8 reports in detail all the variables considered in the model.

Design Spec	**Target Var.**	**Target Value**	**Manip. Var.**	**Range**
CH4IN	H2OUT	1000,05 $\frac{mol}{s}$	CH4-IN	150-500 $\frac{mol}{s}$
FINALCH4	RefDuty + FurDuty	0 kW	EXTRAFUEL	0-300 $\frac{mol}{s}$
CAPRATE	$\frac{CO2OUT}{CO2IN}$	0,1	MEA-IN	1000-10000 $\frac{mol}{s}$
H2OMAKEU	XH2OOUT	XH2OIN	H2O-MAKEUP	5-400 $\frac{mol}{s}$
MEAMAKEU	XMEAOUT	XMEAIN	MEA-MAKEU	0-80 $\frac{mol}{s}$
REB	$\frac{XCO2OUT}{XMEAOUT}$	$\frac{XCO2IN}{XMEAIN}$	RebDuty	4-400 MW

Table 8: Design Specs of traditional plant

3.1.5 Post Combustion MEA model

Ultimately, it was decided to redesign the plant by moving the CCS section with MEA-absorption in location 3, that is the offgas exiting the reformer furnace where all CO_2 produced in the process is concentrated.
The first H_2 production section remains exactly the same as in the previous model, with

the only difference that condensation before entering the PSA is not necessary, but is performed only just after H_2 separation in that component. Then, the 2^{nd} and 3^{rd} sections are exactly inverted, with the adding of a condenser (**COND-2**, operating at T=35 °C and p=1bar) after the furnace in order to remove water and increase CO_2 partial pressure for a better absorption. The condenser is preceded by a cooler (**COOLER-1**), whose aim is to pre-cool the hot exhaust before condensation to prevent damages to the condensing equipment; outlet temperature has been set equal to 140 °C, a moderate temperature for which water at such partial pressure does not condense, with no pressure drops.
Passing to the CCS section, it is basically the same as the previous model one, with the only differences that the absorber works at atmospheric pressure (thus, with no valves needed to model it) and, together with the stripper, has different dimensions since the volumetric flowrate of gas to be treated is different. Moreover, since atmospheric pressure and does not promote exothermic CO_2 absorption, outlet temperature at the bottom of the absorber results to be lower than in the previous case, needing a preheater to enter the stripper at a higher temperature. So, a heat exchanger was installed after the pump, using inside the plant the heat of the liquid stream exiting the absorber, that was previously wasted being given to a cooling fluid. This heat exchanger was modelled as two interconnected heater and cooler (**HXHEAT** and **HXHEAT2**), with imposed outlet temperature of the cooler of 40 °C and no pressure drops.
The assumptions for the components that have been changed from previous plant are reported in table 9, while calculator blocks and design specs remained the same.

Block Name	**Block Type**	**Assumptions/Specifications**
COOLER-1	Heater	Pressure drop: 0 bar. Outlet temperature= 140 °C.
COND-2	Flash2	Valid Phases: Liquid-Vapor. Temperature 35 °C , Pressure 1 bar
ABSORBER	RadFrac	Rate based approach, 20 stages. No reboiler or condenser. Vapor-liquid valid phases, countercurrent. Pressure=1 bar. Packing Rating: Mellapack Sulzer Standard, 10 meters section diameter, dimensions 250Y, 9 meters section packed height.
STRIPPER	RadFrac	Rate based approach, 20 stages. Partial Vapor condenser, Kettle reboiler. Vapor-liquid valid phases, countercurrent. Distillate to feed ratio (molar base)=0,12. Reboiler duty= 56 MW. Stage 1 pressure= 1,6 bar. Packing Rating: Mellapack Sulzer Standard, 14 meters section diameter, dimensions 250Y, 12 meters section packed height.
HXHEAT	Heater	Pressure drop: 0 bar. Outlet temperature= from energy balance
HXHEAT2	Heater	Pressure drop: 0 bar. Outlet temperature= 40 °C

Table 9: Different assumptions for post combustion MEA part

3.2 Chemical Looping Combustion driven plant

Once the model of traditional plant was concluded, the study continued with the analysis of a more innovative layout of SMR plant, based on Chemical Looping Combustion (CLC) as heat supply medium. A schematic of the plants is shown in figure 24.
The structure is similar to the one of the previous plant, with only 2 sections that can be identified.
The first part, where H_2 **production** occurs, is exactly the same of traditional plant. Pressurized CH_4 and H_2O mixture is sent at first to the reformer, and then to WGS reactors to perform the conversion of CH_4, H_2O and CO into H_2. But in this case, H_2 is directly separated by the tail gas soon after the last WGS, since CCS section is not necessary here. The H_2 free gas exiting the PSA at ambient pressure is then sent to a condenser for H_2O removal.
In the second part, **heat supply** requested by the endothermic SMR reactions is genereated by two interconnected fluid bed reactor that carry on an oxygen carrier as fludized mean, so that CLC reactions take place. Thanks to CLC, exiting CO_2 is not mixed with N_2 and can be easily removed by condensation. At the end of the first part, a CH_4 and CO_2 rich offgas gets out of the condenser and is mixed with additional CH_4, in order to make CLC reactions happen and close the thermal balance. . The mixture is compressed and then sent to the fuel reactor together with the oxygen carrier NiO, that is reduced by oxidizing the CH_4 rich mixture. At this point, the gaseous CO_2 rich stream exiting the fuel reactor is sent to a condenser for H_2O removal, while CO_2 is ready for compression. The Ni particles, instead, are sent to the air fluidbed reactor, where they are reoxidized by reacting with compressed air, producing a large amount of heat. At this point, inert N_2 is cooled after rejection in atmosphere, while NiO particles are cooled and recirculated as inlet of the fuel reactor.

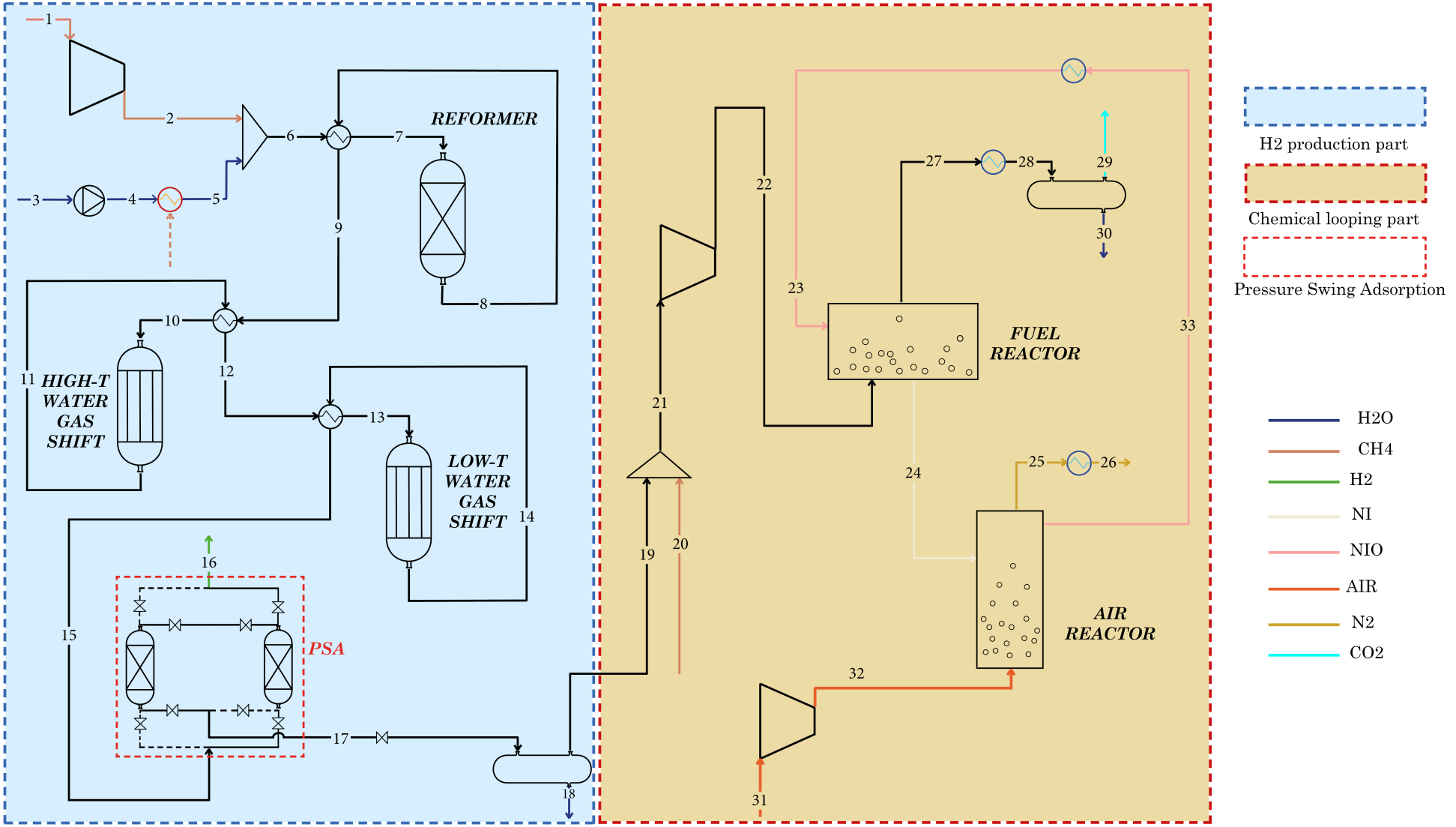

Figure 24: Chemical Looping Combustion plant layout

3.2.1 H_2 production section

As stated in the previous paragraph, the H_2 generation part remains the same as in the traditional plant. A schematic of its layout is shown in figure 25.

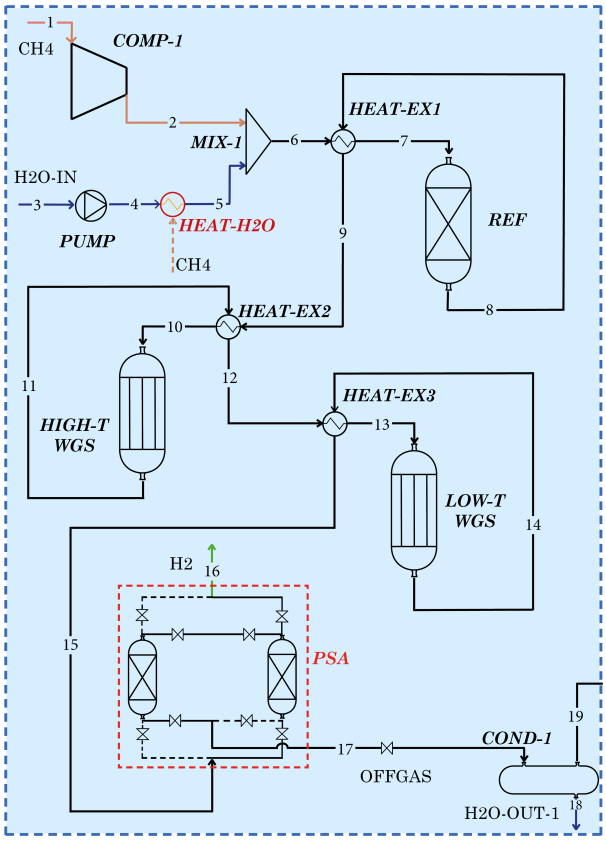

Figure 25: H_2 production section, CLC plant

The model adopted is the same as traditional plant too, but an attempt was conducted in order to replace the equilibrium reactors with another block in ASPEN, called RGibbs reactor. This kind of reactor performs products calculation minimizing the Gibbs free energy of all the reactions that can happen with the inlet reactants, at specified pressure and temperature. Thus, RGibbs does not require stoichiometry of reactions as input, but only its operating conditions.
Thus, it was tried to use a RGibbs reactor to model the reformer and WGS reactors, resulting in a success for the former component, but not the same for the latter ones. As a matter of fact, while total reforming is the favoured reaction at such temperatures and pressures, without any external stoichiometric imposition, WGS is favoured only under specific catalyst activities. This appears clearer if $\Delta\bar{h}$ of WGS (-41 $\frac{kJ}{mol}$) is compared to the one of methanation reaction, that results to be [47]

$$CO_2 + 4H_2 \rightarrow CH_4 + 2H_2O \qquad \Delta\bar{h} = -165\frac{kJ}{mol} \tag{43}$$

Methanation reaction has a $\Delta\bar{h}$ exactly equal to 4 times the one of WGS, in absolute value. Due to low temperature WGS reactions need to be performed at, a more exothermic reaction becomes the predominant reaction in absence of catalysts. In conclusion, RGibbs block results not to be the proper choice to model WGS reactors, whose behaviour is however well characterized by equilibrium ones.

The only differences in modelization from the same section of the traditional plant rely on:

- The reformer (**REF**), whose most proper model has been chosen to be the RGibbs reactor. Operating conditions are the same of the previous model (T=800 °C [43], pressure drops 1 bar).
- A condenser (**COND-1**), used to remove unreacted H_2O, avoiding that part of the heat generated in the following section is used to vaporize and heat up also useless components. It has been modelled as a flash separator, like all the other condensers in this work, at atmospheric pressure and T=23 °C).

In a more structured vision of the work, the list of components with the assumptions made for their modelization is presented also for this section in table 10 .

Block Name	**Block Type**	**Assumptions/Specifications**
COMP-1	Compr	Discharge pressure 25 bar, isentropic efficiency 0,85
PUMP	Pump	Discharge pressure 25 bar, efficiency 0,85
HEAT-H2O	Heater	Flash type: pressure. Pressure drop: 0 bar. Outlet temperature=468 °C
MIX-1	Mixer	Pressure drops=0 bar. Valid phases: Vapor-liquid
HEAT-EX1	HeatX	Hot stream outlet temperature: 700 °C. Countercorrent
REF	RGibbs	1 bar pressure drop; Temperature 800 °C
HEAT-EX2	HeatX	Hot stream outlet temperature: 450 °C. Countercorrent
HIGH-T WGS	REquil	Temperature 350 °C, pressure drop 1 bar, specified WGS reaction
HEAT-EX3	HeatX	Hot stream outlet temperature: 350 °C. Countercorrent
LOW-T WGS	REquil	Temperature 200 °C, pressure drop 1 bar, specified WGS reaction
PSA	Sep2	Outlet Stream H_2: Split fractions defined (0,99995 H_2, rest others)
COND-1	Flash-2	Valid Phases: Liquid-Vapor. Temperature 23 °C, Pressure 1 bar

Table 10: Assumptions for H_2 production part, CLC plant

3.2.2 Heat generation and supply section, 1^{st} model

The last section analyzed within these models is the heat generation and supply one, that provides the necessary energy to make SMR reactions happen. A focus on the schematic

of its layout is shown in figure 26 .

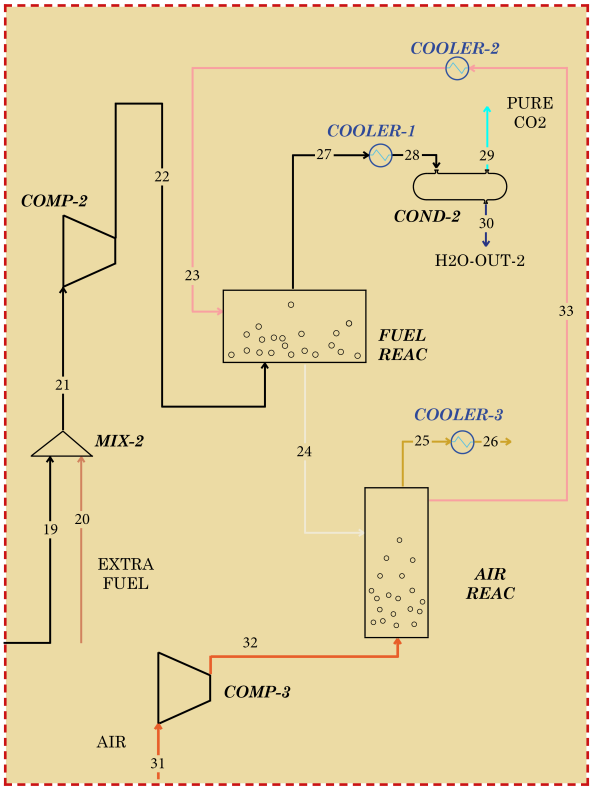

Figure 26: Heat generation and supply section, CLC plant

The external inputs to be given to this part of the system are the extra fuel, the comburent air (both entering the plant at atmospheric conditions) and the NiO to the fuel reactor, since open loop convergence has been chosen to model recirculation of oxygen carrier between interconnected reactors. By doing so, NiO enters the fuel reactor at T=25 °C and p=10 bar. It is worth noting that, having the need of working with solid compounds, their aggregation state has been properly defined in the "properties" section in ASPEN, differently from liquid or gaseous ones that are recognized as "conventional".
For the analysis of this part, that can be recognized as the most relevent added value of the work, two different models were developed. The substantial difference relies in the way the fuel and air reactors were modelled: as a first trial, they were considered as black boxes with the use of RGibbs reactor block, leading to an evolution with the help of Fluidbed reactor block, that allows a deeper analysis of what happens inside them.
Starting with the 1^{st} simpler model, the components involved are the following:

- A mixer (**MIX-2**), used to simulate the blending of additional CH_4 to the offgas. Valid phases are both liquid and vapour, with no pressure drops.
- A compressor (**COMP-2**), used to increase the pressure of the reacting mixture up to 20 bar, to substain velocities needed in the fluidbed reactors. Isentropic efficiency was set equal to the one of the other compressors, that is 0.85 [41].
- The fuel reactor (**FUEL REAC**), where basically endothermic reaction (19) happens with NiO as oxygen carrier and fluidization medium. Since in ASPEN RGibbs references it is stated that RGibbs is also able to calculate chemical equilibrium between conventional solid compounds and others in fluid phases, this block was chosen to perform equilibrium calculations. Temperature was set equal to 900 °C

[17], with outlet pressure of 6.5 bar. In order to complete the modelization of the fuel reactor, another block was necessary to simulate the separation between solid reduced Ni and CO_2 rich gaseous stream. This behaviour was modelled thanks to a simple separator (**SEP-1**), where the split fractions of Ni and NiO were set equal to 1 for the stream that need to cointain them.

- A cooler (**COOLER-1**), used to cool down the exiting hot offgas at 900 °C for preventing its entering in the condenser at such high temperatures. Final temperature was set equal to 140 °C, a moderate value for which the stream liquid fraction remain null, with no pressure drops.
- A condenser (**COND-2**), that can be seen as the only component representing the CCS section in this plant, since all CO_2 produced during the whole process is present in its inlet. Modelled as a flash separator, its operating conditions are T=30 °C and p=6.5 bar.
- The air reactor (**AIR REAC**), where Ni is reoxidized to NiO according to reaction (18), producing a huge quantity of heat. Also in this case, a RGibbs block was used to model the behaviour of the fludized bed reactor, at T=950 °C [17] with no pressure drops, to allow good convergence in open loop. As in the previus reactor, another block was necessary to simulate the separation between solid oxidized NiO and hot N_2 exhaust. This was done through another separator block (**SEP-2**), where the split fractions of Ni and NiO were set equal to 1 for the stream that need to cointain them.
- A compressor (**COMP-3**), used to pressurize comburent air up to 10 bar, with an isentropic efficiency of 0.85.
- A cooler (**COOLER-2**), used to cool the oxidized NiO down to the inlet conditions to the fuel reac (T= 25 °C), with no pressure drops, in order to simulate the closed loop with a "dummy" open one.
- Another cooler (**COOLER-3**), that cools the exiting N_2 down to ambient temperature (T= 25 °C), in order to prevent local modifications of the ambient temperature.

As usual, the components used in this section, the relative block used and the assumptions made to model them are presented in table 11.

Block Name	Block Type	Assumptions/Specifications
MIX-2	Mixer	Pressure drop: 0 bar. Valid phases: Vapor-liquid.
COMP-2	Compr	Discharge pressure: 20 bar, isentropic efficiency 0,85
FUEL REAC	RGibbs	6.5 bar outlet pressure Temperature 900 °C
	Sep	Split fractions solid stream: NI=1, NIO=1, others 0.
COOLER-1	Heater	0 bar pressure drop, 140 °C final temperature
COND-2	Flash2	RValid Phases: Liquid-Vapor. Temperature 30 °C, Pressure 6.5 bar
COOLER-1	Heater	Pressure drop: 0 bar. Outlet temperature= 40 °C.
AIR REAC	RGibbs	0 bar pressure drop; Temperature 950 °C

	Sep	Split fractions solid stream: NI=1, NIO=1, others 0.
COMP-3	Compr	Discharge pressure 10 bar, isentropic efficiency 0,85
COOLER-2	Heater	0 bar pressure drop, 25 °C final temperature
COOLER-3	Heater	0 bar pressure drop, 25 °C final temperature

Table 11: Assumptions for heat generation part, CLC plant

3.2.3 Heat generation and supply section, 2^{nd} model

As heralded in the previous paragraph, a further step was made in order to have a more complete picture of the working conditions of the fluidbed reactors. All the modelization is focused on the calculations performed of a single block, the fluidbed indeed, that is a new entry in ASPEN worksheets and looks like figure 27.

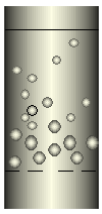

Figure 27: Fluidbed block picture in ASPEN

Starting from the inputs, it requires two streams: one cointaining solids and another cointaining gases. The ouptus are two too, both solid and gaseous stream as in the inputs, calculated basing on the equations inside the block and the specific reactions imposed from outside.
But, the peculiarity of this block is that it requires the Particle Size Distribution (PSD) of the powders input solid stream. Since the only external solid input in the model is the NiO entering the fuel reactor, its PSD needs to be specified.
At a first vision, it has been decided to start from the average diameter of 200 microns proposed by Lyngfelt et all [17], building over it a Gaussian distribution with this mean value and standard deviation of 50 microns reported in figure 28.
The cumulative weight fractions of the distribution are shown in figure 29, instead.
With this configuration, the largest particles have a diameter of around 350 microns, while the smallest around 50 microns. The hypotesis of same PSD maintained at the end of each reactor has been made and implemented in ASPEN in order to retrieve results from the model. So, calculations for the reactors have been made taking into account this f(200,50) distribution.
In order to present the mathematical model that is inherent to the fluidbed block, it can become usefuel to understand its working principle and main characteristics. So, the start-up of the reactor is made by investing an initially stationary solid bed with a fluid, whose velocity needs to be higher or equal than a certain value u_{mf}, called *minimum fluidization velocity* or *terminal velocity* [48]. From that moment on, all the solid-fluid mixture behaves as a single fluid. In particular, if gas is considered as fluidizing medium, when its velocity is slighly higher than u_{mf} only some bubbles are creating in the lower

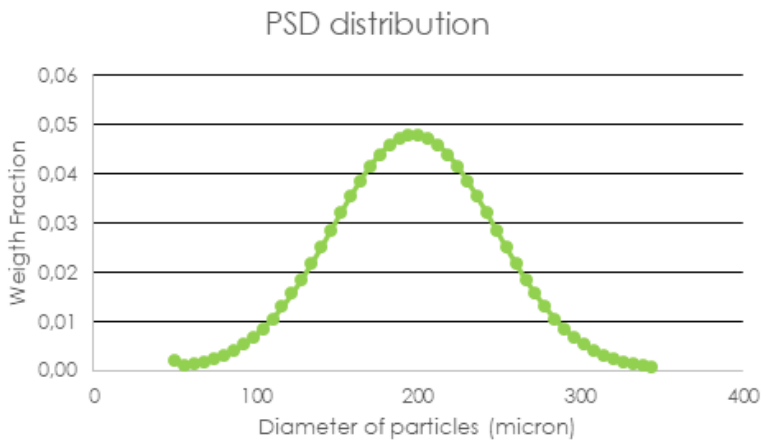

Figure 28: PSD for inlet NiO to fuel reactor

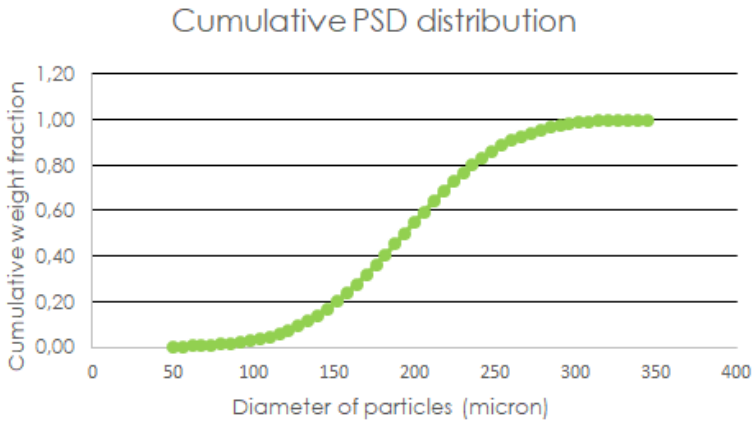

Figure 29: Cumulative PSD for inlet NiO to fuel reactor

part of the reactor, that create only a partial movement of the particles in the so called *bubbling bed*. On the other hand, when gas velocity becomes very high, fluidization gets completed, being not only limited to the formation of bubbles, and leads to the so called *circulating bed*. A visual representation of the two phenomena is shown in figure 30.

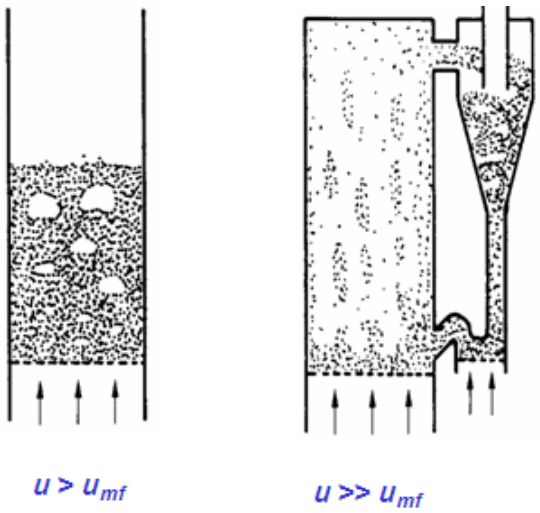

Figure 30: Bubbling bed and Circulating bed reactors

A fluidized bed can be subdivided in two different zones:

- The **bottom** zone, whose height is expressed as H_b, where particles are denser;
- The **upper diluted** zone, whose height is expressed as H_f, where solid matter is more diluted indeed.

Moreover, it is important to define also the *Transport Disengagement Height* (TDH), as the distance between the section where solid matter concentration becomes more or less constant and the bottom of the fluidbed reactor. A visual representation of these zones is given by figure 31.

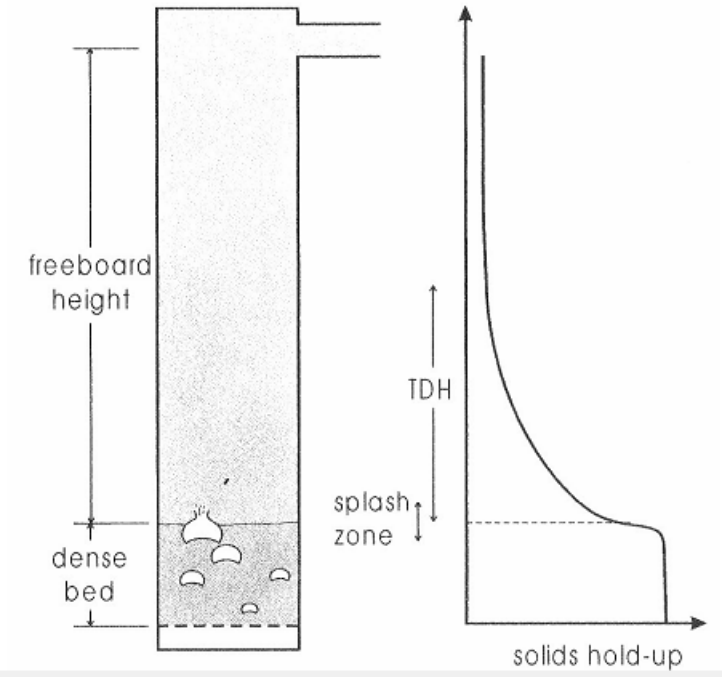

Figure 31: Definition of different zones in fluid bed

Getting more in detail into the mathematical model, the fundamental hypothesis on which it is based is the exponential decay of the concentration of solid matter in the upper diluted zone, as described by Kunii and Levenspiel [48] and shown in figure 32 [50]:

$$c_v(h) = {c_v}^* + ({c_{v,be}} - {c_v}^*) \cdot e^{-ah} \tag{44}$$

where, as can be easily seen from the figure, ${c_v}^*$ is the concentration at infinite hight (calculated by taking into account entrainment coefficients), $c_{v,be}$ is the concentration of the solid matter at terminal velocity in the bottom zone, and a is a an exponential constant whose values range from 2 to 12 [48]. Concentrations of particles in the bottom zone are almost constant, being very dense and with poor fluidization.
Giving this distribution, it is possible to calculate the height of the bottom zone H_b and, consequently, the height of the upper diluted zone H_f since $H_t = H_b + H_f$ is imposed by the user. For doing so, it is necessary to assign a specific value of pressure drops over the reactor ($\Delta p_{Bed,def}$) and imposing it equal to its formulation Δp_{Bed}, expressed as follows:

$$\begin{aligned} \Delta p_{Bed} = g \cdot \int_0^{H_b} \left(\sum_{i=0}^{n} \Delta Q_{3,b,i} \cdot \rho_{s,i} \cdot c_{v,i} + \left(1 - \sum_{i=0}^{n} \Delta Q_{3,b,i} \cdot c_{v,i} \right) \cdot \rho_f \right) \cdot dh + \\ + g \cdot \int_{H_b}^{H_f} \left(\sum_{i=0}^{n} \rho_{s,i} \cdot c_{v,i} + \left(1 - \sum_{i=0}^{n} \cdot c_{v,i} \right) \cdot \rho_f \right) \cdot dh = \Delta p_b + \Delta p_f \end{aligned} \tag{45}$$

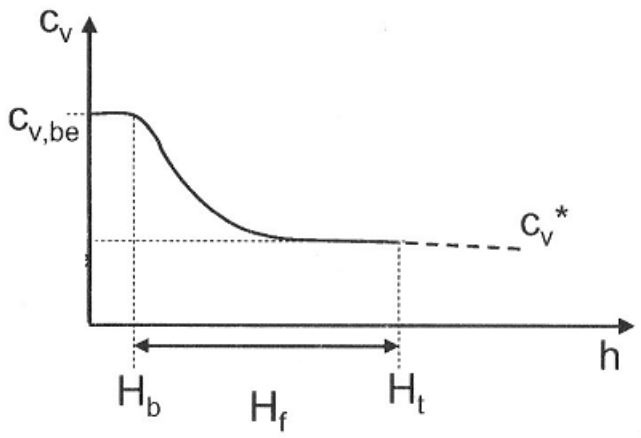

Figure 32: Solid matter concentration distribution over the reactor [50]

where the subscript i refers to the different terminal velocity classes of the particles (that are various since diameters are distributed according to a gaussian distribution), $\Delta Q_{3,b,i}$ is the mass fraction of particles in the bottom zone at terminal velocity class i, $\rho_{s,i}$ is the density of particlea at that terminal velocity class and ρ_f is the density of the gaseous phase.
Terminal or minimum fluidization velocity (u_{mf}) can be calculated from the Ergun correlation [49]:

$$u_{mf} = 7.14 \cdot (1 - \epsilon_{mf}) \cdot \nu_f \cdot S_V \cdot \left[\sqrt{1 + 0.067 \cdot \frac{{\epsilon_{mf}}^2}{(1 - \epsilon_{mf})^2} \cdot \frac{(\rho_s - \rho_f) \cdot g}{\rho_f \cdot {\nu_f}^2} \cdot \frac{1}{{S_V}^3}} - 1 \right] \quad (46)$$

where ν_f is the kinematic viscosity of the gas, ϵ_{mf} is the porosity of the bed at minimum fluidization and S_V is the volume-specific surface area of the solids, defined as:

$$S_V = \frac{Surface\ area\ of\ all\ particles\ in\ the\ bed}{Volume\ of\ all\ particles\ in\ the\ bed} \quad (47)$$

Thus, total pressure drops can be distinguished in their bottom (Δp_b) and upper diluted zone (Δp_b) contributions, as shown in (45).
Knowing that, an optimization problem is performed in order to find the H_b that satisfy the realationship, that is formulated as follows:

$$f(H_b) = |\Delta p_{Bed}(H_b) - \Delta p_{Bed,def}| \rightarrow min! \quad (48)$$

At this point, it it possible to calculate the total mass in the bed according to the following relationship:

$$\begin{aligned} m_T &= \int_0^{H_b} A_t(h) \cdot \left(\sum_{i=0}^{n} \Delta Q_{3,b,i} \cdot \rho_{s,i} \cdot c_{v,i} \right) \cdot dh + \int_{H_b}^{H_t} A_t(h) \cdot \left(\sum_{i=0}^{n} \cdot \rho_{s,i} \cdot c_{v,i} \right) \cdot dh \\ &= m_b + m_f \end{aligned} \quad (49)$$

where $At_(h)$ is the transversal section of the reactor, function of its height, that is an input of the block, while m_b and m_f are the mass of the particles beds in the bottom and upper diluted zone, respectively. It is worth noting that the optimization problem (46) for H_b determination could be done also if starting from the total particle bed definition:

once known H_b, pressure drops over the reactor are calculated through (45). Thus, the block requires those two inputs in a mutually exclusive way.
As far as gas velocity u_g is concerned, it is easily calculated by the classic relationship:

$$u_g(h) = \frac{\dot{m}_g(h)}{\rho_g(T, p(h)) \cdot A_t(h)} \tag{50}$$

where $\dot{m}_g(h)$ is the gas flowrate at height h.
Passing to modelization of the bottom zone, it is modelled as a bubbling bed [51] other inputs required are the number (n_{or}) and diameter (d_{or}) of orifices where gases pass through. By knowing that, the volumetric flow of gases passing through each single orifice ($\dot{V}_{or}$) is:

$$\dot{V}_{or} = \frac{u \cdot A_t}{n_{or}} \tag{51}$$

Once injected, the gases make bubbles form, whose initial diameter of the equivalent sphere ($d_{v,o}$) is given by [52]:

$$d_{v,o} = 1.3\left(\frac{\dot{V}_{or}^2}{g}\right) \tag{52}$$

Knowing its initial value, it is possibile to solve the following differential equation to find the evolution of the diameter of the bubbles with height:

$$\frac{d(d_v)}{dh} = \left(\frac{2 \cdot \epsilon_b}{9 \cdot \pi}\right)\frac{1}{3} - \frac{dv}{3 \cdot \lambda \cdot u_b} \tag{53}$$

with the first positive term that describe coalescence that makes bubbles grow, while the second negative one stands for their splitting. In this relationship, d_v is the diameter of the sphere, while λ represent the mean life of a bubble that is provided by Hilligardt and Werther relationship [53]:

$$\lambda = 280 \cdot \frac{u_{mf}}{g} \tag{54}$$

while ϵ_b is the local bubble volum fraction, calculated as:

$$\epsilon_b = \frac{\dot{V}_b}{u_b} \tag{55}$$

where $\dot{V}_b$ and u_b are, respecively, the visible bubble flow and the local bubble rise velocity, both provided by Hilligardt and Werther as [54]:

$$\dot{V}_b = \psi \cdot (u - u_{mf}) \tag{56}$$

$$u_b = \dot{V}_b + 0.71 \cdot \theta \cdot \sqrt{g \cdot d_v} \tag{57}$$

where ψ and θ are two fludization parameters whose value depends on the Geldart classification of the reactor, that is one of the inputs of the block. The classification is based on solid fluidization behaviour, as empirically observed by Geldart himself [55].
It is now necessary to understand how the concentrated pressure drops due to the exiting of the gases from the orifices. So, first of all the velocity at each single orifice (u_{or}) has to be calculated as follows:

$$u_{or} = \frac{\dot{V}}{n_{or} \cdot \frac{\pi}{4} \cdot {d_{or}}^2} \tag{58}$$

and, consequently, the concentrated pressure drops in the distributor (Δp_{Dis}):

$$\Delta p_{Dis} = \left(\frac{u_{or}}{C_{Dis}}\right)^2 \cdot \frac{\rho_f}{2} \tag{59}$$

where C_{Dis} is the orifice discharge coefficient and is dependent on its form.
After that, TDH needs to be evaluated according to Fournol et al. correlation [56]:

$$TDH = 1000 \cdot \frac{u^2}{g} \tag{60}$$

where u is the gas velocity at the top of the fluidized bed.
Finally, the phenomenon of *elutriation* needs to be completely characterized. It basically consists in the separation of the partilces from the stationary bed by being invested by the gas at sufficient velocity. So, it is necessary to understand which is the elutriated mass flow of particles that belong to a specific terminal velocity class ($\dot{m_{e,i}}$); when the upper diluted zone is taller than TDH, it depends on gas velocity, solid matter terminal velocity and its mass fraction in the bottom zone:

$$\dot{m_{e,i}} = k_{\infty,i} \cdot A_t(H_b) \cdot \Delta Q_{3,b,i} \tag{61}$$

where $k_{\infty,i}$ is a specific elutriation coefficient that can be calculated by means of different correlations. In this model, the Tasirin and Geldart one has been chosen, that is reported below [57]:

$$k_{\infty,i} = A \cdot \rho_g \cdot u^B \cdot exp\left(C \cdot \frac{u_{t,i}}{u}\right) \tag{62}$$

where with $u_{t,i}$ is indicated the terminal velocity for the class i and A, B and C are default fitting parameters that depend on the turbulence of the flow and are inserred by the software.
Now that the model has been completely characterized, the inputs that were given to the two fluidbed reactors are presented and subdivided in the different sections they are inserred in the software. Namely, the sudvision adopted is:

- **Specifications**, where bed mass or pressure drops, and the correlations for calculation of terminal velocity, TDH and elutriation, are specified;
- **Operation**, that requires only valid phases and operational temperature of the reactor;
- **Geometry**, where geometrical dimensions of the reactor are defined;
- **Gas Distributor**, that describes its type, the number and diameter of orifices and the discharge coefficient;
- **Reactions**, where reactions that need to happen are selected after their definition in the omonym section in the worksheet.

All the inputs are summarized in table 12. It is to say that most of the assumptions has been taken by Lyngfelt et al. [17]; when missing, data were supposed to be the default values or personal assumptions based on literature description.

Input		Fuel React	Air React
Specifications	Pressure drops (bar)	0,177	0,035
	Fluid. Vel. Corr.	Ergun	Ergun
	Geldart class.	A	A
	TDH. Corr.	Fournol et al.	Fournol et al.
	Elutriation Corr.	Tasirin and Geldart	Tasirin and Geldart
Operation	Temperature (°C)	900	950
	Valid phases	Vapor only	Vapor only
Geometry	Cross section	Rectangular	Rectangular
	Height	2,5	9,5
	Width	11,4	2
	Depth	7,4	2
Gas Distributor	Type	Perforated plate	Perforated plate
	Number of orifices	40	60
	Orifice diameter (mm)	10	100
	Discharge coefficient	0,8	0,8
Reactions	Ni oxid. and red.	(18)	(19)

Table 12: Assumptions for Fuel and Air Fluidbed reactors

It is worth noting that, by using fluidbed block, no separators are necessary to simulate the cyclone solid separation, since the two outputs are already divided by the block itself. Moreover, reactions (18) and (19) have been defined following a specific kinetic, as described in literature. A Power Law expression has been implemented, that assumes the more general Arrhenius form:

$$k_j = k \cdot T^n \cdot \left(-\frac{E_a}{RT}\right) \tag{63}$$

which is substantially the same as (40), with the adding of polynomial dependence by temperature. Parameters found in literature are reported in table 13[58].

Reaction	**k** $\left[\frac{mol^{1-n} \cdot m^{3n-2}}{s}\right]$	**n**	$E_a\left[\frac{kJ}{mol}\right]$
(18)	0,46	1	23
(19)	0,19	0.2	5

Table 13: Kinetic parameters for Ni oxidation and reduction

Anticipating something related to the following chapter, both the models provided more or less the same results, leading to considering the second one as more complete and representative of the behaviour of the plant. Thus, for all the following considerations, only the second model will be taken as representative of the CLC plant.

3.2.4 Calculator Blocks and Design Specifications

As in the previous plant, also CLC one needs calculator blocks and design specifications to be properly modelled.
Starting from calculator blocks, the same steam to carbon ratio was defined and set equal to 2.5 as starting value: this clearly modifies the flowrate of H_2O entering the reformer, making it 2.5 times the one of the inlet CH_4. The other two calculator blocks are about the inlet NiO to fuel reactor and air to air reactor, whose flowrates were calculated starting from stoichiometry of the reactions, without any excess of reactants. Thus, according to reactions (18) and (19), inlet NiO and Air are calculated as follows:

$$NiOIN = 4 \cdot CH_4 \tag{64}$$

$$AIRIN = \frac{0,5}{0,21} \cdot Ni \tag{65}$$

where CH_4 and Ni are the methane and nickel in input, respectively, to fuel and air reactors.
As far as design specifications are concerned, only calculations of inlet CH_4 to reformer and additional one are required, since all the other inputs are imposed or calculated by means of calculators block. Moreover, there is no need of modifying iteratively any block parameter (as in the case of the reboiler duty), so the analysis is reduced to 2 design specs, as follows:

- **CH4IN**, used to calculate the CH_4 needed to be given to the reformer in order to have, at the end of Low-T WGS reactor, an hydrogen productivity of 1000,05 mol/s, as proposed by Lyngfelt et al. [17].
- **FINALCH4**, used to calculate the molar flow of additonal fuel necessary to provide the right amount of heat to be given to the reformer. In this case, the heat generated by exothermic reaction (18) must be necessary to sbustain both SMR happening in the reformer and reaction (19), that results to be endothermic. The heat globally released by the algebraic sum of (18) and (19) (that is equal to CH_4 combustion) is recalled in the text as "CLCduty".

As in the previous section, all the assumptions made in the design specs definition have been summed up in table 14.

Design Spec	Target Var.	Target Value	Manip. Var.	Range
CH4IN	H2OUT	1000,05 $\frac{mol}{s}$	CH4-IN	150-500 $\frac{mol}{s}$
FINALCH4	RefDuty + CLCduty	0 kW	EXTRAFUEL	0-300 $\frac{mol}{s}$

Table 14: Design Specs of CLC plant

The most important check on the equivalence of the two models was the evaluation of the additional fuel needed, guaranteeing a relative difference lower than 1%. These considerations are driven from the fact that, being the kept unchanged between the two models, the only parameter involved in the calculations of the fluidreactors is the molar flow of additional fuel.

4 Results and Sensitivities

After implementing all the inputs, calculator blocks and design specs, the models were run in order to extract significant results from them.
First of all, the cornerstones of each stream indicated in figure 20 and 24 are taken from ASPEN and reported in tables 15 and 16. More in detail, the parameters that are reported are temperature, pressure, molar flow and composition of the streams.
Then, In order to have a complete overview of the plants performances, two major analyses have been carried on. The first one is related to the H_2 production part of the plants, where operational parameters such as S/C ratio and reformer pressure and temperature have been varied in order to investigate the feedback of the plants. In particular, the variations that were mostly analyzed are the ones in CH_4 conversion and all the external inputs that have a certain weight in economic terms (CH_4 and electrical power). The second study, instead, can be seen as a focus on the detailed model of the fluid bed reactors introduced in the advanced modelling of the Chemical Looping Combustion plants. From ASPEN fluidbed block, indeed, lots of interesting data can be extracted, as pressure, solid matter fraction, gas velocities and molar flow of the different species over the reactor.
Thus, having results about the behaviour of the plants at different operating conditions, the best options were chosen in order to make them work at their best.
It is worth noting that the comparison has been performed considering two plants with the same H_2 productivity (1000 mol/s), imposed by referring to Lyngfelt et all [17]: thus, instead of considering specific parameters over H_2 productivity, absolute ones can be shown in the results, making them clearer to understand.

	1	**2**	**3**	**4**	**5**	**6**	**7**	**8**	**9**	**10**	**11**	**12**	**13**	**14**	**15**	**16**	**17**
Temperature [°C]	25	331	25	25	468	417	535	800	700	450	350	603	350	200	462	35	35
Pressure [bar]	1,01	25	1,01	25	25	25	25	24	24	24	23	23	23	22	22	22	22
Total Flow $\left[\frac{mol}{s}\right]$	393	393	982	982	982	1375	1375	1877	1877	1877	1877	1877	1877	1877	1877	480	1396
Molar Fraction																	
CH_4	1	1	0	0	0	0,29	0,29	0,08	0,08	0,08	0,08	0,08	0,08	0,08	0,08	0	0,1
H_2O	0	0	1	1	1	0,71	0,71	0,33	0,33	0,33	0,27	0,27	0,27	0,26	0,26	1	0
H_2	0	0	0	0	0	0	0	0,46	0,46	0,46	0,52	0,52	0,52	0,53	0,53	0	0,72
CO	0	0	0	0	0	0	0	0,07	0,07	0,07	0,01	0,01	0,01	0	0	0	0
CO_2	0	0	0	0	0	0	0	0,06	0,06	0,06	0,12	0,12	0,12	0,13	0,13	0	0,18
O_2	0	0	0	0	0	0	0	0	0	0	0	0	0	0	0	0	0
N_2	0	0	0	0	0	0	0	0	0	0	0	0	0	0	0	0	0
MEA	0	0	0	0	0	0	0	0	0	0	0	0	0	0	0	0	0
$MEACOO^-$	0	0	0	0	0	0	0	0	0	0	0	0	0	0	0	0	0
H_3O^+	0	0	0	0	0	0	0	0	0	0	0	0	0	0	0	0	0
$MEAH^+$	0	0	0	0	0	0	0	0	0	0	0	0	0	0	0	0	0
HCO_3^-	0	0	0	0	0	0	0	0	0	0	0	0	0	0	0	0	0
CO_3^{--}	0	0	0	0	0	0	0	0	0	0	0	0	0	0	0	0	0
OH^-	0	0	0	0	0	0	0	0	0	0	0	0	0	0	0	0	0

	18	**19**	**20**	**21**	**22**	**23**	**24**	**25**	**26**	**27**	**28**	**29**	**30**	**31**	**32**	**33**	**34**	**35**
Temperature [°C]	40	40	100	100	121	40	93	30	30	69	69	69	35	35	25	35	25	800
Pressure [bar]	1	1	1	2,1	1,6	1,6	1,6	1,6	1,6	20	20	20	1	1	1	1	1	1
Total Flow $\left[\frac{mol}{s}\right]$	158	3107	3092	3092	2943	2943	371	229	142	1189	1000	189	10	179	0	180	1362	1540
Molar Fraction																		
CH_4	0	0	0	0	0	0	0	0	0	0,12	0	0,75	0	0,79	1	0,79	0	0
H_2O	1	0,81	0,8	0,8	0,8	0,8	0,4	0,03	1	0,02	0	0,1	0,98	0,06	0	0,06	0	0,19
H_2	0	0	0	0	0	0	0	0	0	0,84	1	0	0	0	0	0	0	0
CO	0	0	0	0	0	0	0	0	0	0	0	0,01	0	0,01	0	0,01	0	0
CO_2	0	0	0	0	0	0	0,6	0,97	0	0,02	0	0,13	0	0,14	0	0,14	0	0,11
O_2	0	0	0	0	0	0	0	0	0	0	0	0	0	0	0	0	0,21	0,01
N_2	0	0	0	0	0	0	0	0	0	0	0	0	0	0	0	0	0,79	0,70
MEA	0	0,17	0,03	0,03	0,18	0,18	0	0	0	0	0	0	0	0	0	0	0	0
$MEACOO^-$	0	0,01	0,08	0,08	0,01	0,01	0	0	0	0	0	0	0	0	0	0	0	0
H_3O^+	0	0	0	0	0	0	0	0	0	0	0	0	0	0	0	0	0	0
$MEAH^+$	0	0,01	0,08	0,08	0,01	0,01	0	0	0	0	0	0	0,01	0	0	0	0	0
HCO_3^-	0	0	0	0	0	0	0	0	0	0	0	0	0,01	0	0	0	0	0
CO_3^{--}	0	0	0	0	0	0	0	0	0	0	0	0	0	0	0	0	0	0
OH^-	0	0	0	0	0	0	0	0	0	0	0	0	0	0	0	0	0	0

Table 15: Cornerstones traditional SMR plant

	1	**2**	**3**	**4**	**5**	**6**	**7**	**8**	**9**	**10**	**11**	**12**	**13**	**14**	**15**	**16**	**17**
Temperature [°C]	25	331	25	25	468	417	534	800	700	450	350	603	350	200	462	462	462
Pressure [bar]	1,01	25	1,01	25	25	25	25	24	24	24	23	23	23	22	22	22	22
Total Flow $\left[\frac{mol}{s}\right]$	393	393	981	981	981	1374	1374	1875	1875	1875	1875	1875	1875	1875	1875	1000	875
Molar Fraction																	
CH_4	1	1	0	0	0	0,29	0,29	0,08	0,08	0,08	0,08	0,08	0,08	0,08	0,08	0	0,16
H_2O	0	0	1	1	1	0,71	0,71	0,33	0,33	0,33	0,27	0,27	0,27	0,26	0,26	0	0,55
H_2	0	0	0	0	0	0	0	0,46	0,46	0,46	0,52	0,52	0,52	0,53	0,53	1	0
CO	0	0	0	0	0	0	0	0,07	0,07	0,07	0,01	0,01	0,01	0	0	0	0
CO_2	0	0	0	0	0	0	0	0,06	0,06	0,06	0,12	0,12	0,12	0,13	0,13	0	0,28
O_2	0	0	0	0	0	0	0	0	0	0	0	0	0	0	0	0	0
N_2	0	0	0	0	0	0	0	0	0	0	0	0	0	0	0	0	0
Ni	0	0	0	0	0	0	0	0	0	0	0	0	0	0	0	0	0
NiO	0	0	0	0	0	0	0	0	0	0	0	0	0	0	0	0	0

	18	**19**	**20**	**21**	**22**	**23**	**24**	**25**	**26**	**27**	**28**	**29**	**30**	**31**	**32**	**33**
Temperature [°C]	23	23	25	23	309	25	900	950	25	900	140	30	30	25	343	950
Pressure [bar]	1,01	1,01	1	1	20	10	6,75	9,86	9,86	6,75	1	6	6	1	10	9,86
Total Flow $\left[\frac{mol}{s}\right]$	473	402	69	471	471	843	843	1584	1584	891	891	464	427	2004	2004	843
Molar Fraction																
CH_4	0	0,35	1	0,45	0,45	0	0	0	0	0	0	0	0	0	0	0
H_2O	1	0,02	0	0,02	0,02	0	0	0	0	0,48	0,48	0,01	1	0	0	0
H_2	0	0	0	0	0	0	0	0	0	0	0	0	0	0	0	0
CO	0	0,01	0	0	0	0	0	0	0	0	0	0	0	0	0	0
CO_2	0	0,62	0	0,53	0,53	0	0	0	0	0,51	0,51	0,99	0	0	0	0
O_2	0	0	0	0	0	0	0	0	0	0	0	0	0	0,21	0,21	0
N_2	0	0	0	0	0	0	0	1	1	0	0	0	0	0,79	0,79	0
Ni	0	0	0	0	0	0	1	0	0	0	0	0	0	0	0	0
NiO	0	0	0	0	0	1	0	0	0	0	0	0	0	0	0	1

Table 16: Cornerstones CLC plant

4.1 H_2 production part

Since the first part of the plants is the same, the traditional plant was taken as reference model when extracting all those results that involve parameters and effects belonging to that part. In order to make comparisons, instead, both the plant models were obviously run.

4.1.1 Reformer Temperature

The first manipulated parameter is the reforming temperature in the reactor, that dominates the rate of reaction since its increase shifts the equilbrium towards the products (endothermic reaction). This phenomenon is fundamental in order to understand why CH_4 **Conversion**, defined as (3), has the trend reported in figure 33 by varying reformer temperature between 750 and 900 °C [6].

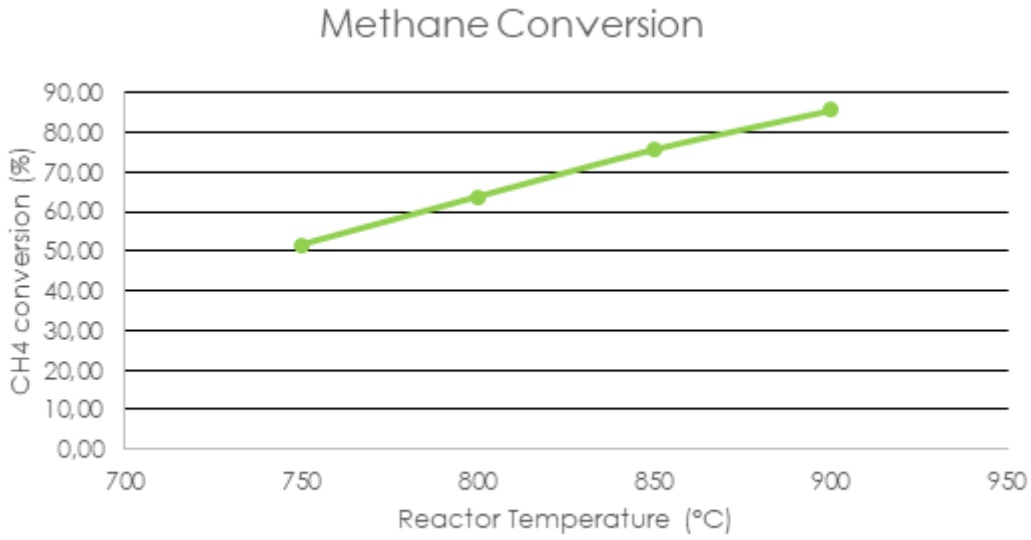

Figure 33: Effect of Reformer Temperature on CH_4 Conversion

As a matter of fact, being the inlet and outlet temperatures of the WGS unchanged and the reforming reaction endothermic, CH4 conversion increases when reactor temperature increases, up to 86% for T=900 °C. Obviously, temperatures higher than 900 °C were not investigated, since fuel reactor works at this temperature, and consequently heat transfer can happen until this temperature.
Another relevant factor that is influenced by reformer temperature is the CH_4 **molar flow in input** to the plants, which can be distingueshed in its 3 contributions (inlet to the H_2 production part, additional inlet to substain the heat supply reactions for reforming and fuel to the H_2O boiler) as shown in figure 34.

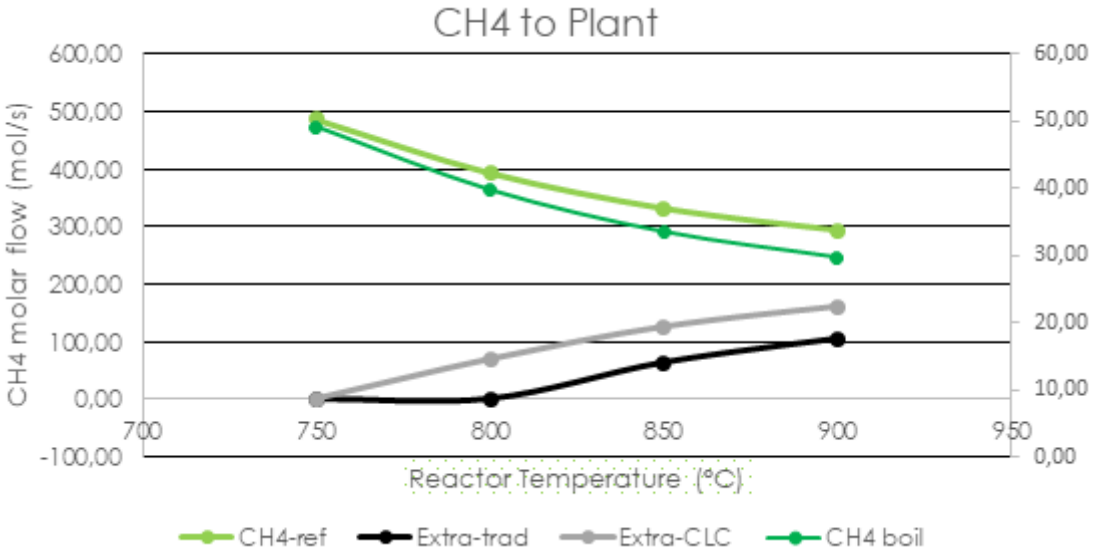

Figure 34: Effect of Reformer Temperature on different CH_4 inlets to plants

If methane conversion increases, obviously CH_4 to reformer decreases, since less methane is necessary in order to produce the same fixed amount of H_2. Fuel requested by H_2O boiler (reported on secondary axis) decreases too, since at fixed Steam to Carbon ratio, less methane means less water to be heated and vaporized. On the other hand, since high temperatures require more heat, the extra fuel requested by the plants increases with temperature.
Then, the three contributions were added to obtain the total inlet CH_4 trends reported in figure 35.

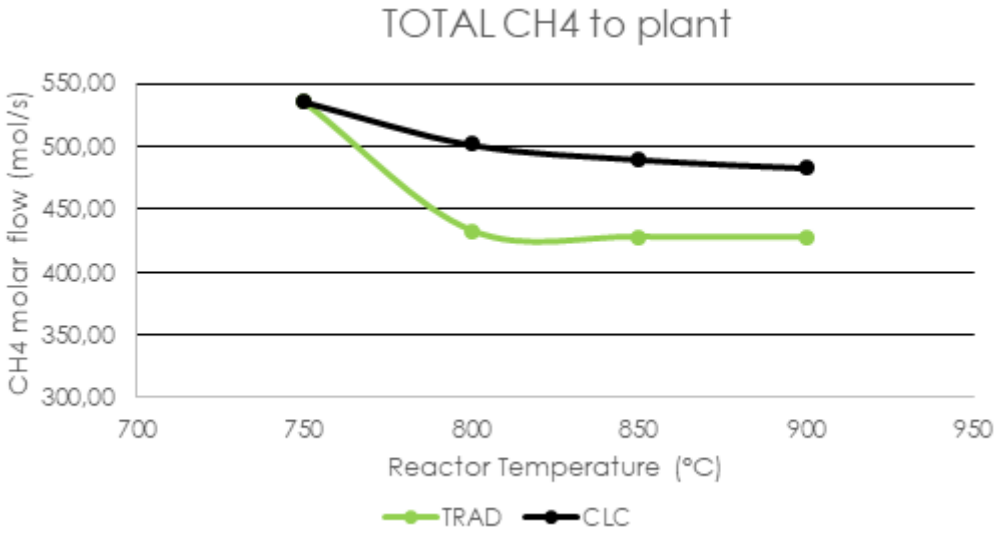

Figure 35: Effect of Reformer Temperature on Total CH_4 inlet to plants

The values of the traditional plant result to be lower of around 55-70 mol/s, depending on the temperature considered, except for T= 750 °C, where no extra fuel is requested since the inlet CH_4 to the reactor is sufficient to substain also the heat supply reaction. In this case, the total CH_4 is represented by the inlet CH_4 to the reactor itself (which remains the same since the H_2 production part is unchanged in the 2 plants). In any case, the fuel required is more or less the same (13-16% more for CLC), confirming the fact that

CLC plants could become a worthy substitute in the future of large scale industrial H_2 generation.
Moreover, only for traditional plant it was chosen to see which could be the effect of reformer temperature on **stripper's reboiler and condenser duty and temperatures**, as reported in figures 36 37.

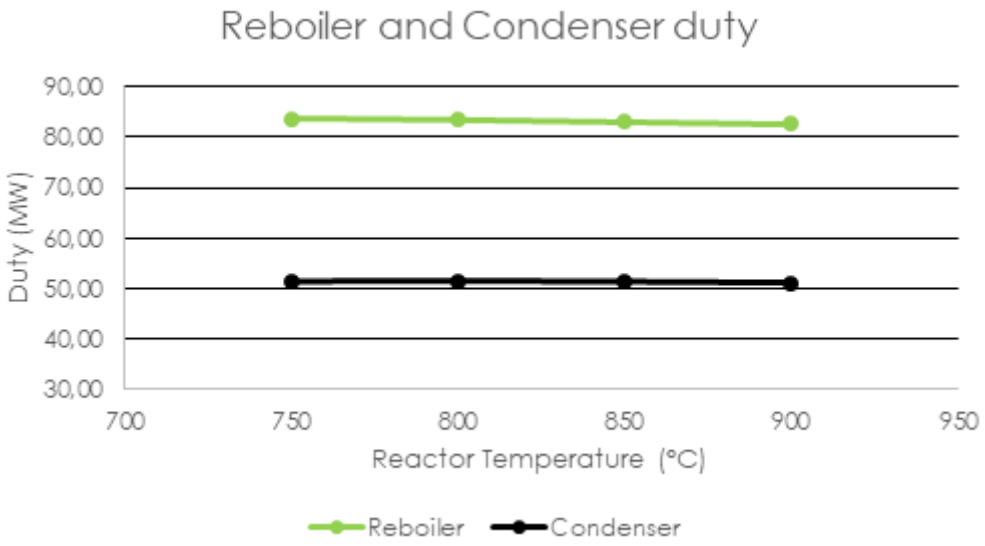

Figure 36: Effect of Reformer Temperature on Reboiler and Condenser Duty

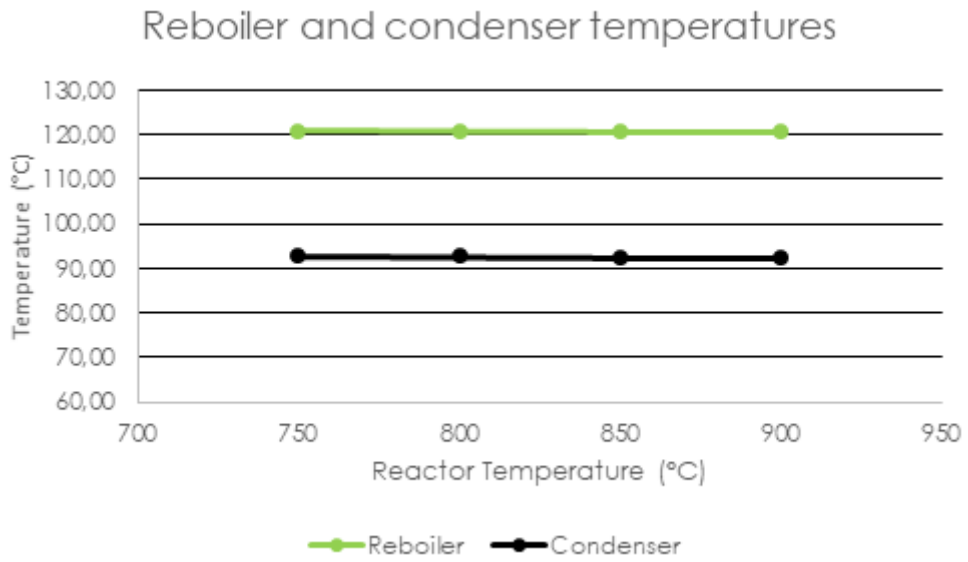

Figure 37: Effect of Reformer Temperature on on Reboiler and Condenser Temperatures

The reason for which this investigation was conducted was that the temperature level affects the molar flow and composition of the offgas exiting the WGS. This in principle could have an effect on the CCS part, that needs extra H_2O where MEA are dissolved to work properly. Since the CO_2 produced remains more or less the same, depending only on temperature levels and efficiencies of the WGS reactors that are unchanged, and H_2O is almost completely removed before the entering on the PSA, the trends of the reboiler and condenser operating parameters against reformer temperature show a very

weak dependence on the temperature of the reactor, mostly due to unreacted CH_4.
As far as values are concerned, it can be easily seen the condenser rejects around 2/3 of the heat required by the reboiler, at a temperature level of around 93 °C against 121 °C of the reboiler.

In conclusion, it has been noticed that the value of T=750 °C presents complications in terms of more input CH4 required, so such low temperature should not be reached in an optimized vision of the plant. The other temperature values, instead, are all feasible, even if the most efficient tradeoff seems to be recognized in **T=850** °C , which is only 50 °C higher than the the first modelling trial value(800 °C, [43]) and within the ranges that can be found in literature [43], [6], [41]. As a matter of fact, the value of T=850 °C allows the use of fewer resources in terms of CH4 in input to the plant, guaranteing a good methane conversion (76%) and a lower H2 dilution in the product gas at the exit of the absorber; moreover, T= 850 °C is a quite moderate temperature value, that implies reduced thermal stresses and the possibility of using materials less temperature-resistant and, consequently, less expensive.

4.1.2 Steam to Carbon Ratio

After that, it was decided to vary the S/C ratio between 2 and 3.5, as previously done by Antzara et al. [6], in order to see its influence on methane conversion and input fuel to the plant.
The former has a trend that reminds the one for reformer temperature, as shown in figure 38.

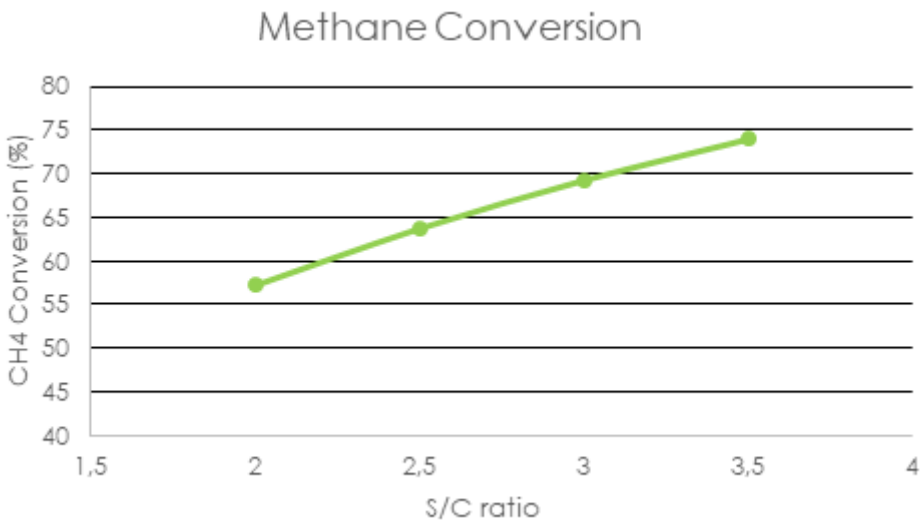

Figure 38: Effect of S/C ratio on CH_4 conversion

This could be explained by the fact that, when the concentration of reactants is higher, the rate of reaction is higher, pushing the reaction itself more towards the products because the probability of contact between the molecules of reactants increases. Obviously, this is not free in terms of resources: when S/C ratio increases, the reaction becomes more energy consuming and so more additional fuel is requested by the plant, as shown by figure 39.Moreover, since increasing S/C ration means increasing the quantity of water required, also the CH_4 requested by the H_2O boiler (reported on secondary axis, as before) increases linearly.

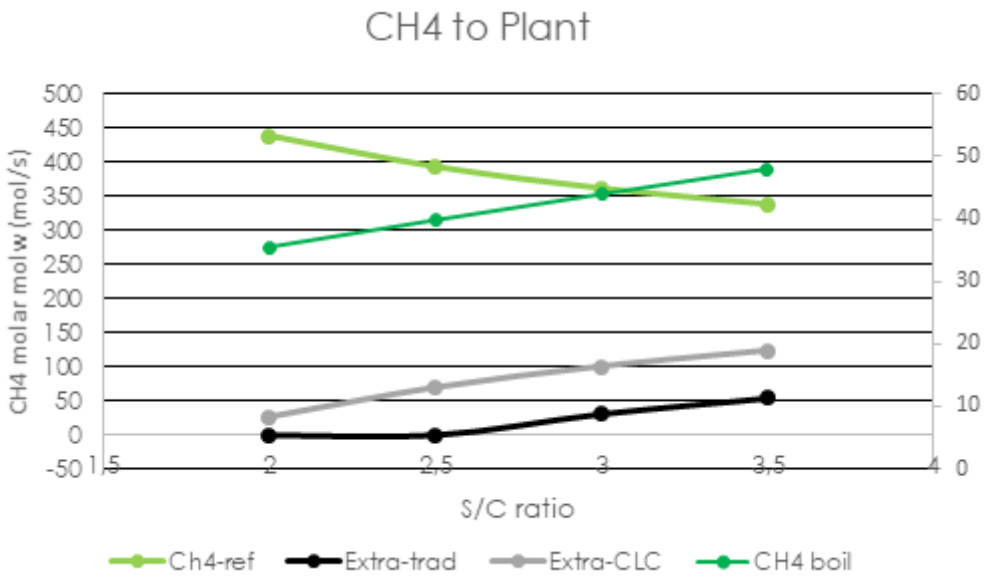

Figure 39: Effect of S/C ratio on on different CH_4 inlets to plants

Even in this case, the additional fuel for the traditional plant is always lower than the CLC plant. Finally, the total CH_4 required by the plants is shown in figure 40.

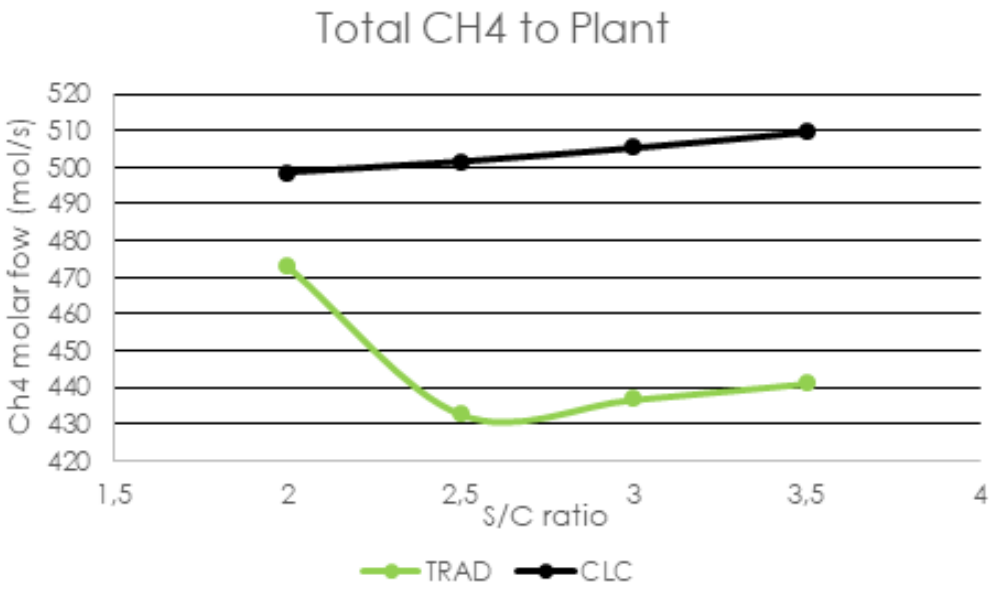

Figure 40: Effect of S/C ratio on total CH_4 inlet to plants

The trend is quite steady for CLC plant, while for the traditional one it appears to have a maximum at S/C=2. The difference in absolute values remains always in the 25-70 mol/s range, but the S/C ratio value that appears as the best tradeoff between input resources seems to be **2.5**: as a matter of fact, it is a good value that allows the use of less CH_4 as shown by the previous results, but also of process water. Thus, in the optimized configuration of the plants, this value will be chosen for final and techno-economical evaluations.

4.1.3 Reformer Inlet Pressure

The last parameter in the H_2 production part that was chosen to be manipulated is the reformer inlet pressure, by varying the discharge pressure of methane compressor and water pump from 10 to 25 bar, as proposed by Antzara et al. [6]. In addition, the value of p=30 bar was investigated, in order to understand the feedback of the plants also at pressures slightly higher than the attempt proposed in the models. As in the previous parts, the CH_4 conversion was considered, resulting to be inversely proportional to the inlet pressure, as shown by figure 41.

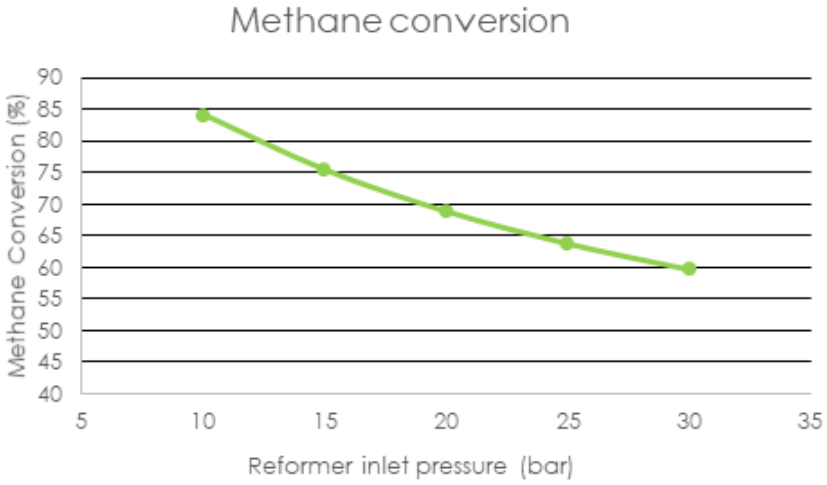

Figure 41: Effect of Pressure on CH_4 conversion

This indicates that the total reforming reaction (6) is not favoured by an increase in pressure, implying that more methane is necessary to substain the reactions at higher pressure. It can easily explained if Le Chatelier's principle is considered, whose general view is that the system tends to naturally re-establish the equilibrium that is broken by external perturbations. In this case, an increase in the gaseous pressure causes a decrease in the volume occupied by them, forcing the system to go towards a situation in which less volume is handled; thus, an increase in pressure pushes the reactions towards the direction where there is a decrease in the number of moles.
This can be seen analytically if the expression of $K_p(T)$, known as **equilibrium constant** of a reaction, is considered. $K_p(T)$ can be expressed through temperature dependences of the form [59]:

$$ln(K_p(T)) = C_1 + \frac{C_2}{T} + C_3 \cdot ln(T) + C_4 \cdot T \tag{66}$$

where C_1, C_2, C_3 and C_4 are fitting parameters that come from experimental results. Thus, at fixed and constant T, $K_p(T)$ is well defined and constant too; it can then be expressed as:

$$K_p(T) = \left(\frac{p}{p_0}\right)^{\sum_{i=1}^{N+M} \nu_i} \cdot \frac{\prod^P {y_i}^{\nu_i}}{\prod^R {y_i}^{\nu_i}} \tag{67}$$

where p_0 is a reference pressure that can be arbitrarily chosen (usually, 1 bar), ν_i is the stoichiometric coefficient of generic species i, with its sign (positive if i is a product, negative if i is a reactant), N and M are the numbers of reactants and products, respectively, and y_i is the molar fraction of generic species i.

It is worth noting that at fixed T, being $K_p(T)$ constant, if $\sum_{i=1}^{N+M} \nu_i > 0$ (i.e. the reaction has an incresing number of moles from left to right) and p increases, the second term of the product $\left(\frac{\prod^P {y_i}^{\nu_i}}{\prod^R {y_i}^{\nu_i}}\right)$ has to decrease, meaning that the equilibrium is shifted back to the reactants.
This completely explains why CH_4 conversion has the trend reported in figure 41 with pressure, and has the same implications in terms of additional fuel requested, since the unreacted methane is re-used in the heat production part of the plants. The trends of the 3 contributions of inlet fuel are reported in figure 42.

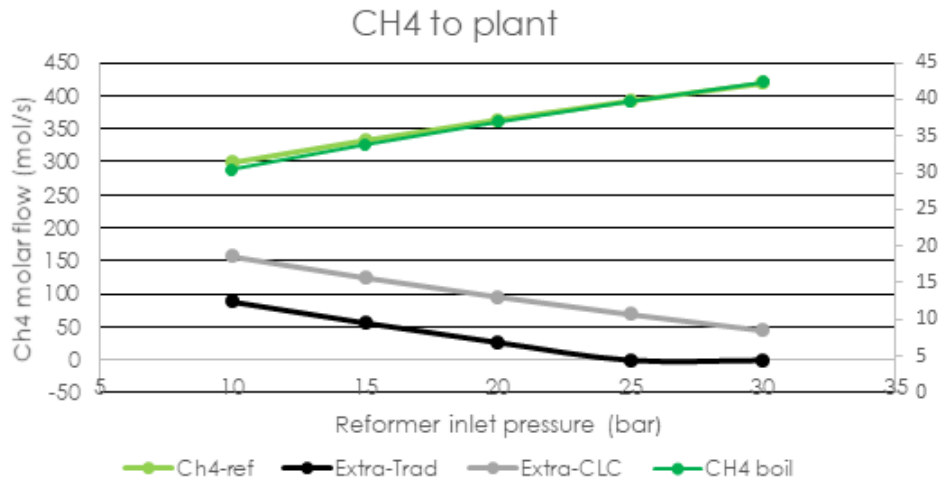

Figure 42: Effect of Pressure on on different CH_4 inlets to plants

It can be noticed the same positive difference between CLC and traditional plants in terms of additional fuel requested, while the trend is linear for each pressure level. Obviously, methane to the reformer increases linearly with an increase in pressure since its conversion decreases; in addition, when pressure increases, also saturation temperature increases, resulting in higher duty and fuel to be given to the H_2O boiler.
But as usual, in order to understand which pressure level gives the possibility to use fewer resources, the total CH_4 inlet fuel should be analyzed and is represented in figure .

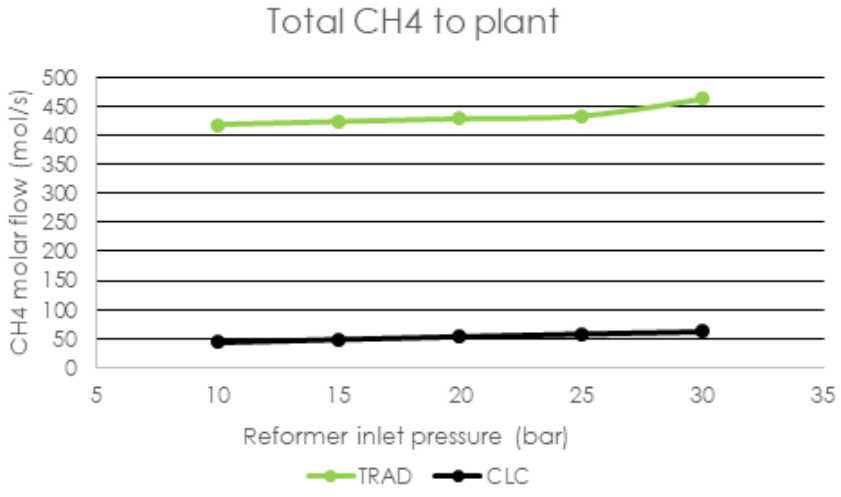

Figure 43: Effect of Pressure on total CH_4 inlet to plants

It can be noticed that varying this parameter has not a significant effect of the total CH_4 required by both plants, with a weak linear increasing trend. The only value to be avoided is p=30 bar, that causes an increment in total CH_4 required by the plant since there is an excess of unreacted CH4 also at the end of the reformer furnace. It is worth noting that such high values were not investigated by Antzara et al. [6], maybe due to these undesirable behaviours in terms of external resources needed. However, also in this last case differences are not so accentuated, and the gap in terms of CH_4 required by the two plants remain around 55-70 mol/s, depending on the pressure considered.
The last factor that needs to be taken into account is the electrical power needed by the auxiliaries, since it expects to increase by increasing the operating pressure. The values are reported in figure 44 .

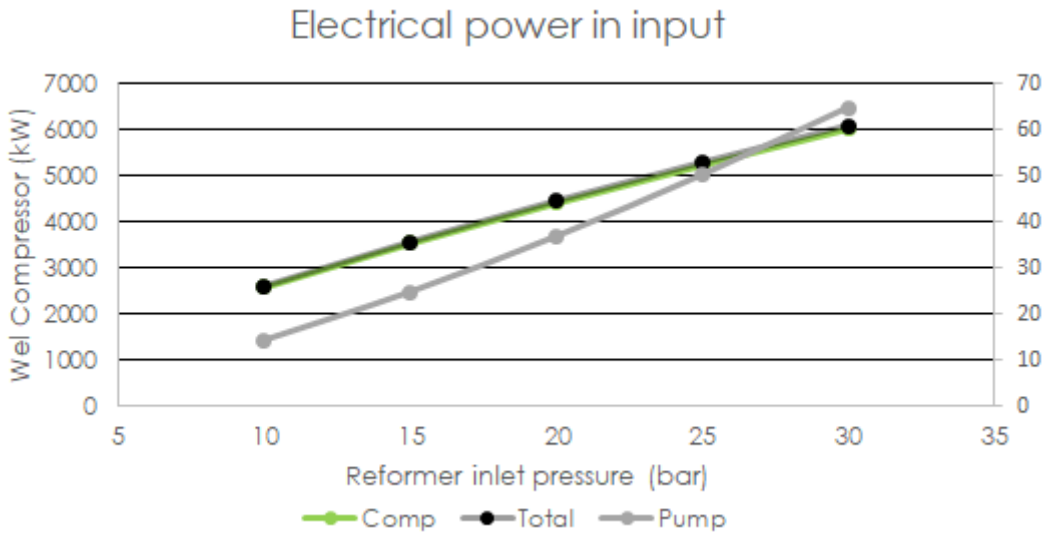

Figure 44: Effect of Pressure on electrical power in input to plants

Both compressor and pump electrical needs are reported, as well as the sum of the 2, that shows how the pump contribution is negligible with respect to the compressor one (2 orders of magnitude lower, reported in the secondary axis), as expected. Values are quite significant (6 MW for pressures around 30 bar) and should not be forgotten in a balance of plant analysis, while the trend is almost linear for each pressure level.
So, the choice of the pressure level should take into consideration the economics of both resources, trying not to go towards too high values. On the other hand, it would be desireable to work at significant pressures for two reasons:

1. When compressed, gases occupy less space. So, reactors can be smaller and also the infrastructures where they are located can be cointained, even if thickness of the material should be increase to substain those conditions;

2. If CO_2 capture is put in location 1 for traditional plant, a higher partial pressure would be a benefit for its adorption.

Thus, a good compromise between all those factors could be a pressure of **20 bar**, that would be the choice adopted for the analysis of the final configurations.

4.2 Fluid Bed Reactors

As stated before, the aim of this paragraph is to continue the detailed focus on fluid bed reactors modelization by getting all those results that came from the use of the advanced block, instead of the simple black box represented by RGibbs reactor.
After analyzing the results, an improved configuration was proposed for both the reactors. Finally, the influence of different PSD was also investigated, in order to understand if the value of mean diameter of 200 micron proposed by Lyngfelt et al. [17] was the proper option.

4.2.1 Fuel reactor

It was observed that the fluidbed reactor block requires in input several data, allowing the collection of multiple detailed results too.
So, the first data which can be obtained by ASPEN are the **molar flows** of each gaseous component over the reactor itself. Since ASPEN provides us only the molar compositions in each subdomain in which the height of the reactor has been divided, a mass balance for each component has been considered in each node of the ASPEN mesh. This led to m 3x3 linear systems, where m is the number of nodes, whose generic form for node i is:

$$\begin{cases} n_{CH_4 i+1} = y_{CH_4 i+1} \cdot (n_{TOT i+1} - n_{CH_4 i} + n_{CH_4 i+1} + \\ \qquad + n_{H_2O i+1} - n_{H_2O i} + n_{CO_2 i+1} - n_{CO_2 i}) \\ n_{CO_2 i+1} = y_{CO_2 i+1} \cdot (n_{TOT i+1} - n_{CH_4 i} + n_{CH_4 i+1} + \\ \qquad + n_{H_2O i+1} - n_{H_2O i} + n_{CO_2 i+1} - n_{CO_2 i}) \\ n_{H_2O i+1} = y_{H_2O i+1} \cdot (n_{TOT i+1} - n_{CH_4 i} + n_{CH_4 i+1} + \\ \qquad + n_{H_2O i+1} - n_{H_2O i} + n_{CO_2 i+1} - n_{CO_2 i}) \end{cases} \tag{68}$$

where y and n express, respectively, the molar fraction and flow of the species indicated in the subscript. Being the initial conditions at node 1 well known, since each stream entering and exiting a block is completely characterized, and getting the molar fractions by ASPEN data, each system can be solved in the unknowns $n_{CH_4 i+1}$, $n_{CO_2 i+1}$ and $n_{H_2O i+1}$ with the help of Matlab. Thus, it allows to understand the molar flow of each component over the height of the reactor, as shown from figure 45.

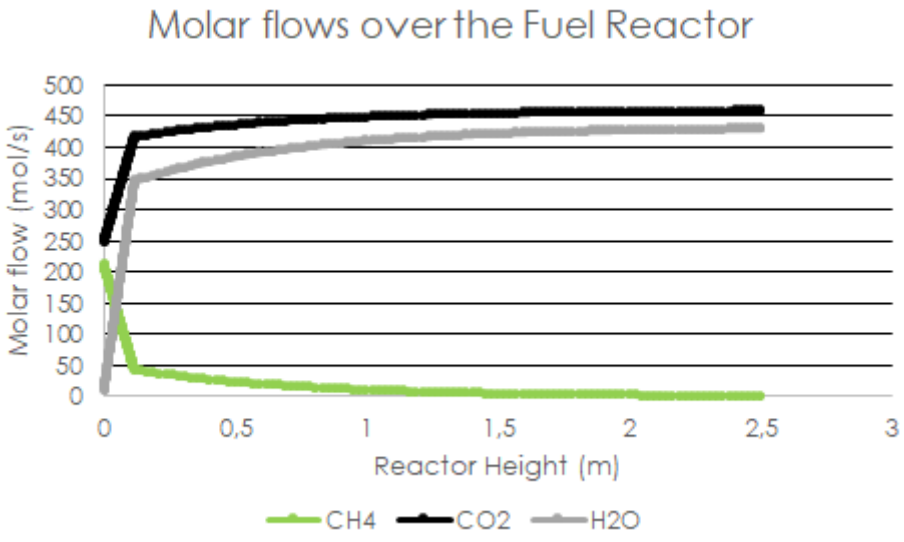

Figure 45: Molar flow of different species over the fuel reactor

From these profiles, it seems that the reactions occur mostly in the first part of the reactor (over 75% of CH_4 reacts), and then there is a "knee" from which the conversion becomes more gradual. This is due to the fact that particles are mostly concentrated in the bottom zone, where fluidization is not complete and gravity dominates. As a matter of fact, the height of bottom zone calculated by ASPEN is equal to around 0.12 meters, that corresponds to the point where sharp conversion starts to become much less accentuated. Since at about 1,5 meters the reaction seems to be almost completely developed, maybe the initial choice of the height is not optimal and can be reduced.
This particular behaviour has an important impact on the **velocities** of the gases over the height of the reactor, as shown by the figure 46 .

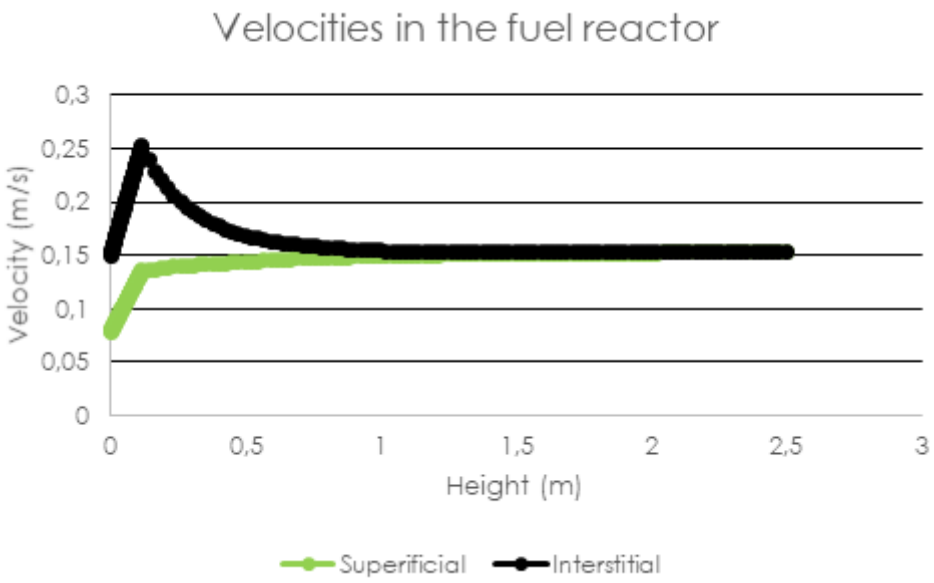

Figure 46: Velocities over the fuel reactor

Two different velocities are reported: the **superficial** velocity takes into account the entire cross section of the reactor for its determination, while the **interstitial** one is calculated by considering only the volume fraction occupied by the gases and not by solid particles.
It appears clear that their behaviours need to be necessarily different. While for the superficial one the trend follows literally the one of the CO_2 and H_2O molar flow, underlining its only strong dependence on the flowrate of gases passing through a constant cross section, the interstitial velocity has a different trend. As a matter of fact, If in the very first part the sharp production of gases makes it increase a lot in a linear way, at the end of the bottom zone it exponentially decreases up to the same values of the superficial one. It suggests that, when the product gas formation starts to become more gradual, there is still a significant part of solid matter that makes the interstitial velocity assume values higher than the superficial one, util they reach the same value at around 1,5 meters where particles are almost not present anymore: this is another signal that the first attempt in terms of reactor height was not the proper choice in terms of material usage and component performances.
In terms of absolute values, velocities are in the order of 0.1-0.2 m/s (also half for superficial one in the very first sections): such low values confirm the fact that fluidization is poor and needs very low orifices' diameter to occur.
The previous way of reasoning is then confirmed by the **solid fraction** profile over the height of the reactor, shown in figure 47.

Figure 47: Solid matter fractions over the fuel reactor

It confirms the idea that most of the solid particulate is kept in the bottom zone, making the reactions mostly occurr there, and that from 1,5 meters on there are no particles in the reactor, making that zone useless. Moreover, the trend of the solid fraction follows also the one of the distributed pressure drops over the reactor. This is explained by the fact that gases are more subject to friction and contact with particles when they pass through the first solid-dense zones. Moreover, if the same volumetric flowrate passes through a reduced cross section due to the presence of solid matter, velocities increases as seen before and this causes more pressure drops in the fluid passing through the particles and over the walls of the reactor. These factors are stricly interconnected, and their trends are reported in figure 48.

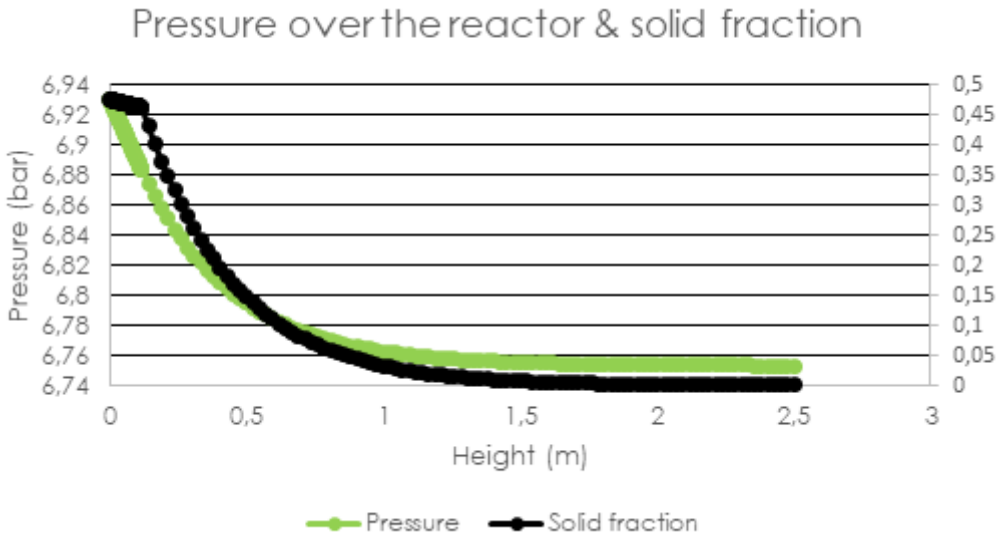

Figure 48: Solid matter fractions and pressure over the fuel reactor

It is clear that this reactor design is not the optimal choice for this kind of plants, and some geometrical parameters need to be rearranged in order to find a more efficient configuration. These considerations are presented in the following paragraph.

4.2.2 Improved Fuel Reactor

In order to work with a more efficient device, some geometrical improvements were implemented in the reactor.
First of all, the total height of the reactor was set equal to 2 meters, considering that the reaction was almost completelty developed after 1,5 meters. This value choice was dictated by the fact that it allows reduction of material but also a continuous conversion of fuel. As a matter of fact, if it was reduced up to 1,5 meters, the minimization method (48) used by the ASPEN mode would calculate a too high bottom zone that makes all the reactions happen there. With this new total height, the bottom zone resulted to be around 0,14 meters high, leading to the conversion profiles shown in figure 49.

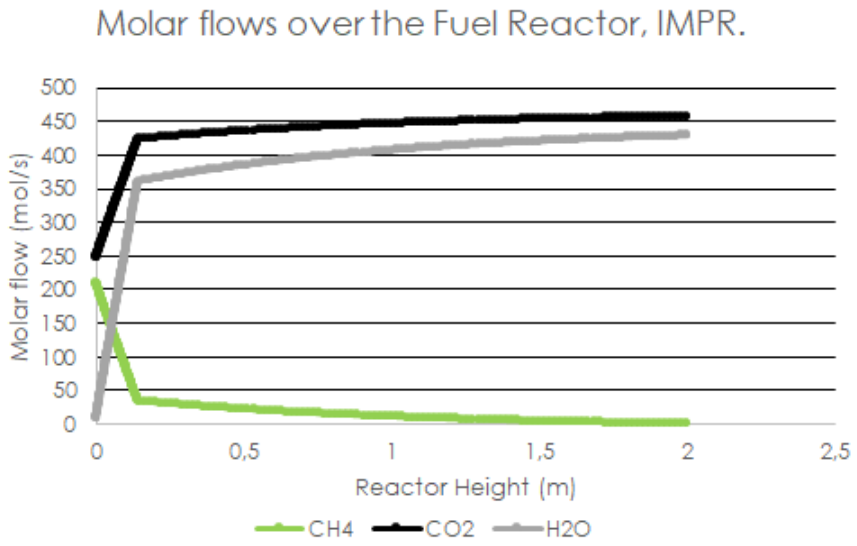

Figure 49: Molar flow of different species over the improved fuel reactor

Secondly, it has been decided to reduce the cross section in order not to make the reactor totally horizontal-disposed and to increase the velocities for a better fluidization.

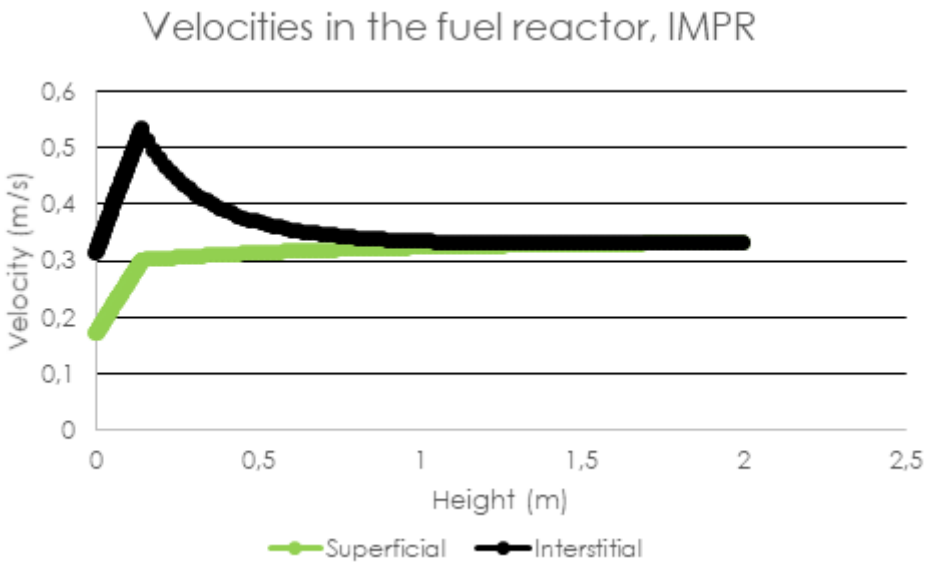

Figure 50: Velocities over the improved fuel reactor

The value chosen is a squared 6x6 m cross section, that brings with it a strong reduction in materials usage e leads to the velocity profiles shown in figure 50, even if reactor tubes need to be more "packed" due to reduction in space available.
In terms of absolute values, they reach around 2.5 times the previous ones, that confirms the effect of reduced cross section and slighlty increased height of bottom zone; anyway, the trend is perfectly tracing the non-optimized one, showing that the same effects of pressure and solid fraction are present.
So, the effective solid fraction trend is the expected one as shown in figure 51.

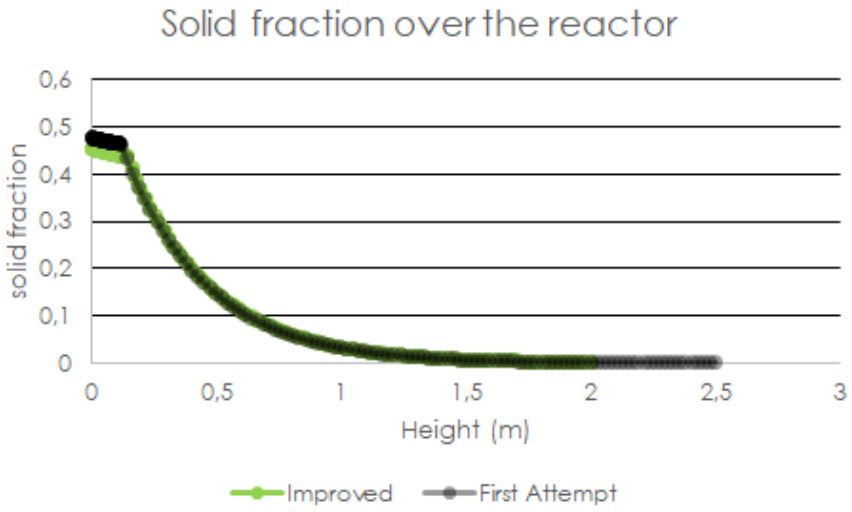

Figure 51: Solid matter fractions over the improved fuel reactor

As can be easily seen, the solid fraction trends are very similar, even if very slight decreases are present, especially in the part next to the bottom zone, while at the end thery are coincident. The values in the bottom zone are lower because more or less the same amount of material is present, and so being its height higher than previous case it needs to re-arrange in this way.
Finally, the pressure over the reactor is investigated as shown in figure 52.

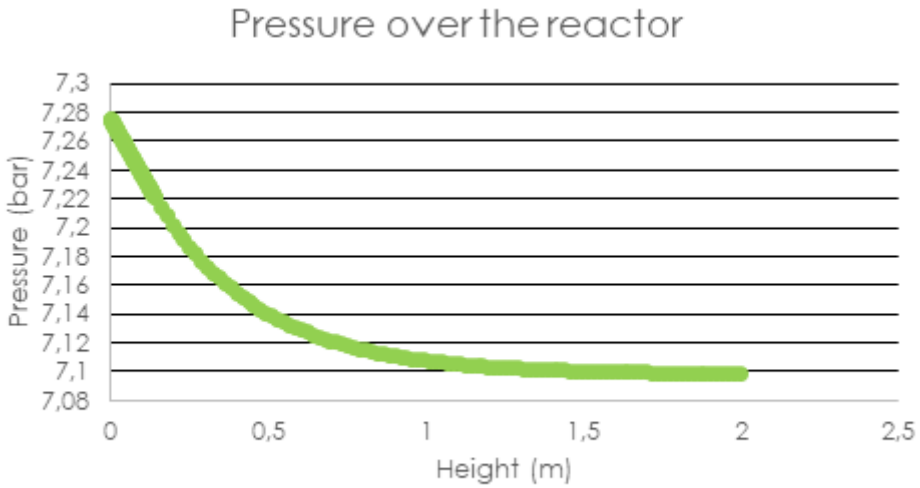

Figure 52: Pressure over the improved fuel reactor

It can be noticed that the trend is exactly the same as before, while values are slightly different in absolute terms. This is due to the fact that the strong pressure drops are due to the passage of the flowrate through very small orifices, with the small differences that can be reconducted to the different air flowrate into the reactor, that comes from stoichiometry starting from different values of CH_4, since pressure and temperature of reformer have been changed from the 1^{st} attempt.
In conclusion, the geometrical improvements undergone in the fuel reactor led to consistent savings in terms of space and cost for materials and to a better fludization, against a more compact layout of the reformer tubes inside it.

4.2.3 Air Reactor

As for the fuel reactor, also in the air reactor the same profiles and results can be extracted and analyzed.
First of all, it can be analyzed how oxygen present in the air reacts throughout the reactor, by making a simple mass balance on this component for each node of the height discretization, due to the fact that it is the only gaseous reacting specie. The resulting trend is shown in figure 53.

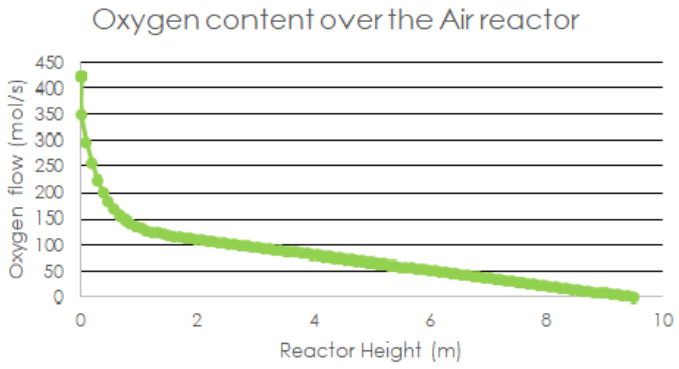

Figure 53: Molar flow of oxygen over the air reactor

It is clear that, being the fluidization higher, the reaction is much more well geometrically distributed than in the previous component, even if most of the reactions occur in the first zone as well. This behaviour is mostly due to the very low height of the bottom zone, that results to be 0,0034 meters (around 2 orders of magnitude lower than in the fuel reactor) and implies a more homogeneous distribution of the particles over the whole reactor. It is worth noting that almost all the oxygen reacts with the metal in the oxidation reaction, confirming that the stoichiometric approach followed in the definition of the model works well.
As usual, the two different kinds of velocity are analyzed and reported in figure 54.

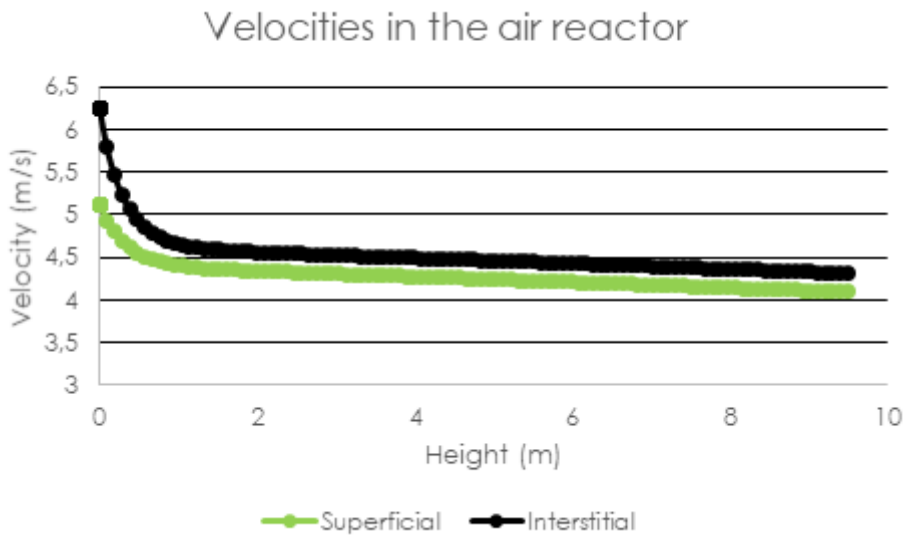

Figure 54: Velocities over the air reactor

The interstitial velocity remains higher than superficial for the same definition reason than before, while in this case the trend is always decreasing due to the fact that no gaseous products are present, but only disappearing reactants. Values are on the order of 5 m/s, meaning that substantial fludization regime has been established as required.
It can be noticed that, in this case, values never coincide: this can be due to the presence of solid matter in each section of the reactor. Moreover, the interstitial velocity follows a more accentuadet exponential decreasing trend in the first part; these last two factors can be the effect of the shape of the solid fraction over the reactor, as shown in figure 55.

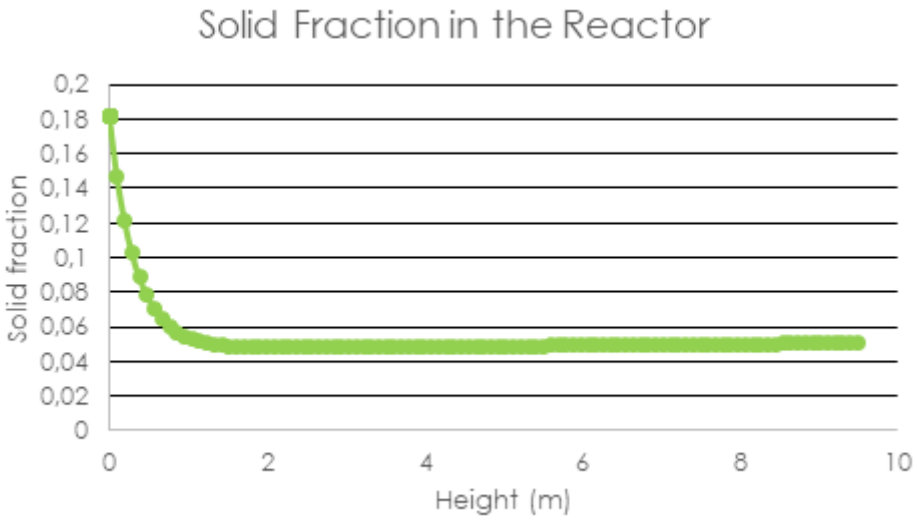

Figure 55: Solid matter fractions over the air reactor

The behaviour is consistent both with the velocities one, that shows an exponential decrease in the very first part and then becomes steady and non null from about 2 meters on.
Finally, the pressure behaviour is indicated in figure 56.

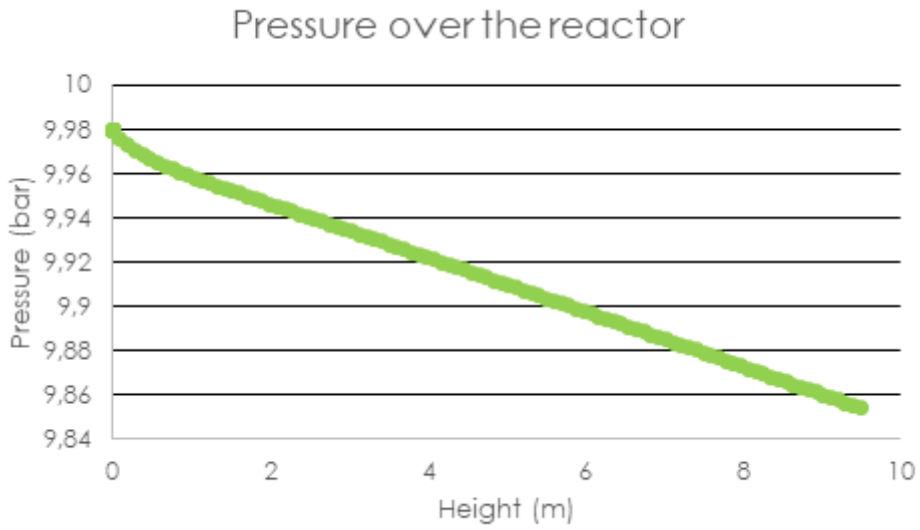

Figure 56: Pressure over the air reactor

It is evident that the trend is consistent with solid matter one (slightly more accentuated at the beginning and linear decreasing from about 2 meters on), while it is more interesting to notice that values remain quite high and similar to the pressure of the inlet air stream, equal to 10 bar. This is due to the very reduced concentrated pressure drops that occur at the exit of the orifices, being their diameter consistently high.
So, in the following part it is discussed how the system can be improved moving towards a more efficient and convenient device.

4.2.4 Improved Air Reactor

In this case, the geometry seems to be suitable to guarantee the fluidization required by the system, and since conversion appers to be quite gradual in each section of the reactor, there is no need of reducing the cross section.
But a significant parameter that can be varied in this case is represented by the open area of the orifices in the perforated plate of the bottom zone, defined as the ratio of the orifice area over the bottom surface of the reactor. As reported by Paiva et all, typical values for this parameter range from 0.1% to 8.6% [60]: in the analyis presented in this work, the lower value considered was 0,7%, since too low values would lead to extreme turbulent velocities in the reactor.
The monitored operating parameters were the maximum superficial velocity and solid fraction (happening at the inlet of the reactor), as well as the additional fuel requested and the pressure at the inlet of the reactor, whose behaviours are reported in the following figures.

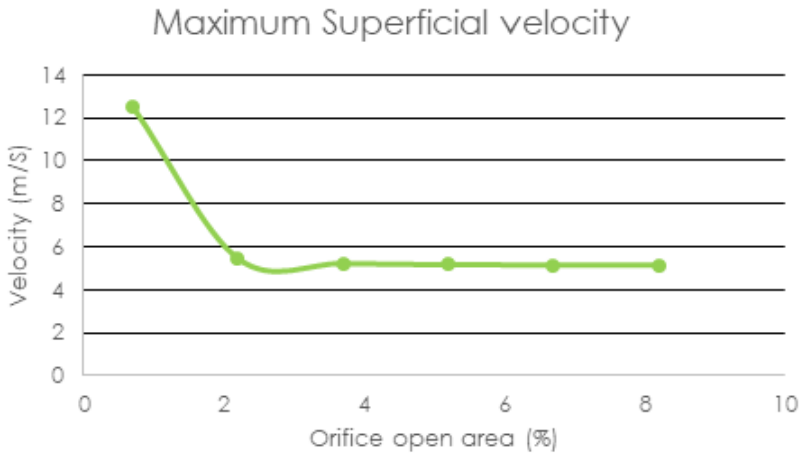

Figure 57: Maximum superficial velocity over different orifice areas

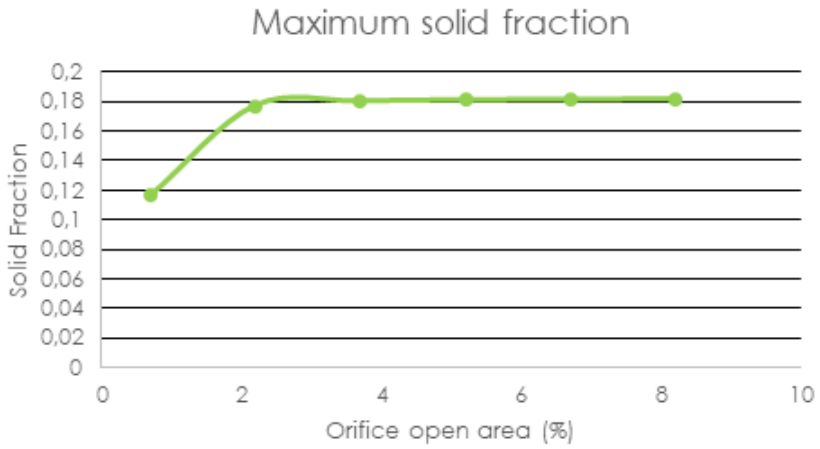

Figure 58: Maximum solid fraction over different orifice areas

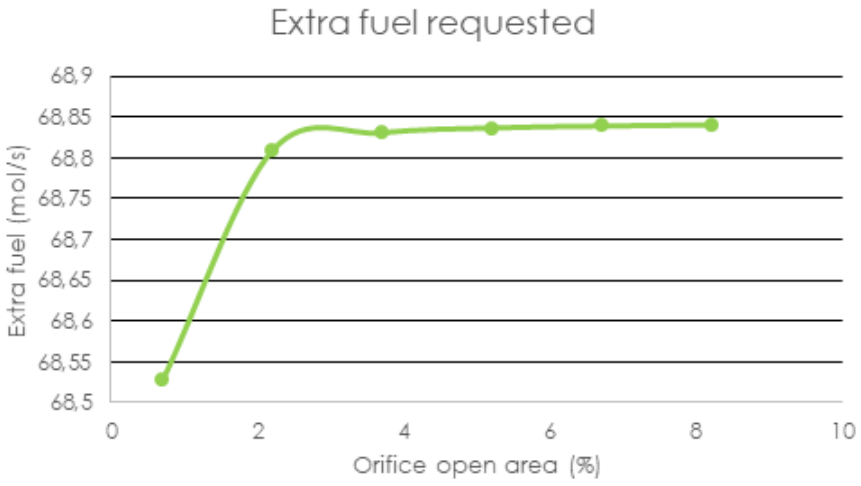

Figure 59: Extra fuel requested over different orifice areas

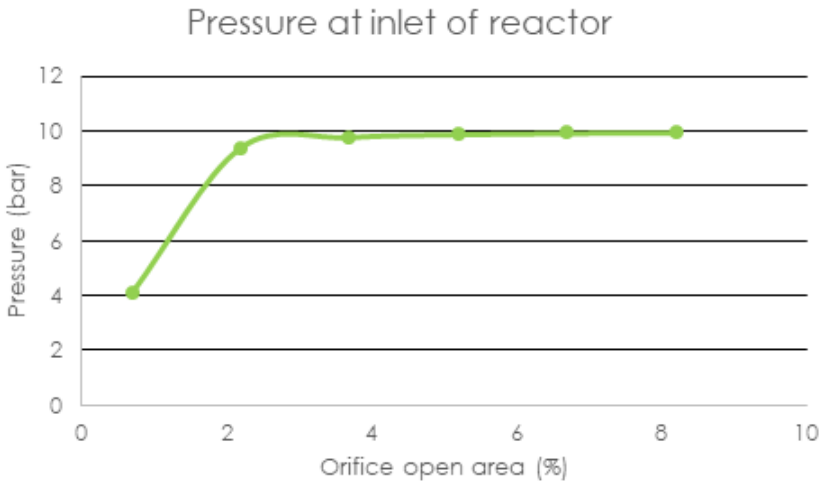

Figure 60: Pressure at inlet of reactor over different orifice areas

It can be easily noticed that, for each investigated parameter, a plateau is present from 2,2% on, even if for extra fuel requested the absolute variations are negligible also for the case at 0,7%. As far as maximum superficial velocity and inlet pressure are concerned, instead, the influence of the open area starts to become more significant: at 0,7% open area, the former becomes almost doubled due to the reduced section, while the latter has a sharp decrease (from around 10 to 4 bar) due to consequential concentrated pressure drops.
In conclusion, the value chosen for the improvement is 3,7%, a good tradeoff that corresponds to 60 orifices with diameter equal to 5,6 cm, around half of the first hypotesis values.
The reasons for this choice were multiple. First of all, it is a value for which velocities are maintained at desirable lveles; moreover, sharp depressurization does not occur, with an exit pressure of NiO of 9.78 bar against 10 bar of input in the fuel reactor. This allows to treat the model in open loop, ensuring a relative error lower than 2,2% and a faster convergence. Secondly, it allows to have a small part of the bottom surface that is drilled for the orifices: when open area increases, in fact, there are more stress intensity factors in correspondence to the holes, that leads to an increase in mechanical stress that makes more probable the collapse of the entire structure in case of accident.

4.2.5 Influence of Different PSDs

Finally, it has been decided to test other PSD values for investigating if deviations from the 200 micron mean value proposed in the model of Lyngfelt et al. [17] are optimal or not.
Three different Gaussian distributions were considered, with mean values respectively of 150,200, and 250 microns as reported in figure 61 and fixed standard deviation at 50 microns.

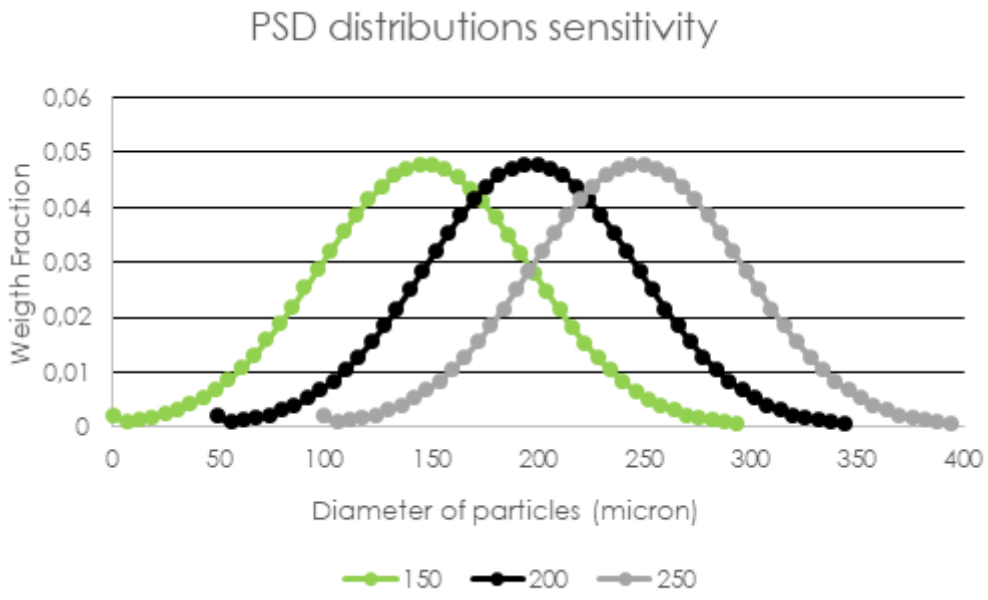

Figure 61: Different PSDs considered for sensitivity analysis

The influence on different parameters was analyzed, starting from the additional fuel to the plant which has the trend shown in figure 62.

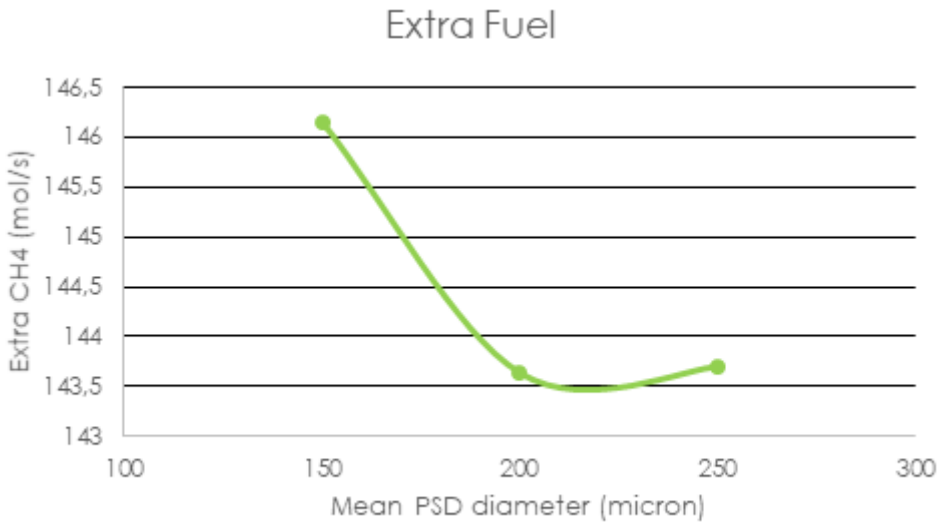

Figure 62: Influence of different PSDs on extra fuel requested

It is worth noting that if values are quite steady for 200 and 250 micron mean diameters, around 3 mol/s more are required to substain the reforming reaction in terms of heat if smaller particles are inserred. Moreover, since the modification has been introduced only in the heat supply part, leaving the H2 prodution one unchanged, these 3 mol/s of CH_4 are surely not compensated by a decrease in the CH_4 entering the reformer and need to be paid as extra input resource. The value of 150 microns seems to be not so interesting, indeed.
The influence on the interstitial velocities is shown in figure 63.

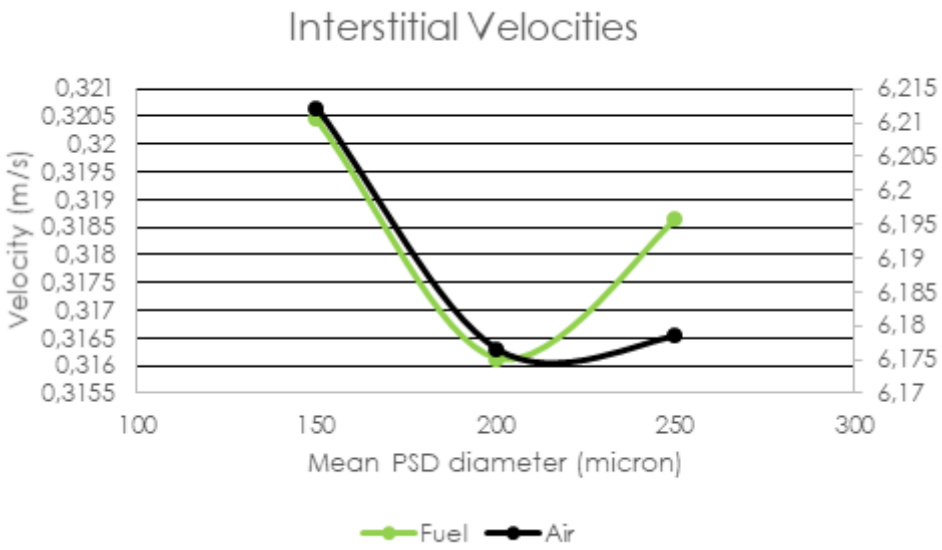

Figure 63: Influence of different PSDs on interstitial velocity

In absolute terms, there are not strong variations, even if minimums can be detected at 200 microns mean diameter. Since the analysis is proposed to the optimized solutions for the reactors, there is no need of fluidization (and consequently of high velocities) for the fuel reactor, so velocities can be maintained at lower and safer values that minimizes elutriation of unreacted particles out of the reactor.
This trend could be explained if the solid fraction profiles in the bottom zone is analyzed, as proposed in figure 64.

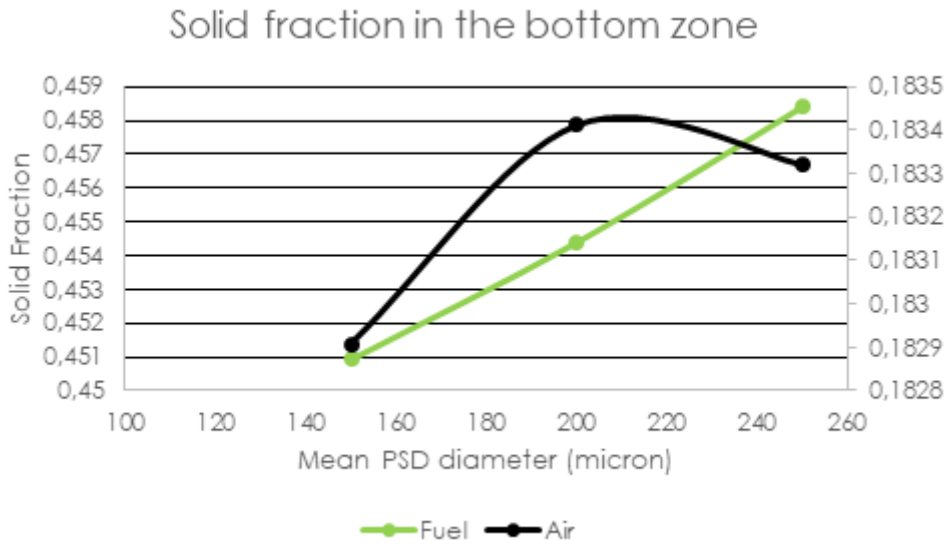

Figure 64: Influence of different PSDs on solid fraction in the bottom zone

As a matter of fact, in the fuel reactor solids fraction increases when mean diameter increases, as expected, while for air reactor variations are imperceptible.
But if for values from 200 microns on the extra fuel requested remains the same, for d=150 microns it has a sharp increase, that results in higher flowrates entering the fuel reactor and, consequently, also the air one (since the needed air is calculated as the stoichiometric one in the model). If the open area and the cross section are maintained constant, an

increase in volumetric flowrate results in an increase in velocity reported for the case at d=150 microns.
Finally, the effect on inlet pressure in the reactors is analyzed as shown in figure 65.

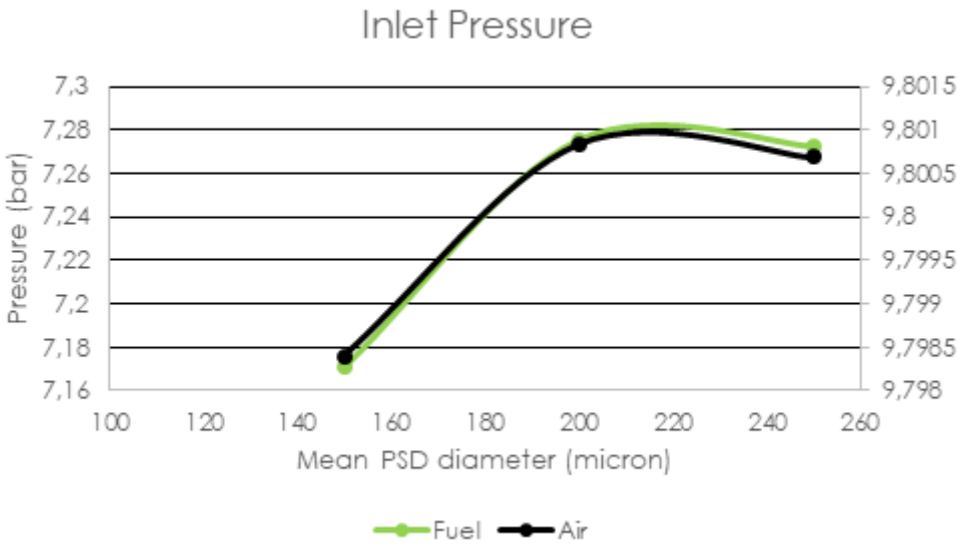

Figure 65: Influence of different PSDs on inlet pressure to the reactors

Both the trends are steady for values from 200 microns on, even if in absolute terms in the air reactor the variation is imperceptible also for d=150 microns, whereas for the fuel one the depressurization appears to be more conistent, but always cointained (around 0.1 bar).
In conclusion, the value of 200 microns chosen by Lyngfelt et al. [17] results to be the best option since, in addition to avoiding problems in extra resources and pressure drops at fuel reactor inlet, guarantees the lowest value of solid fraction in the bottom zone of both reactors (among the remaining value of 250 micron). This implies a better homogenization of the solid matter over the reactor and, consequently, a better distributed conversion of fuel and oxygen.

4.3 MEA in Post-Combustion location

In order to have a clearer picture of the traditional plant, it was decided to analyze some key parameters of the plant if the MEA-based adsorption system were put to treat the final offgas in location 3. They are reported in the form of comparison with Pre-PSA location (location 1) in table 17:

	Pre PSA (loc. 1)	Post Combustion (loc. 3)
Absorber diameter (m)	3	10
Absorber packed height (m)	4	9
Stripper diameter (m)	16	14
Stripper packed height (m)	13,5	12
Absorber Pressure (bar)	16	1
Absorber stage 1 temp. (°C)	98,92	45,95
Stripper duty (MW)	84,21	114,44

H_2O in CCS Loop (mol/s)	2535	3595
MEA in CCS loop (mol/s)	539	764
CO2 captured (%)	57,13	90
Extra fuel (mol/s)	81,81	100,95
Extra fuel (MW)	65,45	80,76

Table 17: Comparison between MEA locations 1 and 3

First of all, since the volumetric flowrate of gaseus products to be treated is changed, in Post Combustion CCS system the absorber and stripper dimensions have been chosen proportionally to the inlets and outlets quantities. In particular, the new absorber is much bigger than before, due to the high quantity of N_2 that enters it, while the stripper is smaller due to reduced outlet temperature of the gaseous $CO_2 - H_2O$ mixture.

Moreover, as anticipated in section 2.2.3 , location 1 has the benefit to be pressurized (16 bar), while adsorption in location 3 occurs at atmospheric pressure. Thanks to higher pressure, CO_2 absorption in location 1 is more favoured as stated by the Henry Law, where concentration of the species in the solution is proportional to its partial pressure in the starting gaseous mixture. This could be easily observed by looking at the temperature of the liquid outlet at absorber bottom stage: in the first case, temperature is 53 °C higher than in post combustion one, meaning that exothermic adsorption reactions are favoured.

The effect of pressure, combined with higher quantity of gas to be treated, can be also seen in the resources required for making CO_2 adsorption occur at same efficiency rate (90%). As a matter of fact, location 3 requires about 42% more H_2O and especially MEA to be inserred in the CCS loop, leading to higher costs of resources and infrastructures materials, like pipes. Besides, stripper duty results to be higher due to increased flowrate of liquid solution to regenerate, resulting in additional waste heat to be provided. In case it were not be sufficient to use waste heat from near facilities, additioal fuel would be requested to substain the stripping process.

In addition, since in Post-Combustion layout all the CO_2 produced by WGS reactions is not eliminated before entering the reformer furnace, its presence makes it necessary to introduce more additional fuel to the reformer furnace (about 19 mol/s) to be heated.

Concluding, Post-Combustion location is clearly not the best one in terms of operating conditions that promote CCS processes, but has the significant advantage of enabling the plant to capture much more CO2 than in location 1 (90% against 57%).
Thus, it is worh noting that there is not a better location in absolute terms, but the choice of the plant layout should take into consideration what objectives it wants to maximize: location 1 is the best solution for economic plans, while location 3 becomes of relevant importantance when environmental issues become the main problems to be managed and solved.

4.4 Final Comparison and Considerations

After deeply analyzing each plant and chosing the best configuration, a sum up of the most important operational indicators for traditional plant with pre-PSA MEA and CLC one is presented in table 18.

	Traditional SMR	CLC driven SMR
CH_{4in} (mol/s)	311,63	311,43
CH_{4in} (MW)	249,30	249,14
H_2O_{in} (mol/s)	779,07	778,57
Extra fuel (mol/s)	81,81	143,64
Extra fuel (MW)	65,45	114,91
Total CH_4 to plant (mol/s)	425,03	486,65
Total CH_4 to plant (MW)	314,76	364,05
CO_2 captured (%)	57,13	100,00
CO_2 purity (%)	97,29	98,45
CH_4 conversion (%)	80,53	80,58
H_2 yield (%)	99,62	99,62
Electric power in (MW)	30,59	54,53

Table 18: Final Comparison between Traditional and CLC plant

As already stated and supported by these data, parameters regarding the first part of the plants are substantially the same, since changes in the arrangement of different equipment are present only in the second part and no operational condition of the first part has been changed from one plant to the other.

It can be enhanced that both the plants need around 311 mol/s of CH_4 entering the reformer as well as exactly 2.5 times the quantity of H_2O (779 mol/s), with a good CH_4 conversion (around 80%) and excellent H_2 yield (close to 100%).

The big difference is provided by the fact that the traditional plant requires around 62 mol/s less of additional fuel requested, with a reduction of around 13% of the total CH_4 requested by the plant (425 mol/s against 487 mol/s). This can be reasoably due to the increased complexity of the heat supply process in the CLC plant (coupled redox reactions in fluid bed reactors where only the oxygen carrier oxidation has to be able to provide heat both for its subsequent reduction and methane reforming, against a simple combustion in a furnace). This is reflected in an increase in the operational costs of the CLC plant against the state of the art that needs to be accurately managed and taken into account. In any case, the difference is not so accentuated, and thus it can be concluded that CLC technologies can be a good competitor to tradtional SMR in the next future due to their good operations.

Another weak point of the CLC plant from the operational point of view is the higher electrical power needed to make the complete system work. As a matter of fact, it requires around 55 MW to work, against 31 MW for the traditional plant, with an increase of around 78% of the input electrical power. The reason for that relies on the additional compressors for offgas and air needed to pressurize the inlets to the fluid bed reactors in the CLC plant, that are not present in the traditional one, whereas only an additional little pump is needed to slightly increase the pressure of the CO_2 rich outlet stream of the absorber. The impact of each single component on the total energy requirement is shown in figures 66 and 67.
It can be easily noticed that in the CLC plant the two compressors account for the 44%

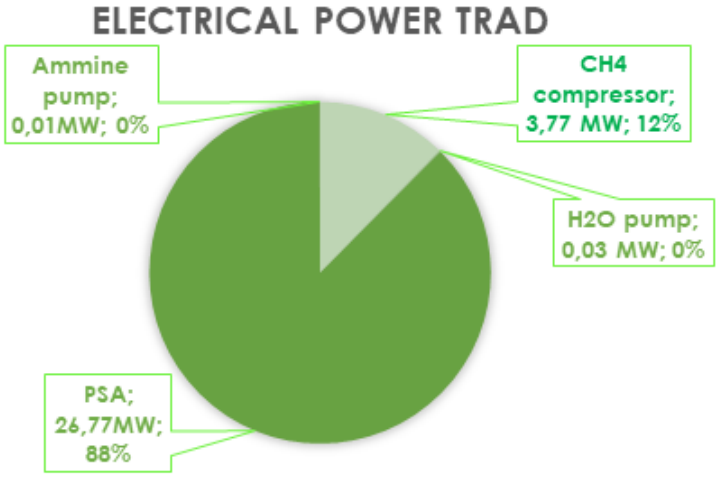

Figure 66: Allocation of electrical input power, Traditional SMR

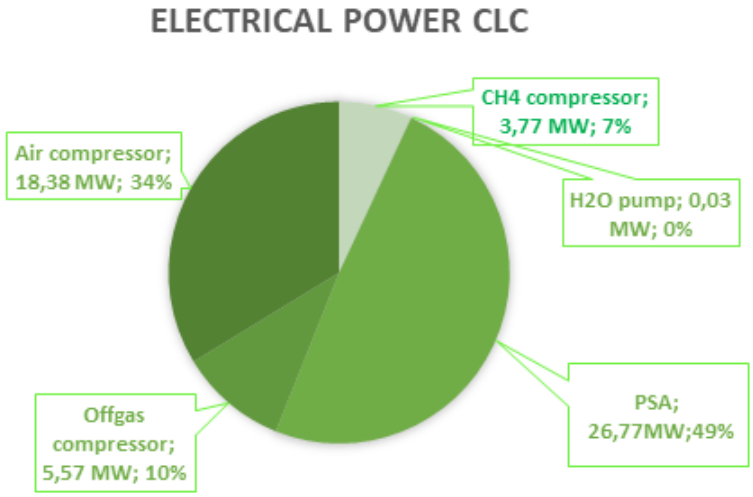

Figure 67: Allocation of electrical input power, CLC driven SMR

of the total consumption, while the most energy-demanding device remains the Pressure Swing Adsorption, since it has to be cyclically pressurized and depressurized in order to make the selective sorbents work properly. Due to the fact that PSA was modelled as a simple separator, its energy demand needed to be evaluated on literature basis, where a value of 0,3 kWh/Nm^3H2 was found and adopted for calculations [61], resulting in 26,77 MW power requirement. Moreover, pumps for water and MEA solution require a negligible energy provision as expected.

In the end, it was found that the strength of the CLC plant relies in the complete CO_2 capture and removal with a simple condenser locate in end-of-pipe position, while the ammine-based system is able to catch only a part of the CO_2 entering the absorber (in this model, this value has been set to 90%) and additional CO_2 is produced by the offgas combustion, leading to an overall 57% CO_2 captured. This deserves also economic considerations, since non-negligible carbon taxes are applied to CO_2 emissions: the best purely economic tradeoff needs to account also for these aspects.

Finally, CO_2 purity remains quite high in both cases (97-98%), depending mostly by the operative conditions of the final condenser that separate it from water.

5 Techno-Economic Analysis

Finally, both plants are evaluated in terms of economic feasibility in order to understand their penetration potentialities in the market. The economic indicators of similar plants were already evaluated in literature [41] [62] [63]. In order to perform such an assessment, the calculation of CAPEX (CAPital EXpenditure) and OPEX (OPerative EXpenditure) is necessary, that needs to be integreted with a cash flow analysis; these three main parts are singularly analyzed in different subsections.

5.1 CAPEX

In order to estimate the CAPEX, the cost of the bare plant main equipment needs to be calculated. Moreover, in order to take into account all those facilities and infrastructure that are not included in the basic equipment, the cost of basic equipment needs to be increased considering reference value found in literature. By doing this, the different levels of capital cost are calculated.

5.1.1 Cost of Components

The first step of the economic assessment of a plant is the calculation of the cost of its basic components. This is done by following an approach based on cost-functions of the following form [64]:

$$\log_{10} {C_p}^0 = K_1 + K_2 \cdot \log_{10} A + K_3 \cdot (\log_{10} A)^2 \tag{69}$$

where ${C_p}^0$ is the bare cost of the component (\$), K_1 K_2 and K_3 are fitting constants that are characteristic of the single component and A is the value of the capacity parameter of the single component, that is taken as representative of its size. In particular, for the components present in these plants, A could be represented by:

- The **Fluid Power (kW)** for compressors, that is an indication of how much power is given to the gas to be compressed;
- The **Shaft Power (kW)** for pumps, that is an indication of how much mechanical power is needed to run the device;
- The **Duty (kW)** for burners and water boilers, that is an indication of the thermal power given to the fluids;
- The **Surface Area (m^2)** for heat exchangers, coolers and condensers, that can be easily calculated by the following relationship:

$$S = \frac{\dot{Q}}{U \cdot \Delta T_{ML}} \tag{70}$$

where S is the surface area (m^2), $\dot{Q}$ is the heat exchanged in the component (W), U is the global heat transfer coefficient $\left(\frac{W}{m^2 K}\right)$ and ΔT_{ML} is the average temperature difference between the two sides of the heat exchanger, that can be expressed as follows:

$$\Delta T_{ML} = \frac{\Delta T_I - \Delta T_{II}}{ln\left(\frac{\Delta T_I}{\Delta T_{II}}\right)} \tag{71}$$

where ΔT_I and ΔT_{II} are, respectively, the temperature differences at the the opposite ends of the component. By doing this way, it is possibile to use a compact relationship as (70) for the whole heat exchanger, not considering the fact that the temperature difference varies over its length.
The global heat transfer coefficient U was chosen from literature ranges for each type of device and heat transfer media [65].
The details for the dimensioning of each heat exchanger are shown in appendix A, tables 28 and 29. It is worth noting that, for condensers or coolers, water from 15 to 30 °C was chosen as reference cooling fluid.

- The **Volume** (m^3) for all the process vessels used in the plants, that comprise the reformer, both the WGS reactors, the absorber, the stripper and the PSA. As far as the asborber and the stripper are concerned, the geometric dimensions are one of the input of the model; thus, the volume can be easily calculated from these data. On the other hand, black boxes in geometrical terms were used to model the other process vessels in the plants, so their volume should be evaluated by following another pathway. Thus, since the volumetric flowrates of gases that pass through the vessels can be extracted by ASPEN, it was sufficient to find the average residence time τ (s) of the compounds inside each vessel to find the required volume according to the following realationship:

$$V = \frac{\dot{V}_{in} + \dot{V}_{out}}{2} \cdot \tau \tag{72}$$

where V is the volume (m^3), while $\dot{V}_{in}$ and $\dot{V}_{out}$ are, respectively, the volumetric flowrates of the streams entering and exiting the specific vessel. An average value between $\dot{V}_{in}$ and $\dot{V}_{out}$ is considered since their values are different, due to different operating conditions at the inlet and outlet of the vessels and the chemical reactions that happen inside them. The values of $\dot{V}_{in}$ and $\dot{V}_{out}$ extracted by ASPEN, together with the values of τ taken by literature [66] [67] [68], are reported for each specific component in table 19.

Component	$\dot{V}_{in}\left(\frac{m^3}{s}\right)$	$\dot{V}_{out}\left(\frac{m^3}{s}\right)$	τ **(s)**	**Volume** (m^3)
REF	3,87	7,85	5,6 [66]	32,8
HIGH T WGS	5,05	4,59	2,3 [67]	11,1
LOW T WGS	4,59	3,68	2,3 [67]	9,5
PSA	2,13	2,13	172 [68]	356,6

Table 19: Characteristics of process vessels

As far as the **CLC Reactors** are concerned, instead, no specific cost functions were found in literature to express their cost in a precise way. Thus, it was estimated by scaling another cost found in literature on the basis of H_2 productivity.
After estimating ${C_p}^0$, a correction needs to be implemented in case the value of the parameter A falls out the validity ranges of equation (69), that are specific for each type of component. The relationship that needs to be used is the following:

$$ {C_p}^0{}_C = {C_p}^0 \cdot \left(\frac{Q}{Q_B} \right)^n \tag{73} $$

where ${C_p}^0{}_C$ is the cost of the component after the scaling correction, Q is the capacity value (that coincides with the value parameter A), Q_B is the capacity value of the reference case and n is the cost exponent, that is specific of the component. In other terms, if Q is larger than the entire range, Q_B is represented by the highest value of the range; if Q is lower than the entire range, instead, Q_B assumes the lowest value of the range. The values of n are taken by literature [66], and they are representative of how much the deviation in the capacity parameter influences the deviation in the costs. In case no specific components can be found in literature, a value of 0,6 was chosen according to the so called Six-Tenth Rule [69]; the value of 0,6 is, indeed, an average one between the ones that were evaluated in literature.
Finally, since the intent is to propose an analysis that can be useful for present purposes, it was necessary to apply another correction to take into account time deviations of the cost of components. This is done by means of CEPCI (Chemical Engineering's Plant Cost Index), that are provided year by year and can be used to convert a cost from one reference year to another with the help of the following relationship:

$$ C_y = C_x \cdot \left(\frac{CEPCI_y}{CEPCI_x} \right) \tag{74} $$

where the subscripts x and y refer, respectively, to two different reference years.
For this work, the values that need to be collected are the ones for 2009 and 2016, since costs were estimated by literature references written in those years, and obviously the one of 2019 to make them actual. They are briefly summarized in table 20.

Year	**CEPCI**
2009	521,9 [70]
2016	541,7 [71]
2019	619,2 [72]

Table 20: CEPCI for different years

All the parameters used to calculate ${C_p}^0$, ${C_p}^0{}_C$ and ${C_p}^0{}_{C2019}$ and their resulting values are shown in Appendix A, tables 30 and 31, for both plants. The total cost of components resulted to be around 12,5 M$ for the traditional SMR plant, and 17 M$ for the CLC one.

5.1.2 Levels of Capital Cost

In order to take into account all the staff that surrounds the basic equipment needed to run the plants, an approach described by NETL was followed [73]. It basically consistes in considering some percentage increases to be applied to other values previously calculated (the bare cost of components, for example). Thus, CAPEX could be sudbdivided into 4 different levels that accounts for different extra services or infrastructures to be paid. Specifically, the levels are:

1. The **Bare Erected Cost (BEC)**, that accounts for the cost of components and the infrastructures and facilities surrounding the equipment, as well as all the labour necessary to erect them. Its different contributions are:

   - The cost of components, calculated in the previous paragraph;
   - Each process utilities and offsite units costs, estimated to be around 25% of the main plant subsystems cost, that is the cost of components [41];
   - Pipes, valves, instrumentation, electrical and other components, estimated to be around 20% of the main plant subsystems cost plus the offsite units and utilities [41];
   - Building and structure costs, estimated to be around 40 % of the main plant subsystems cost plus the offsite units and utilities [41].

   The BEC resulted thus to be around 25 M$ for the traditional plant and 34 M$ for the CLC one.

2. The **Engineering, Procurement and Costruction Cost (EPCC)**, that accounts for the BEC with the addition of all those costs associated to services such as contractor permitting, engineering design and general management costs. Its additional different contributions are:

   - The installation cost factor, estimated to be around 60% of the total equipment cost (coincident with the BEC) [41];
   - The engineering and supervision, estimated to be around 15% of the total equipment cost [74];
   - The contractor fees, estimated to be around 20% of the total equipment cost [74].

   The EPCC resulted thus to be around 48,7 M$ for the traditional plant and 66,5 M$ for the CLC one.

3. The **Total Plant Cost (TPC)**, that accounts for the EPCC and all those contingencies that can follow the adoption of such a project. Its additional different contributions are:

   - The process contingencies, that are estimated to be 10% of the EPCC for the traditional plant, and 25% of the EPCC for the CLC one [73]. The contingencies are different between the two cases since, while traditional SMR is a mature and well established technology in the blue hydrogen production market, only some demo plants are operating for the CLC one [37].
   - The project contingencies, that are estimated to be around 15 % of the sum of EPCC and process contingencies [74].

The TPC resulted thus to be around 61,5 M$ for the traditional plant and 95,7 M$ for the CLC one.

4. The **Total Overninght Capital (TOC)**, that accounts for the TPC and the owner's costs, including the cost of land. Its additional different contributions are:

   - The owner's costs (pre-production, inventory capital, financing and others), estimated to be around 15% of the TPC [41];
   - The cost of land, estimated to be around 15% of the TPC [41];

   The TOC, and consequently the CAPEX, resulted thus to be around **77 M$** for the traditional plant and **120 M$** for the CLC one.

Finally, the different costs for each contribution assessed are summarized in table 21.

Level			**Trad**	**CLC**
BEC	Main plant subsystems	Cost (M$)	12,48	17,06
	Utilities and offsite units	% of main subsystems	25%	25%
		Cost (M$)	3,12	4,27
	Pipe, valves, instrumentation etc.	% of (main subsystems + utilities and units)	20%	20%
		Cost (M$)	3,12	4,27
	Building and structure	% of (main subsystems + utilities and unit)	40%	40%
		Cost (M$)	6,24	8,53
	BEC	Cost (M$)	24,97	34,13
EPCC	Engineering and supervision	% of total equipment 15%	15%	
		Cost (M$)	3,74	5,12
	Installation	% of total equipment	60%	60%
		Cost (M$)	14,98	20,48
	Contractors fees	% of total equipment	20%	20%
		Cost (M$)	4,99	6,83
	EPCC	Cost (M$)	48,68	66,55
TPC	Process contingencies	% of EPCC	10%	25%
		Cost (M$)	4,87	16,64
	Project contingencies	% of (EPCC + Process contingencies)	15%	15%
		Cost (M$)	8,03	12,48

	TPC	Cost (M$)	61,58	95,66
TOC	Owner's costs	% of TPC	15%	15%
		Cost (M$)	9,24	14,35
	Land	% of TPC	10%	10%
		Cost (M$)	6,16	9,57
	TOC	Cost (M$)	76,98	119,57

Table 21: Different Levels of Capital Cost, Details

5.2 OPEX

After estimating the capital investment needed to build the plants, the yearly operational expense needs to be calculated too. The fundamental assumption that governs the whole OPEX analysis relies in the yearly operational hours, that were considered to be equal to 8000 [41].
OPEX can be easiy sudvivided into **direct and fixed manufacturing costs**, together with other additional costs that are considered as **general expenses**.
Staring with direct manufacturing costs, the first and most important contribution to them is certainly the cost of **raw materials**, that can be resumed into 3 macro-categories:

1. **Natural Gas**, which represents the most consistent expenditure, whose price (8,7 $/GJ) was taken from Eurostat reference for non household medium size consumers, at 2019 snd considering European average price [76].

2. **Electricity**, which stands for another big slice of the total, whose price (0,0957 $/kWh) was taken from Eurostat reference for non household medium size consumers, at 2019 snd considering European average price too [77].

3. **Process water**, which does not accounts for a great part of the total OPEX, but needs to be considered in the global balance. Its cost was found in literature, assumpted to be about 0,11 $/ton [75].

The costs of each raw material, for both plants, are reported in table 22.

Raw Material	**Cost TRAD (M$/year)**	**Cost CLC (M$/year)**
CH_4	91,8	105,8
Electricity	23,4	41,7
Process Water	0,054	0,046

Table 22: Raw Materials costs comparison

Another cost to be considered is the **substitution** of the MEA in the traditional plant and the catalyst in the CLC one, even if this was evaluated not to have such a great impact in the final balance.
In order to calculate the cost for MEA substitution, it was necessary to extract the molar flow from ASPEN and suppose a residence time τ of about 180 seconds, in order to obtain the total quantity of MEA in the plant. Then, it was found in literature a reference price for MEA (1760 \$/ton) [41], so it was easy to calculate the final cost for MEA, that resulted to be around **0,042 M\$/year** with the assumption that all the MEA in the plant is substituted each 3 months.
As far as catalyst substitution in CLC plant is concerned, the calculation is easier; as a matter of fact, ASPEN provides directly the total quantity of solid catalyst present in both CLC reactors. Thus, it was sufficient to multiply that value by the cost of NiO found in literature (15400 \$/ton) [41], in order to obtain the final cost for catalyst substitution **(4,27 M\$/year)**, with the same assumption that all the material is replaced one time each three months.
After that, the cost of **labour** (C_L) should be evaluated. The estimation is based on some general assumptions taken by Vergis [63], presented in table 23.

Working weeks per year per operator	49
N. of operating shifts per week per operator	5
N. of operating shifts per year per operator	245
N. of shifts per year	1095

Table 23: Starting assumption for C_L calculation

At this point, the number of operating shifhts per shift N_{OL} has to be calculated by means of Alkhayat and Gerrard correlation [78], reported below:

$$N_{OL} = \sqrt{6.29 + 31.7P^2 + 0.23N_{MP}} \tag{75}$$

where P is the number of steps that comprise handling, distribution and trasportation, solid matter control and removal, while N_{MP} is the number of processing steps that comprise heating, cooling, compression, mixing and reaction, found in literature for SMR [63] and re-adapted for CLC. Once having this value, it is sufficient to multiply it for the number of total yearly shifts to obtain the total number of operating shifts per year. It is now sufficient to divide this last result for the number of operating shifts per year per operator, to obtain the number of operators yearly needed. Supposing an average yearly salary of 40000 \$/operator, it it possible to calculate the cost of operating labour C_L. All the results for both plants are summarized in table 24.

	TRAD	CLC
P	4	5
N_{MP}	6	6
N. of operating shifts per shift	23	28
N. of operating shifts per year	25185	30660
N. of operators per year	103	125
Average annual salary per operator ($/year)	40000	40000
Labour cost C_L (M$/year)	4,1	5

Table 24: Final C_L calculation

Moreover, there are several other parts that form the direct manufacturing costs, evaluated just as percentages of the labour or investment cost. The estimations were made by referring to Vergis [63], and involved the calculation of:

- **Direct supervisory and clerical labour**, that is the cost for engineering and amministrative support, and stands for about 18 % of C_L;
- **Maintenance and repair**, that is the cost for maintenance labour, and stands for about 6 % of total cost of investment excluding the cost of land (FCIL);
- **Operating supplies**, that is the cost for additional staff required by operators (lubrificants, protective equipmente etc.), and stands for about 0.9 % of total cost of investment excluding the cost of land (FCIL);
- **Operating supplies**, that is the cost for additional staff required by operators (lubrificants, protective equipmente etc.), and stands for about 0.9 % of total cost of investment excluding the cost of land (FCIL);
- **Laboratory Charges**, that is the cost for continuous technological testing in laboratory, and stands for about 15 % of total cost of investment excluding the cost of land (FCIL);
- **Patens**, that is the cost for the use of patented inventions or technologies, and stands for about 3 % of total direct manufacturing costs.

So, in the end the direct manufacturing costs accounts for **140 M$/year** for the traditional plant and **187,5 M$/year** for the CLC one. Details of their different contributions can be found in Appendix B, table 32.
On the other hand, manufacturing costs have also a fixed component that should be evaluated. This can be easily summarized in two main contributions:

- **Plant overhead costs**, that comprise all those operative costs associated with internal and external facilities, and stand for about 70,8 % of the C_L plus 3,6 % of FCIL;
- **Local taxes and insurance**, that stand for about 3,2 % of FCIL.

So, the fixed manufacturing costs amount to **7,7 M$/year** for the traditional plant and textbf11 M$/year for the CLC one.
Finally, the last contribution to the OPEX is represented by the so called "General Expenses", that comprise the costs for:

- **Administration**, that stand for about 17,7 % of the C_L plus 0,9 % of FCIL;
- **Distribution and selling**, that stand for about 1,1 % of total direct manufacturing costs;
- **Research and development**, that stand for about 5 % of total direct manufacturing costs.

The general expenses result thus to be equal to **11 M$/year** for the traditional plant and **14,9 M$/year** for the CLC one.
Each contribution of fixed manufacturing costs and general expenses, for both plants, is reported in Appendix B, tables 33 and 34.
In last analysis, it was considered also the presence of the carbon tax, in an European location, for the traditional plant that is the only one that emits CO_2 in the atmosphere. Considering the data and the trends of the energy perspectives of IEA in 2016 [4], it was possible to extract an average value of carbon tax to be applied to the traditional plant, equal to 32,8 $/ton. Thus, by simply extracting the flowrate of CO_2 leaving the plant and multiplying it for the annual operation hours, the total quantity of CO_2 emitted can be calculated, and consequently the costs associated to carbon tax **(6,93 M$/year)**.
In the end, the final OPEX was estimated to amount to **165,5 M$/year** for the traditional plant and **213,4 M$/year** for the CLC one.

5.3 Cash Flow Analysis

Once known the investment cost and the yearly operational one, it is necessary to understand all those processes that lead to earning (or loosing) money from the yearly incomes and outcomes.
The first thing to be considered is the so called **depreciation**, that is a sort of fiscal benefit that goverments apply in order to promote the born of new building and plants. It basically consists in the recovery of part of the investment during the first years of the plant operating, by applyng a fiscal detraction on part of the investment cost, where no taxes are applied. In other terms, if a standard depreciation period of 10 years is considered, the depreciation rate is defined as:

$$DEP\,rate = \frac{TOC}{10} \tag{76}$$

This depreciation rate represents a tax-free quantity that can be subtracted by the incomes, as it is seen in the next considerations.
After considering all the costs to be substained for the operational working of the plants, the focus passes on the **revenues** that can be exctracted from them. They basically consist in the money that can be obtained by H_2 selling to the customers. Thus, being the H_2 productivity the same for both plants, it is sufficient to find a selling price for H_2 to easily determine the revenues. In a report of the National Renewable Energy Laboratory (NREL), it was found that a valid range of selling price for H_2 could be 3-10 $\frac{\$}{kg}$ [80]. So, for this first analysis an average value of 6 $\frac{\$}{kg}$ was chosen as selling price. The revenues

that can be obtained by H_2 selling amount, indeed, to **345,6 M$/year**, for both plants. At this point, yearly **cash flow** needs to be evaluated. Cash flow can be easily defined as the difference between all the costs and the incomes; obviously, at year 0 there are no revenues and only the investment costs is present, while starting from year 1 the OPEX costs and revenues are considered. Moreover, if the cash flow is positive, **taxes** are imposed on that. So, making the assumption that the plant could be located in Italy, the taxation rate that needs to be assumed is related to IRPEF different aliquots. In this specific case, since revenues are so high, taxation rate t can be approximated with a single fixed one, relative to the maximum band (over 75k€) that amounts to t= 43 % [81]. Thus, the cash flow can be expressed as:

$$\begin{aligned} Cash\ Flow\left(\frac{M\$}{year}\right) &= Incomes - Costs - Taxes \\ &Incomes - Costs - t \cdot (Incomes - Costs - Dep\,rate) \end{aligned} \tag{77}$$

for the first 10 years, where depreciation is present, and as:

$$\begin{aligned} Cash\ Flow\ \left(\frac{M\$}{year}\right) &= Incomes - Costs - Taxes \\ &Incomes - Costs - t \cdot (Incomes - Costs) \end{aligned} \tag{78}$$

for the remaining years. The lifetime of the plants was supposed equal to 25 years [41]. After that, it is necessary to understand how to estimate the **present cash flow** of a predicted cash flow in the future. This can be done by taking into consideration the value of money in time, by means of the **discount rate i**. In this analysis, the discount rate can be approximated with the Weighted Average Cost of Capital (WACC), that is determined on the basis of the financial structure chosen for the investment. The financial structure basically depends on:

- The type of the investor, that can be nor Investor-Owned Utility (IOU) or Independent Power Producer (IPP);
- The risk of the investment, that can be lower or higher depending on the maturity of the technology in the market.

Since the plants can be seen as inserred in a wider network of energy infrastructure, an IOU investor was chosen for both plants. On the other hand, due to the higher maturity of the traditional plant with respect to CLC one, the risk associated to that investment is lower than in CLC, and this is reflected on the financial structures themselves. The WACC is determined by means of a weighted average on cost of equity (C_E) and cost of debt (C_D), as follows:

$$WACC = \%_E C_E + \%_D C_D \tag{79}$$

where all the parameters depend on the financial structure chosen. Moreover, taxation rate needs to be applied to the cost of debt to obtain the after tax WACC, as follows:

$$After\ Tax\ WACC = \%_E C_E + \%_D C_D \cdot (1 - t) \tag{80}$$

So, in the end the after tax WACC resulted to be **5,67** % for the traditional plant and **6,24** % for the CLC one. Details of the financial structures used for WACC calculation were taken by NETL [73] and are reported in Appendix C, tables 35 and 36.

At this point, the Net Present Value (NPV) can be evaluated with the following relationship:

$$NPV(\tau) = -I + \sum_{n=1}^{\tau} \frac{B_n}{(1 + WACC)^n} \tag{81}$$

where I is the investment cost, coincident with the CAPEX, n are representative of the years, and B_n is the cash flow at year n. The resulting NPVs for both plants, over their whole lifetime, is shown in figure 68, while puntual values for each year are reported in appendix C, table 37.

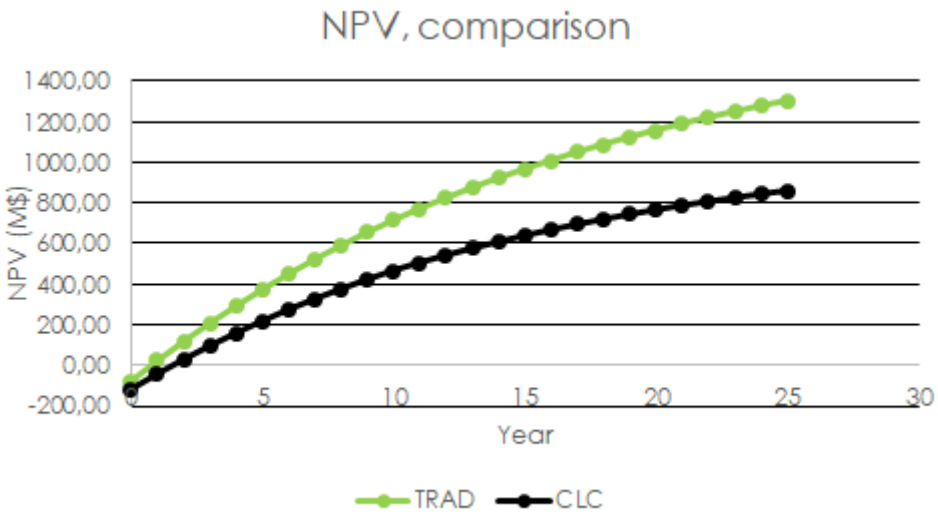

Figure 68: NPV comparison, Traditional and CLC plants

As can be easily seen, the investment seems to be very promising, since it is recovered very quickly. Thus, together with NPV at final operational year of the plant, the so called Payback Time (PBT), that is the time at which NPV=0 and so the investment is recovered, is considered as key indicator of the quality of the investment. Both are reported in figure 69.

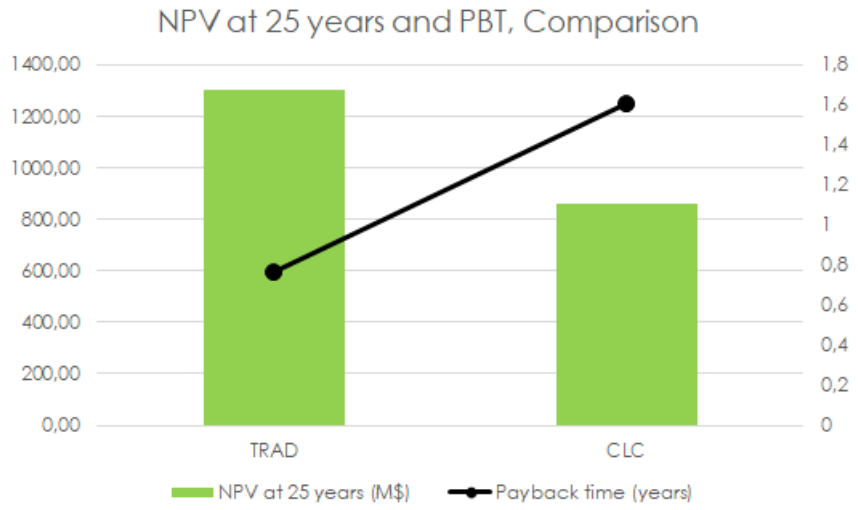

Figure 69: NPV at 25 years and PBT comparison, Traditional and CLC plants

As expected, the traditional SMR plant allows higher earnings and lower PBT with respect to CLC one. CLC plant has a reduction of about 34% of the NPV at 25 years (860 M$ against 1300 M$ of the tradtional one), while the PBT results to be 1.4 years against 0.8 of the traditional.
Finally, it can become useful to analyze the cost of production of H_2 for both plants, in order to have another indicator. The most proper one for this purpose results to be the Levelized Cost Of Hydrogen (LCOH), that can be expressed as [41]:

$$LCOH\left(\frac{\$}{kg_{H_2}}\right) = \frac{Annual\ Capital\ Cost + Operational\ Cost}{Annual\ H_2\ Productivity} \tag{82}$$

The Annual Capital Cost (ACC) can be calculated as follows:

$$ACC = CRF \cdot C_{Total} \tag{83}$$

where C_{Total} is the total investment cost (TOC), while Capital Recovery Factor (CRF) is an indication of the different value of investment during lifetime of the plant, and is defined as:

$$CRF = \frac{i(1+i)^n}{(1+i)^n - 1} \tag{84}$$

where i is the discount rate, coincident with after tax WACC, and n is the lifetime of the plant (25 years in this case).
The resulting LOCHs are shown in figure 70.

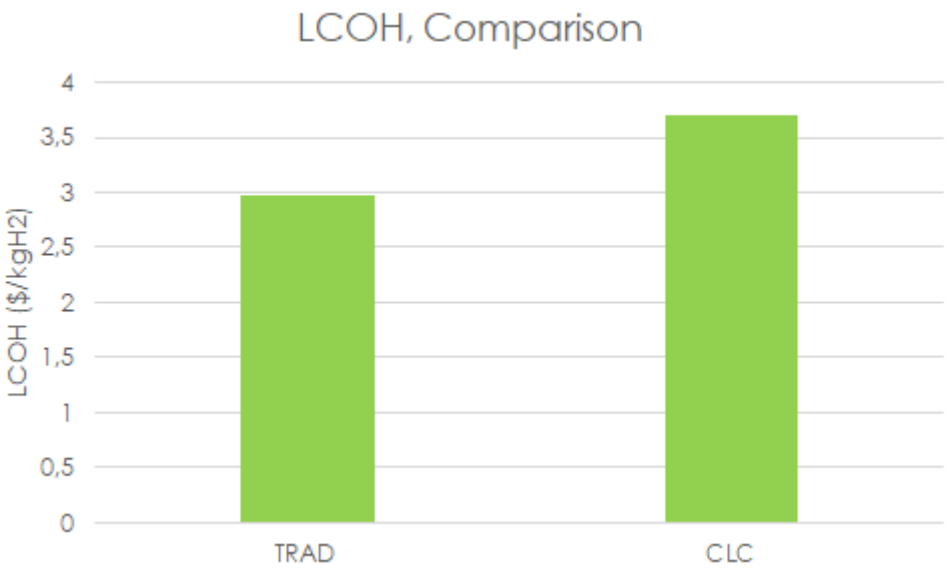

Figure 70: LCOH comparison between traditional and CLC plant

As expected, LCOH is higher in CLC plant (3,7 against 2,97 $\left(\frac{\$}{kg_{H_2}}\right)$ of the traditional one), mainly due to the higher external resources needed to properly work.

5.4 Sensitivities

The techno-economic analysis was mainly performed with literature assumptions for many influencing parameters. The aim of this part is to show how the variation of the most relevant paameters (cost of CH_4 and electricity, selling price of hydrogen, carbon tax) has an impact of the indicators previously identified (NPV, PBT and LCOH).

5.4.1 Cost of Raw Materials, Present and Future scenarios

The first sensitivity was done by considering the possible future trends for cost of electricity and CH_4, together with carbon tax, predicted by IEA in 2016 [79]. Since the data analyzed referred to household consumption, it was considered only their increasing or decreasing trend in time to scale up the EUROSTAT average European price used in the analysis [76] [77]. For carbon tax, instead, the value proposed by IEA were chosen [79]. All the assumptions are reported in table 25.

Parameter	**2019**	**2030**	**2050**
$CH_4 \left(\frac{\$}{GJ}\right)$	8,7	11,2	13,6
Electricity $\left(\frac{\$}{kWh}\right)$	0,096	0,11	0,125
Carbon Tax $\left(\frac{\$}{Ton}\right)$	32,8	81,8	140,9

Table 25: Assumptions for future trends sensitivities

The years chosen for the analysis are clearly 2019 (present year of this work) and both medium term (2030) and long term (2050) scenario, in order to assess the feasibility of such plants in each time framework. It is worth noting that, being impossible to retrieve and predict CEPCI for future years, the CAPEX estimation remains the same of present case; however, since CAPEX does not influence so much the analysis, while OPEX resulted to be the dominant term, the approximation can be considered acceptable.
Thus, the previsions for future terms show a decrease in the profitability of the investment, as shown by figures 71, 72, 73, 74, 75, 76,, due to the sharp increase of raw materials costs and carbon tax. Obviously, if LCOH depends only on costs, for NPV at the end of the lifetime and consequently payback time, the selling price of hydrogen in the future has a great influence. So, the suggestion is to use these last two indicators only as media for understanding how much the cost of raw materials and carbon tax influence them.
Results show a strong dependence on those costs, underlining how those technologies should be imoplemented in present or short-term time to get maximum profitability from them. It is to say that all these considerations trascend the environmental matter, that could become more and more relevant with respect to economic one, especially in the next future; in fact, those plants are able to create profit and to avoid pollution and climate change.

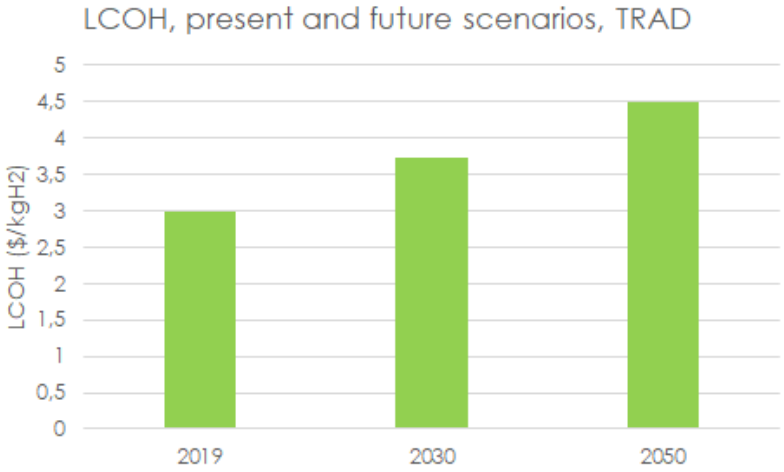

Figure 71: LCOH sensitivity, present and future scenarios, Traditional plant

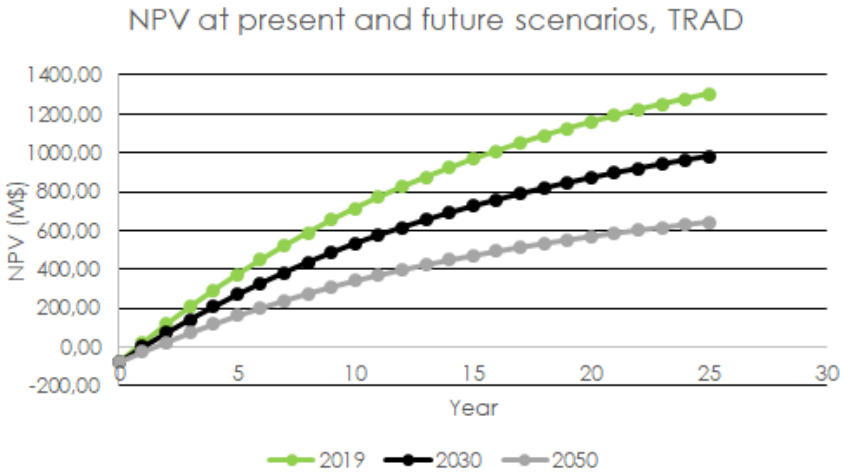

Figure 72: NPV sensitivity, present and future scenarios, Traditional plant

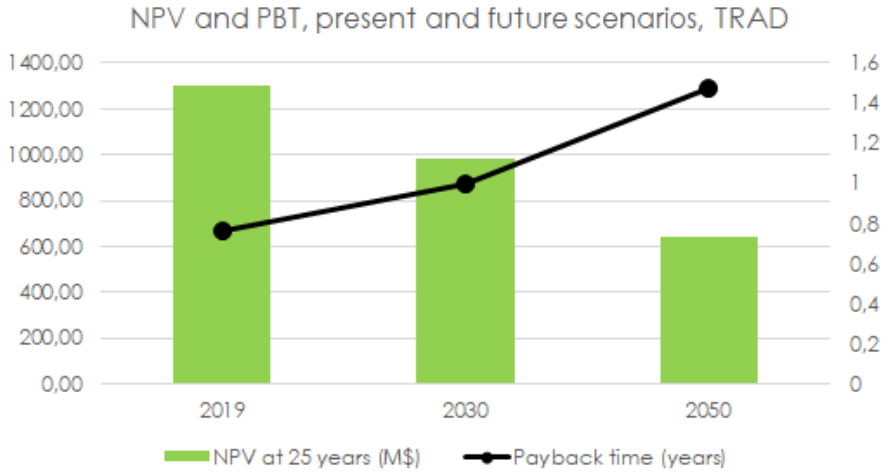

Figure 73: NPV at 25 years and PBT sensitivity, present and future scenarios, Traditional plant

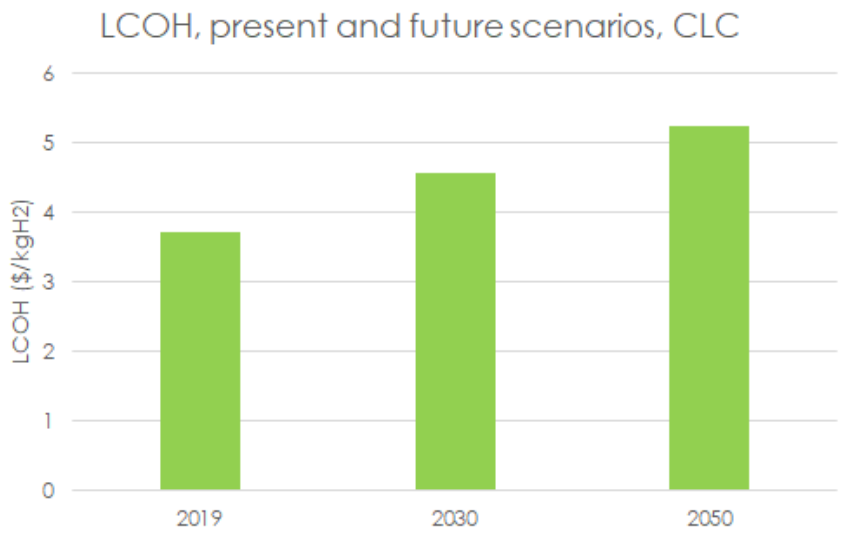

Figure 74: LCOH sensitivity, present and future scenarios, CLC plant

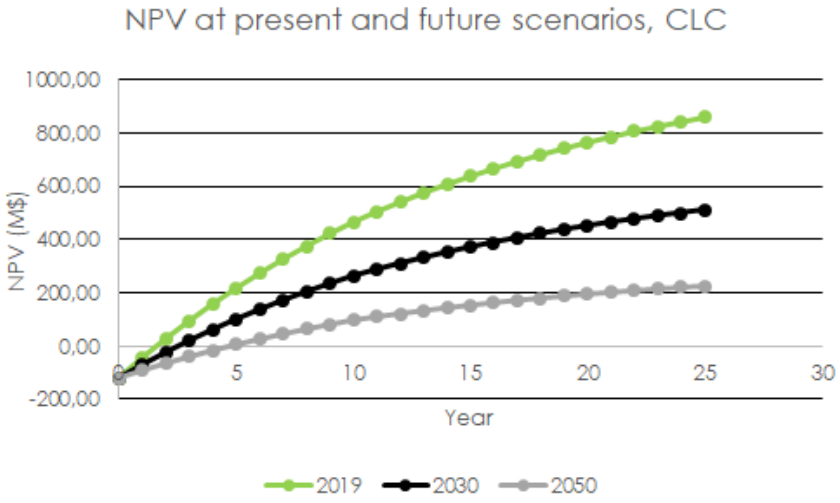

Figure 75: NPV sensitivity, present and future scenarios, CLC plant

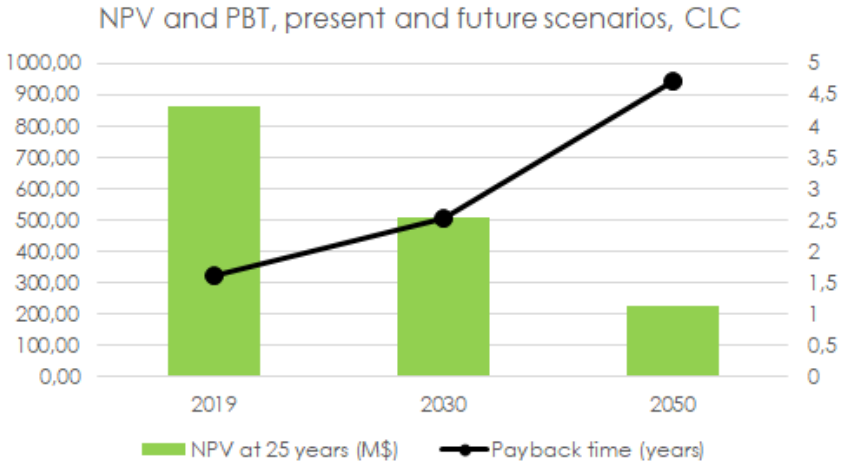

Figure 76: NPV at 25 years and PBT sensitivity, present and future scenarios, CLC plant

5.4.2 Cost of Raw Materials, different European countries

The second sensitivity that was performed regards the differences in electricity and CH_4 price for the different European countries. The idea was to select the worst and the best country to install such plants, in terms of raw materials costs, and thus identify the two extreme bounds of the profitability range for the investment.
Since CH_4 cost is responsible for over 60% of the total operational costs, the European countries chosen were the ones with lowest and highest cost of CH_4, respectively Belgium and Finland [76]. In order to make the comparison easier, the European average values, that are the same proposed in the very first economic analysis, are shown together with these new results. The values used for the analysis are presented in table 26 [76] [77].

Parameter	**Belgium**	**Average UE**	**Finland**
$CH_4\ \left(\frac{\$}{GJ}\right)$	6,70	8,70	13,48
Electricity $\left(\frac{\$}{kWh}\right)$	0,089	0,096	0,070

Table 26: Assumptions for future trends sensitivities

For this analysis too, the effect of such prices in LCOH, NPV and PBT were analyzed and shown in figures 77, 78, 79, 80, 81, 82, for both plants. It is worth noting that the choice of the country is less influent than the effect of time, as far as raw materials prices are concerned. In particular, there are no significant differences between Belgium and UE average, meaning that maybe Finland is a singular case where those plants are not so profitable.

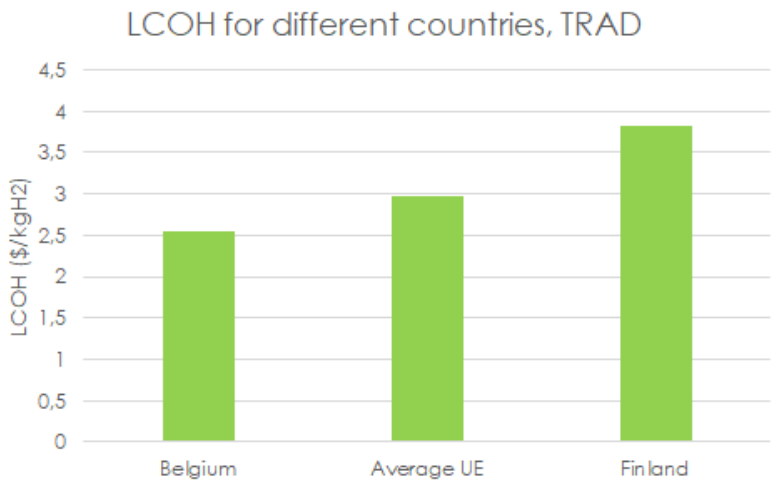

Figure 77: LCOH sensitivity, different European countries, Traditional plant

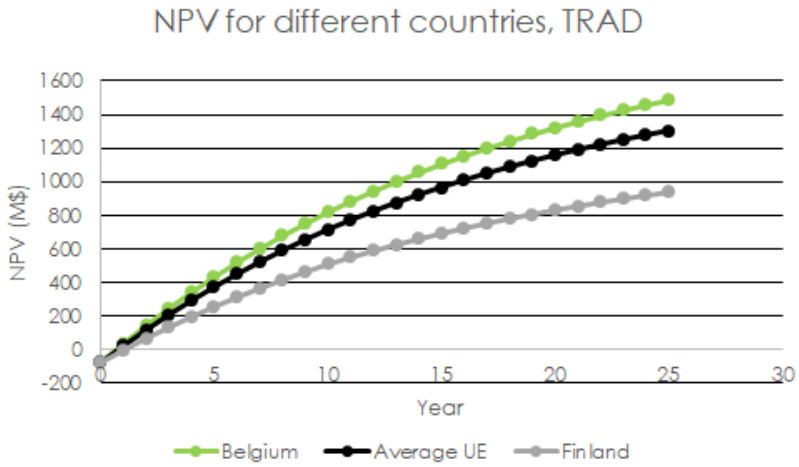

Figure 78: NPV sensitivity, different European countries, Traditional plant

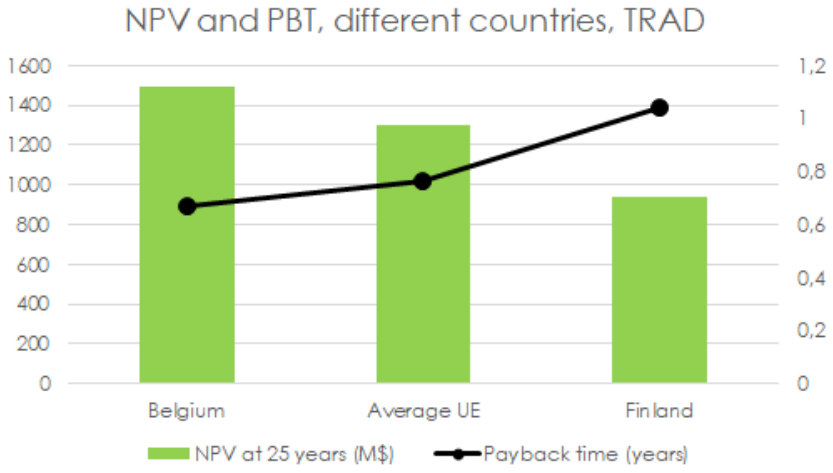

Figure 79: NPV at 25 years and PBT sensitivity, different European countries, Traditional plant

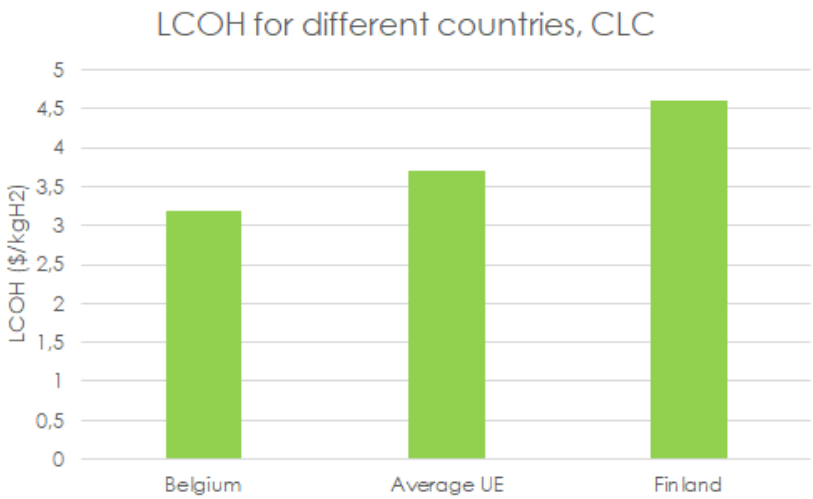

Figure 80: LCOH sensitivity, different European countries, CLC plant

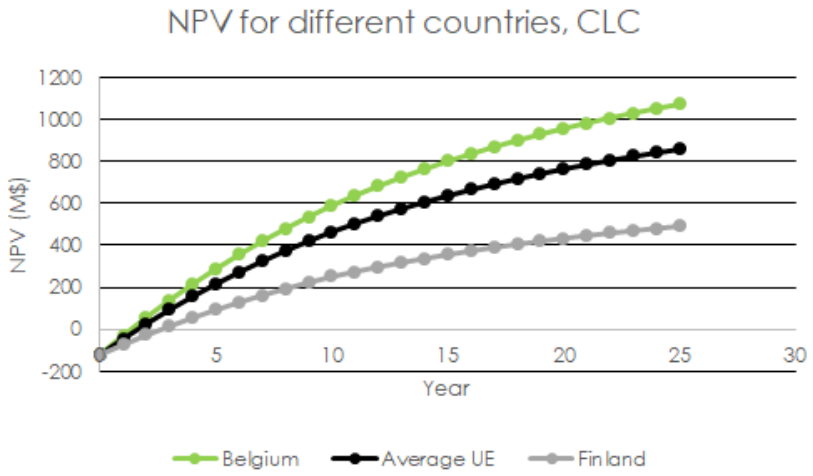

Figure 81: NPV sensitivity, different European countries, CLC plant

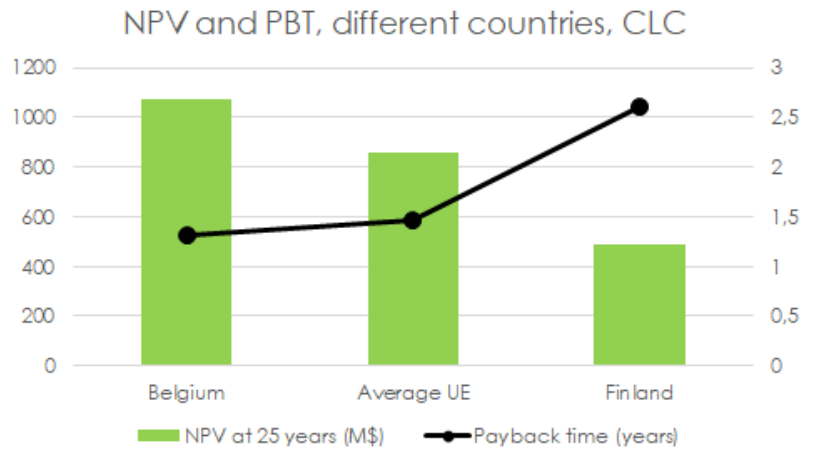

Figure 82: NPV at 25 years and PBT sensitivity, different European countries, CLC plant

5.4.3 Selling Price of Hydrogen

The last parameter analyzed is, indeed, the price at which hydrogen is sold at the final consumer.

According to NREL, 3-10 $\frac{\$}{kg_{H_2}}$ could be a potential range for this value [80], menaning that revenues can be extremely different by changing this parameter. As a matter of fact, it has a great impact on the NPV and PBT indicators, as shown by figures 83, 84, 85, 86. It is worth nothing that, leaving OPEX and CAPEX unchanged, the LCOH is unchanged too, so this indicator is not the right one to measure the impact of different revenus.

The values chosen for the sensitivities are 4, 6, 8 and 10 $\frac{\$}{kg_{H_2}}$; results show that with 4 $\frac{\$}{kg_{H_2}}$ as selling price, the investment is very poor in the traditional plant and it is quasi-null in the CLC plant, meaning that this is the most important parameter to be monitored when doing feasibility analyisis for such plants. For values higher than 6 $\frac{\$}{kg_{H_2}}$, the situation is extremely rosy and the investment is recovered in very little time, for both plants. Obviously, CLC plant performances are always worse than traditional one, being CAPEX and OPEX unchanged.

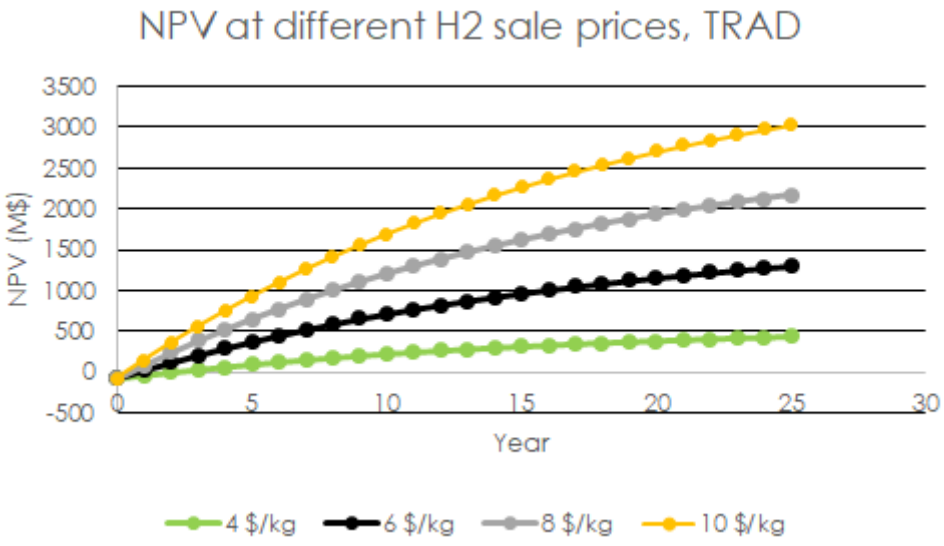

Figure 83: NPV sensitivity, different hydrogen selling prices, Traditional plant

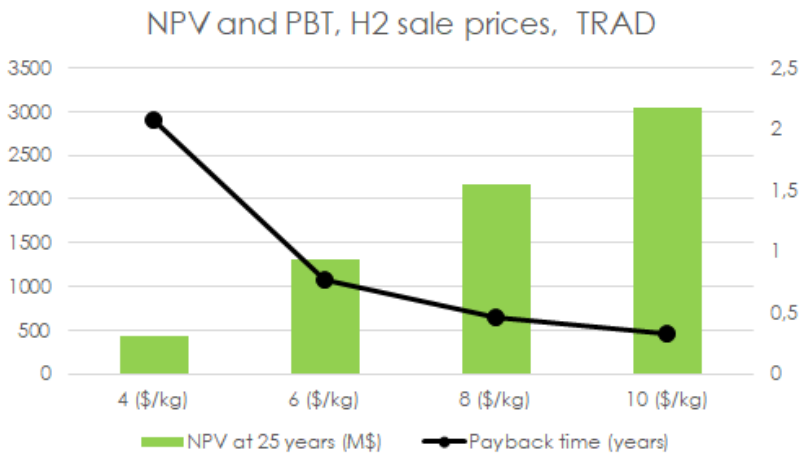

Figure 84: NPV at 25 years and PBT sensitivity, different hydrogen selling prices, Traditional plant

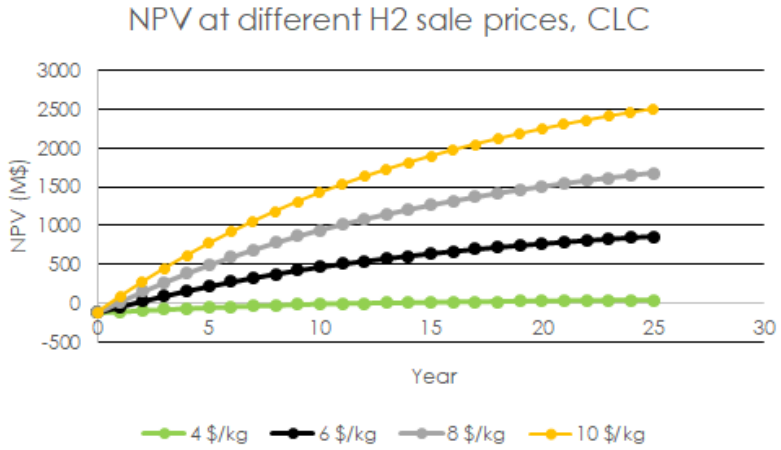

Figure 85: NPV sensitivity, different hydrogen selling prices, CLC plant

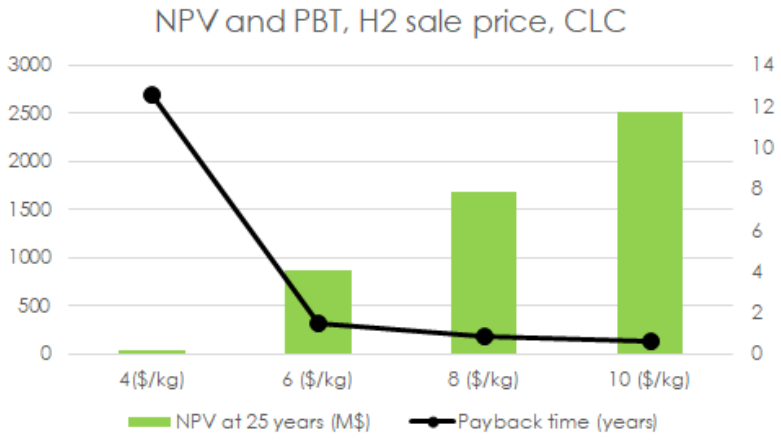

Figure 86: NPV at 25 years and PBT sensitivity, different hydrogen selling prices, CLC plant

5.5 Cost for CO_2 Compression, Transportation and Storage

As can be derived from the whole analysis, the purpose of this work is to assess the potentialities of the two different plants in terms of H_2 production and CO_2 capture. By doing this way, differences in the technological process are enhanced, without considering the compression and storage steps that follow CO_2 separation.
In a further vision, also these factors can be considered. The Sustainable Gas Institute of the Imperial College of London suggests that maximum values available in literature for total abatement costs (capture, compression, transportation and sequestration) are around 160 $\$/ton_{CO_2}$ [82]. For the traditional SMR plant, this can be translated into an annual cost of around 45 M$, that stands for about 0,78 $\$/kg_{H_2}$ more in the LCOH. A small part of these costs is given by CO_2 capture, that is already counted in the previous analysis. By simply eliminating CAPEX and OPEX related to the CO_2 capture section, they are estimated to be around 0,05 $\$/kg_{H_2}$.
As far as compression is concerned, instead, it can be easily estimated considering a single compressor that pressurizes CO_2 from 1.6 bar to 110 bar [25]. Supposing an isentropic efficiency of 0.85 as the previous compressors and obtaining inlet and outlet enthalpies from NIST databases [83], it was possible to calculate the power requested from the compressor W_{comp} by:

$$W_{comp} = \dot{m}_{CO_2} \cdot (h_{out} - h_{in}) \tag{85}$$

where $\dot{m}_{CO_2}$ is the mass flowrate of compressed CO_2, while h_{out} and h_{in} are, respectively, the enthalpies of the outlet and inlet stream of the compressor. The size of the compressor resulted to be 4,34 MW, implying additional costs in terms of investment, electricity required to run it and maintainence. Applying the same procedure of the entire techno-economic analysis, this resulted to impact for about 0.2 $\$/kg_{H_2}$ in the total LCOH.
Thus, the cost allocation for CCS resulted to be the following 27:

Issue	**Cost** ($\$/kg_{H_2}$)
Capture	0,05
Compression	0,2
Trasportation and Storage	0,53

Table 27: Cost allocation for CCS

where transportation and storage costs are obtained by difference from the total costs estimated by Sustainable Gas Institute [82].
Another literature source that confirms the order of magnitude of CCS impact in LCOH formation is the last IEA report about hydrogen future. In Europe, LCOH is estimated to be 1.73 $\$/kg_{H_2}$ without CCS and 2.32 $\$/kg_{H_2}$ with CCS, with a difference of 0.59 $\$/kg_{H_2}$ [84]. As can be clearly seen, the orders of magnitude are the same, with some differences in the absolute values of the two costs. This can be related to the fact that average SMR plants considered by IEA are larger in terms of size, impacting positively in scaling costs for equipment and maintainence: the specific cost of hydrogen production resulted then to be lower than the one calculated for the modelled plant, which has a medium size, as well as the difference between CCS and no CCS cases.

6 Conclusions and Future Work

The final aim of this work is to present a multifaceted comparison between the state of the art in the production of blue hydrogen, that is the traditional SMR plant, and the CLC one. The need for thinking about a new disruptive way of blue H_2 production come from environmental issues: if H_2 would play a crucial role in the decarbonization scenario, also its production should be carbon-free.
In this vision, a Chemical Looping Combustion driven SMR plant can be the right answer. As a matter of fact, there are several studies about Demo plants from 10 to 1000 MWth, while from 2020 on a fully commercial development of 10 MWth ones is predicted [37]. Moreover, it allows eliminating all the CO_2 produced in the process by simple condensation, since no inerts are present, reaching 100% of CO_2 captured against 57 % of the traditional plant.
The CLC reactors modelling itself can be considered as the most relevant added value of this work. The fluidbed block allows to obtain several results about the reactors, that range from geometrical distribution of molar flows of different species to calculation of the different solid matter concentration and quantity. Moreover, the fluidbed model seems to work quite well because it was compared to a simpler one, where black-box RGibbs reactors were used, validating its adherence by looking at similar values obtained for manipulated variables.
Other great advantages of both the models proposed are their flexibility and readiness in terms of escalation. As a matter of fact, it is sufficient to change the imposed hydrogen productivity together with the bounds of the manipulated variables to obtain a well-performant model of the same plant with another scale. The only inputs that need to be reprocessed from outside are the geometric parameters of the components that need them, namely the CLC reactors, the absorber and the stripper.
In addition, the performance of the MEA system in two different locations (pre-PSA and post-combustion) has been analyzed by moving and scaling the CO_2 capture section to the final part of the plant. It was confirmed that post-combustion is not the best location in terms of operating parameters (lower pressure and concentrations), leading to additional input resources needed (15 MW of CH_4 more), but allows a higher CO_2 capture at same absorber efficiency. In this case, about 90% of the CO_2 produced can be captured.
After modelling both plants, it was found that the traditional plant requires fewer input resources that CLC one, both in terms of CH_4 (13 % less) and electricity (44 % less). The former is probably due to the increased complexity of the heat generation process in the fluid bed reactors, while the latter is attributed to the presence of two additional compressors to pressurize gases entering the CLC reactors. This fact leads to higher profitability of the traditional plant; moreover, the cheaper components used for carbon capture in the traditional plant with respect to fluidbed reactors have an impact also on its investment cost, resulting to be around 77 M$ against 120 M$ of the CLC one. In any case, being OPEX the dominant term for these kinds of plants, the traditional one is much more economically performant than CLC, with an LCOH of around 3 $\frac{\$}{kg_{H_2}}$, compared to 3,7 $\frac{\$}{kg_{H_2}}$ of the CLC one. The investment leads to very high NPV at the end of lifetime (1300 M$ for traditional plant and 860 M$ for CLC one), with very low PBT of the order of 1 year; if the investment is made in the next future, instead, OPEX will be higher according to IEA [79], meaning that the present time is the best one to build such plants for a very next decarbonization scenario.

This work can be considered as a starting point for further evaluations. First of all, the choice of the precise location of such plants could become a relevant added value. As a matter of fact, the model can be optimized by maximizing heat recovery both internally, by a pinch approach between the components, and externally, considering the waste heat of the near industries or plants and its thermal levels. Moreover, the costs of natural resources and selling price of hydrogen would be much more punctual and precise, allowing less uncertainty in the definition of a feasibility study.
Secondly, it could be useful to understand how to scale up these plants to reach the correct size needed also by H_2 distribution purposes. Once known the pipeline availability of the location chosen, then the plant capacity required to completely fulfill the grid needs is defined; on the other hand, by setting the plant capacity because of economic or strategical issues, then the pipelines should be properly dimensioned.
Moreover, a deeper investigation about the determination of transportation and sequestration costs, as well as a more precise model for compression, could be an interesting added value for the validation of CCS case. Dimensioning of multi-stage interrefrigerated compression, pipeline and storage would be required for this analysis.
Finally, it could become interesting to analyze the possible insertion of these systems in a varied H_2 production and distribution infrastructure. For example, if the core of H_2 production for the European delivery can be North Africa, it will be surely significant to include both SMR and water electrolyzers in the definition of the H_2 generation pathway, due to its abundance of renewable energy to produce also green H_2.

Appendix A - Cost Of Components, Details

Heat exchanger	**Duty (Kw)**	T_{coldin}°C	$T_{coldout}$(°C)	T_{hotin}(°C)	T_{hotout}(°C)	**U** $\left(\frac{W}{m^2K}\right)$	$\Delta T_{ML}(K)$	$Surface(m^2)$
HEAT-EX1	8826	409	586	850	700	277	325	98
HEAT-EX2	14056	350	600	700	450	100	325	432
HEAT-EX3	14056	200	457	600	350	147	325	295
COND-1	38262	15	30	457	35	133	2100	137
COOLER-1	23104	15	30	121	40	51	600	754
STR-COND	51667	15	30	93	93	70	3300	222
STR-REB	84213	99	121	150	130	30	750	3750
COND-2	7259	15	30	93	30	34	2100	103
COND-3	12	15	30	70	30	25	2100	0,23

Table 28: Characteristics of Heat Exchangers, Traditional Plant

Heat exchanger	**Duty (Kw)**	$T_{cold_{in}}$°C	$T_{cold_{out}}$(°C)	$T_{hot_{in}}$(°C)	$T_{hot_{out}}$(°C)	**U** $\left(\frac{W}{m^2K}\right)$	$\Delta T_{ML}(K)$	$Surface(m^2)$
HEAT-EX1	8825	409	586	850	700	277	325	98
HEAT-EX2	14061	350	600	700	450	100	325	432
HEAT-EX3	14061	200	456	600	350	147	325	295
COND-1	22836	15	30	461	23	106	2100	102
COOLER-1	29612	15	30	900	140	384	300	257
COND-2	22435	15	30	140	30	48	2100	224
COOLER-2	40985	15	30	950	25	201	300	679
COOLER-3	44436	15	30	950	25	201	300	736

Table 29: Characteristics of Heat Exchangers, CLC Plant

Component	**A Param.**	**A value**	**Min**	**Max**	K_1	K_2	K_3	C_p^0 **(M$)**	**n**	$C_p^0{}_C$ **(M$)**	$C_p^0{}_{C2019}$ **(M$)**
COMP-1	Fluid Power (kW)	3773,4	450	3000	2,29	1,36	-0,10	0,60	0,84	0,73	0,86
PUMP-1	Shaft Power (kW)	31,4	1	300	3,39	0,05	0,15	0,007	0,67	0,007	0,008
HEAT-H_2O	Duty (kW)	46218,1	1200	9400	6,96	-1,48	0,32	1,18	0,60	3,06	3,64
HEAT-EX1	Surface area (m^2)	98,1	10	1000	4,19	-0,25	0,20	0,03	0,59	0,03	0,04
REF	Volume (m^3)	32,8	5	45	3,35	-0,28	0,00	0,001	0,53	0,001	0,001
HEAT-EX2	Surface area (m^2)	432	10	1000	4,19	-0,25	0,20	0,08	0,59	0,08	0,09
HIGH T WGS	Volume (m^3)	11,1	5	45	3,35	-0,28	0,00	0,001	0,53	0,001	0,001
HEAT-EX3	Surface area (m^2)	295,1	10	1000	4,19	-0,25	0,20	0,06	0,59	0,06	0,07
LOW T WGS	Volume (m^3)	9,5	5	45	3,35	-0,28	0,00	0,001	0,53	0,001	0,001
COND-1	Surface area (m^2)	137,1	10	1000	4,19	-0,25	0,20	0,04	0,59	0,04	0,04
ABSORBER	Volume (m^3)	28,3	0	520	3,50	0,45	0,11	0,02	0,30	0,02	0,03
PUMP-2	Shaft Power (kW)	10,6	1	300	3,39	0,05	0,15	0,004	0,30	0,004	0,005
COOLER-1	Surface area (m^2)	753,9	10	1000	4,19	-0,25	0,20	0,16	0,59	0,14	0,16
STRIPPER	Volume (m^3)	2714,3	0	520	3,50	0,45	0,11	0,32	0,30	0,53	0,63
STR-REB	Surface area (m^2)	3750,3	10	1000	4,19	-0,25	0,20	0,16	0,60	0,36	0,43
STR-COND	Surface area (m^2)	222,4	10	1000	4,19	-0,25	0,20	0,05	0,59	0,05	0,06
COND-2	Surface area (m^2)	103,2	10	1000	4,19	-0,25	0,20	0,03	0,59	0,03	0,04
PSA	Volume (m^3)	365,6	0	520	3,50	0,45	0,11	0,23	0,30	0,23	0,27
COND-3	Surface area (m^2)	0,23	10	1000	4,19	-0,25	0,20	0,014	0,59	0,001	0,002
FURNACE	Duty (kW)	68541	3000	100000	3,07	0,66	0,02	5,15	0,60	5,15	6,11

Table 30: Cost of components, parameters, traditional plant

Component	A Param.	A value	Min	Max	K_1	K_2	K_3	$C_p{}^0$ (M$)	n	$C_p{}^0{}_C$ (M$)	$C_p{}^0{}_{C2019}$ (M$)
COMP-1	Fluid Power (kW)	3769,5	450	3000	2,29	1,36	-0,10	0,60	0,84	0,73	0,86
PUMP-1	Shaft Power (kW)	31,5	1	300	3,39	0,05	0,15	0,01	0,67	0,01	0,01
HEAT-H_2O	Duty (kW)	47606,1	1200	9400	6,96	-1,48	0,32	1,18	0,60	3,12	3,70
HEAT-EX1	Surface area (m^2)	98,0	10	1000	4,19	-0,25	0,20	0,03	0,59	0,03	0,04
REF	Volume (m^3)	32,8	5	45	3,35	-0,28	0,00	0,001	0,53	0,001	0,001
HEAT-EX2	Surface area (m^2)	432,1	10	1000	4,19	-0,25	0,20	0,08	0,59	0,08	0,09
HIGH T WGS	Volume (m^3)	11,1	5	45	3,35	-0,28	0,00	0,001	0,53	0,001	0,001
HEAT-EX3	Surface area (m^2)	295,1	10	1000	4,19	-0,25	0,20	0,06	0,59	0,06	0,07
LOW T WGS	Volume (m^3)	9,5	5	45	3,35	-0,28	0,00	0,001	0,53	0,001	0,001
COND-1	Surface area (m^2)	102,4	10	1000	4,19	-0,25	0,20	0,03	0,59	0,03	0,04
COMP-2	Fluid Power (kW)	5574,8	450	3000	2,29	1,36	-0,10	0,60	0,84	1,01	1,20
CLC REACTORS	/	/	/	/	/	/	/	/	0,60	6,46	7,38
COOLER-1	Surface area (m^2)	257,1	10	1000	4,19	-0,25	0,20	0,05	0,59	0,05	0,06
COND-2	Surface area (m^2)	224,1	10	1000	4,19	-0,25	0,20	0,05	0,59	0,05	0,06
COMP-3	Fluid Power (kW)	18384,8	450	3000	2,29	1,36	-0,10	0,60	0,84	2,75	3,27
COOLER-2	Surface area (m^2)	678,8	10	1000	4,19	-0,25	0,20	0,12	0,59	0,12	0,14
COOLER-3	Surface area (m^2)	736,0	10	1000	4,19	-0,25	0,20	0,12	0,59	0,12	0,15

Table 31: Cost of components, parameters, CLC plant

Appendix B - OPEX, Details

Contribution	TRAD (M$/year)	CLC (M$/year)
Raw Materials	115,2	147,6
Substitutions	0,04	4,3
Labour	4,1	5,0
Direct Supervisory and clerical labour	0,7	0,9
Mainteinance and repairs	4,2	6,6
Operating supplies	0,6	1,0
Laboratory Charges	10,6	16,5
Patents	4,2	5,6
Direct Manufacturing costs	139,8	187,5

Table 32: Different Direct Manufacturing costs contributions

Contribution	TRAD (M$/year)	CLC (M$/year)
Plant overhead costs	5,5	7,5
Local taxes and insurance	2,3	3,5
Fixed Manufacturing costs	7,7	11

Table 33: Different Fixed Manufacturing costs contributions

Contribution	TRAD (M$/year)	CLC (M$/year)
Administration costs	1,4	1,9
Distribution and selling costs	1,7	2,3
Research and Development	7,9	10,7
General Expenses	11,0	14,9

Table 34: Different General Expenses contributions

Appendix C - Cash Flow, Details

Type of Security	% of total	Current cost	WACC	After Tax WACC
Equity	50%	4,5%	2,25%	
Debt	50%	12%	6%	
Total			8,25%	5,67%

Table 35: IOU low risk financial structure, Traditional Plant

Type of Security	% of total	Current cost	WACC	After Tax WACC
Equity	45%	5,5%	2,48%	
Debt	55%	12%	6,6%	
Total			9,08%	6,24%

Table 36: IOU high risk financial structure, CLC Plant

Year	NPV TRAD (M$)	NPV CLC (M$)
0	-76,98	-119,57
1	23,29	-43,82
2	118,18	27,48
3	207,98	94,59
4	292,96	157,77
5	373,38	217,24
6	449,49	273,21
7	521,51	325,90
8	589,66	375,50
9	654,16	422,18
10	715,20	466,12
11	771,16	504,85
12	824,12	541,29
13	874,23	575,60
14	921,66	607,89
15	966,54	638,29
16	1009,01	666,91
17	1049,21	693,84
18	1087,25	719,19
19	1123,24	743,06
20	1157,31	765,52
21	1189,54	786,66
22	1220,05	806,56
23	1248,92	825,30
24	1276,24	842,93
25	1302,10	859,53

Table 37: NPV comparison between traditional and CLC plant, detail

References

[1] Intergovernmental Panel on Climate Change, 2018, *"Global Warming of 1.5 °C"*

[2] Navigant, 2019, *"Gas for climate. The optimale role for gas in a net-zero emissions energy system"*

[3] Fuel Cells and Hydrogen Joint Undertaken, 2019, *"Hydrogen Roadmap Europe. A sustainable pathway for the European energy transition"*

[4] International Energy Agency (IEA), 2019, *"Hydrogen- tracking clean energy progress"*

[5] International Renewable Eergy Agency (IRENA), 2018, *"Renewable Energy Prospects for the European Union"*

[6] A. Antzara, E. Heracleous, D.B. Bukur, A.A. Lemonidou, 2015, *"Thermodynamic analysis of hydrogen production via chemical looping steam methane reforming coupled with in situ CO_2 capture"*

[7] A. Gumilar, Ray Elshout Energy, Systems Engineering, 2010, *"Hydrogen Production by Steam Reforming"*, Online resource available at `https://chemeng-processing.blogspot.com/2010/05/hydrogen-production-by-steam-reforming.html`

[8] M.C.Annesini, R. Augelletti, I. Fabriani, M. A. Murmura, L. Turchetti, 2012, *"Analisi tecnico-economica del processo di upgrading del biogas mediante Pressure Swing Adsorption"*

[9] M.A. Murmura, M.Diana, R.Spera, M.C.Annesini, 2016, *"Modeling of autothermal methane steam reforming: Comparison of reactor configurations"*

[10] M.H. Halabi , M.H.J.M. de Croon , J. van der Schaaf , P.D. Cobdenb, J.C. Schouten, 2008, *"Modeling and analysis of autothermal reforming of methane to hydrogen in a fixed bed reformer"*

[11] Sheldon H.D. Lee, Daniel V. Applegate, Shabbir Ahmed, Steven G. Calderone, Todd L. Harveyb, 2005, *"Hydrogen from natural gas: part I—autothermal reforming in an integrated fuel processor"*

[12] Hsuan Chang, Yih-Hung Chen, Yun-Tsz Chen and Chii-Dong Ho, 2018, *"Multi-objective Optimization of Mixed Membrane Reactors for Autothermal Reforming of Methane"*

[13] Chang-Hyun Kim, Jae-Yun Han, Sehwa Kim, Boreum Lee, Hankwon Lim, Kwan-Young Lee, Shin-Kun Ryi, 2018, *"Hydrogen production by steam methane reforming in a membrane reactor equipped with a Pd composite membrane deposited on a porous stainless steel"*

[14] Bernardo Castro-Dominguez, Ivan P. Mardilovich, Liang-Chih Ma, Rui Ma, Anthony G. Dixon, Nikolaos K. Kazantzis, Yi Hua Ma, 2016, *"Integration of Methane Steam Reforming and WaterGas Shift Reaction in a Pd/Au/Pd-Based Catalytic Membrane Reactor for Process Intensification"*

[15] Jornandes Dias Silva, Cesar Augusto Moraes de Abreu, 2016, *"Modelling and simulation in conventional fixed-bed and fixed-bed membrane reactors for the steam reforming of methane"*

[16] Genyin Yea, Donglai Xiea, Weiyan Qiaoa, John R. Graceb, C. Jim Limb, 2009, *"Modeling of fluidized bed membrane reactors for hydrogen production from steam methane reforming with Aspen Plus"*

[17] Magnus Rydén, Anders Lyngfelt, 2006, *"Using steam reforming to produce hydrogen with carbon dioxide capture by chemical-looping combustion"*

[18] Marìa Ortiz, Luis F. de Diego, Alberto Abad, Francisco Garcìa-Labiano, Pilar Gayàn, Juan Adaànez, 2012, *"Catalytic Activity of Ni-Based Oxygen-Carriers for Steam Methane Reforming in Chemical-Looping Processes"*

[19] A. Hafizi, M.R. Rahimpour, Sh. Hassanajili, 2016, *"Hydrogen production via chemical looping steam methane reforming process: Effect of cerium and calcium promoters on the performance of Fe_2O_3/Al_2O_3 oxygen carrier"*

[20] Andy Antzaraa, Eleni Heracleousa, Dragomir B. Bukurc, Angeliki A. Lemonidouam, 2014, *"Thermodynamic analysis of hydrogen production via chemical looping steam methane reforming coupled with in situ CO_2 capture"*

[21] Magnus Rydèn, Pedro Ramos, 2012, *"H_2production with CO_2 capture by sorption enhanced chemical-looping reforming using NiO as oxygen carrier and CaO as CO_2 sorbent"*

[22] K. Johnsen, H.J. Ryub, J.R. Graceb, C.J. Limb, 2006, *"Sorption-enhanced steam reforming of methane in a fluidized bed reactor with dolomite as CO_2-acceptor"*

[23] Patricia Aida Pichardo, 2019, *"Design and Optimization Studies as Applied to Hydrogen Production"*

[24] Natural-Gas-Derived Hydrogen in the Presence of Carbon Fuel Taxes and Concentrated Solar Power - ACS Sustainable Chemistry & Engineering (ACS Publications). Available at: `https://pubs.acs.org/doi/abs/10.1021/acssuschemeng.7b02745`

[25] J.C. Meerman, E.S. Hamborgb, T. van Keulena, A. Ramìreza, W.C. Turkenburga, A.P.C. Faaij, 2012, *"Techno-economic assessment of CO_2 capture at steam methane reforming facilities using commercially available technology"*

[26] Patricia Luis, 2016, *"Use of monoethanolamine (MEA) for CO_2 capture in a global scenario: Consequences and alternatives"*

[27] Stephanie A. Freeman, Jason Davis, Gary T. Rochelle, 2010, *"Degradation of aqueous piperazine in carbon dioxide capture"*

[28] Andrea Lanzini, 2018, *"Carbon capture and sequestration (CCS) processes"*, lecture material for the course of "Polygeneration and Advanced Energy Systems"

[29] IEAGHG, 2018, *" The Carbon Capture project at air products' Port Arthur hydrogen production facility"*

[30] Wenrong Shi, Huawei Yang, Yuanhui Shen, Qiang Fu, Donghui Zhang, Bo Fu, 2018, *"Two-stage PSA/VSA to produce H_2 with CO_2 capture via steam methane reforming (SMR)"*

[31] Jun Zhang, Paul A. Webley, Penny Xiao, 2008, *"Effect of process parameters on power requirements of vacuum swing adsorption technology for CO_2 capture from flue gas"*

[32] R. Soltani, M.A. Rosen, I. Dincer, 2014, *"Assessment of CO_2 capture options from various points in steam methane reforming for hydrogen production"*

[33] Guido Collodi, Foster Wheeler, 2010, *"Hydrogen Production via Steam Reforming with CO_2 Capture"*

[34] Jaeheum Junga, Yeong Su Jeonga, Youngsub Lima, Chi Seob Leeb, Chonghun Hana, 2013, *"Advanced CO_2 Capture process using MEA scrubbing: Configuration of a Split Flow and Phase Separation Heat Exchanger"*

[35] Muhammad Asif, Chul-u Bak, Woo-Seung Kim, 2014, *"Energy Minimization and Ammonia Abatement for CO_2 Capture Using a Blend of Ammonia and 2-Amino-2-Methyl-1-Propanol Solution"*

[36] L. Barelli, G. Bidini, F. Gallorini, S. Servili, 2008, *"Hydrogen production through sorption-enhanced steam methane reforming and membrane technology: A review"*

[37] J. Fan, L. Zhu, P. Jiang, L. Li, H. Liu, 2016, *"Comparative exergy analysis of chemical looping combustion thermally coupled and conventional steam methane reforming for hydrogen production"*

[38] Ling Zhou, Zheming Zhang, Ramesh K. Agarwal, 2014, *"Simulation and validation of chemical-looping combustion using ASPEN plus"*

[39] William X. Meng, Subhodeep Banerjee, Xiao Zhang, Ramesh K. Agarwal, 2015, *"Process simulation of multi-stage chemical-looping combustion using Aspen Plus"*

[40] Udara Sampath P.R.Arachchige, Morten Christian Melaaen, 2012, *"Aspen plus simulation of CO2 removal from coal and gas fired power plants"*

[41] A. Boyano, A.M. Blanco-Marigorta, T. Morosuk, G. Tsatsaronis, 2010, *"Exergoenvironmental analysis of a steam methane reforming process for hydrogen production"*

[42] Paolo di Marco, 2007, *"Appunti ed Esercizi di Fisica Tecnica e Macchine Termiche"*

[43] D. Wayne Blaylock, Teppei Ogura, William H. Green, and Gregory J. O. Beran, 2009, *"Computational Investigation of Thermochemistry and Kinetics of Steam Methane Reforming on Ni(111) under Realistic Conditions"*

[44] Ferrara G., Lanzini A., Leone P., Ho M., Wiley D., 2017, *"Exergetic and exergoeconomic analysis of post-combustion CO_2 capture using MEA-solvent chemical absorption"*

[45] Guojie Qi, Shujuan Wang, Hai Yu, Paul Feron, Changhe Chen, 2013, *"Rate-Based Modeling of CO_2 Absorption in Aqueous NH_3 ina Packed Column"*

[46] S. Moioli, L. A. Pellegrini, S. Gamba, 2012, *"Simulation of CO2 capture by MEA scrubbing with a rate-based model"*

[47] Zhongyang Luo, 2017, *"Low-Rank Coals for Power Generation, Fuel and Chemical Production; Chapter 10: Coal-to-liquids and polygeneration using low rank coals"*

[48] D. Kunii, O. Levenspiel, 1991, *"Fluidization Engineering"*

[49] S. Ergun, 1952, *"Chem. Eng. Prog. 48"*

[50] C. Klett, 2005, *"Time-Dependent Behavior of the Particle Size Distribution in Fluidized Bed Systems with Recirculation of Solids, PhD thesis"*

[51] J. Werther, J. Wein, 1994, *"Expansion behavior of gas fluidized beds in the turbulent regime"*

[52] J.F. Davidson, D. Harrison, 1963, *"Fluidised particles"*

[53] K. Hilligardt, J. Werther, 1987, *"Influence of Temperature and Properties of Solids on the Size and Growth of Bubbles in Gas Fluidized Beds"*

[54] K. Hilligardt, J. Werther, 1986, *"Local bubble gas hold-up and expansion of gas/solid fluidized beds"*

[55] D. Geldart, 1973, *"Types of gas fluidization, Powder Technology, 7"*

[56] A.B. Fournol, M.A. Bergougnou, C.G.J. Baker,1973, *"Solids entrainment in a large gas fluidized bed"*

[57] S.M. Tasirin, D. Geldart, 1998, *"The entrainment of fines and superfines from fluidized beds"*

[58] Cristina Dueso, María Ortiz, Alberto Abad, Francisco García-Labiano, Luis de Diego, Pilar Gayán, Juan Adánez, 2012, *"Reduction and oxidation kinetics of nickel-based oxygen-carriers for chemical-looping combustion and chemical-looping reforming"*

[59] David M. Austgen, Gary T. Rochelle, Xiao Peng, Chau-Chyun Chen, 1989, *"Model of Vapor-Liquid Equilibria for Aqueous Acid Gas-Alkanolamine Systems Using the Electrolyte-NRTL Equation1"*

[60] J. M. Paiva, C. Pinho, R. Figueiredo, 2004, *"The Influence of the Distributor Plate on the Bottom Zone of a fluidized bed approaching the transition from bubbling to turbulent fluidization"*

[61] W. Liemberger, M. Groβ, M. Miltner, H. Prazak-Reisinger, M. Harasek, 2016, *"Extraction of green hydrogen at fuel cell quality from mixtures with natural gas"*

[62] Luk Ho Ting, Lei Ho Man, Ng Wai Yee, Ju Yihan and Lam Koon Fung, 2012, *"Techno-economic Analysis of Distributed Hydrogen Production from Natural Gas"*

[63] Midhun Thomas Vergis, 2007, *"Economics of Steam Methane Reformation and Coal Gasification For Hydrogen Production"*

[64] Richard Turton, Richard C. Bailie, Wallace B. Whiting, Joseph A. Shaeiwitz, 2009, *"Analysis, Synthesis, and Design of Chemical Processes, Third Edition"*

[65] Engineers Edge, *"Overall Heat Transfer Coefficient Table Chart"*, `https://www.engineersedge.com/thermodynamics/overall_heat_transfer-table.htm`, accessed 16/11/2019

[66] Robert H. Perry, Don W. Green, James O. Maloney, 1997, *"Perry's Chemical Engineers' Handbook, Seventh Edition"*

[67] Yogi Wibisono Budhi, Dhinny Dwi Putri, Afifa Husna, Hans Kristian Irawan, Manabu Miyamoto, Shigeyuki Uemiya, 2017, *"Dynamic operation of water gas shift reaction over $Fe_2O_3/Cr_2O_3/CuO$ catalyst in Pd/Al_2O_3 membrane reactor"*

[68] Mauro Luberti, 2015, *"Design of a H_2 Pressure Swing Adsorption process at an advanced IGCC plant for cogenerating hydrogen and power with CO_2 capture"*

[69] Randall W. Whitesides, 2012, *"Process Equipment Cost Estimating by Ratio and Proportion"*

[70] `http://folk.ntnu.no/magnehi/cepci_2011_py.pdf`, Accessed 17/11/2019

[71] `https://imgv2-1-f.scribdassets.com/img/document/410567937/original/6fcfff5870/1567762671?v=1`, Accessed 17/11/2019

[72] `https://imgv2-1-f.scribdassets.com/img/document/410567937/original/6fcfff5870/1567762671?v=1`, Accessed 17/11/2019

[73] National Energy Technology Laboratory (NETL), 2011, *"Cost estimation methodology for NETL assessments of power plant performances"*

[74] Yinglong Wang, Guoxuan Li, Zhiqiang Liu, Peizhe Cui, Zhaoyou Zhu, Sheng Yang, 2019, *"Techno-economic analysis of biomass-to-hydrogen process in comparison with coal-to-hydrogen process"*

[75] Calin-Cristian Cormos, 2012, *"Integrated assessment of IGCC power generation technology with carbon capture and storage (CCS)"*

[76] `https://ec.europa.eu/eurostat/databrowser/view/ten00118/default/bar?lang=en`, Accessed 17/11/2019

[77] `https://ec.europa.eu/eurostat/databrowser/view/ten00117/default/table?lang=en`, Accessed 17/11/2019

[78] Alkhayat WA, Gerrard AM., 1984, *"Estimating Manning Levels for Process Plants"*

[79] International Energy Agency (IEA), 2016, *"Energy Technology Perspectives 2016"*

[80] Joshua Eichman, Aaron Townsend, Marc Melaina, National Renewable Energy Laboratory (NREL), 2016, *"Economic Assessment of Hydrogen Technologies Participating in California Electricity Markets"*

[81] `https://www.pmi.it/impresa/contabilita-e-fisco/52519/irpef-scaglioni-e-aliquote.html`, Accessed 21/11/2019

[82] Sustainable Gas Institute, Imperial College London, 2016, *"Can Technology Unlock 'Unburnable Carbon' ?"*

[83] National Institute of Standards and Technologies (NIST), *"Thermophysical Properties of Fluid Systems"*, online database available at `https://webbook.nist.gov/chemistry/fluid/`, Accessed 30/11/2019

[84] International Energy Agency (IEA), 2019, *"The Future of Hydrogen. Seizing today's opportunities"*